

LINKING SATELLITE IMAGERY TO BRIGHT SUNSHINE HOURS FOR THE  
ESTIMATION OF GLOBAL SOLAR IRRADIATION

A THESIS SUBMITTED TO  
THE GRADUATE SCHOOL OF NATURAL AND APPLIED SCIENCES  
OF  
MIDDLE EAST TECHNICAL UNIVERSITY

BY

SELMİN ENER RUŞEN

IN PARTIAL FULFILLMENT OF THE REQUIREMENTS  
FOR  
THE DEGREE OF DOCTOR OF PHILOSOPHY  
IN  
PHYSICS

FEBRUARY 2013



Approval of the thesis:

**LINKING SATELLITE IMAGERY TO BRIGHT SUNSHINE HOURS FOR THE  
ESTIMATION OF GLOBAL SOLAR IRRADIATION**

submitted by **SELMİN ENER RUŞEN** in partial fulfillment of the requirements for the degree of **Doctor of Philosophy in Physics Department, Middle East Technical University** by,

Prof. Dr. Canan Özgen

Dean, Graduate School of **Natural and Applied Sciences**

\_\_\_\_\_

Prof. Dr. Mehmet Zeyrek

Head of Department, **Physics**

\_\_\_\_\_

Prof. Dr. Bülent G. Akınoğlu

Supervisor, **Physics Dept., METU**

\_\_\_\_\_

**Examining Committee Members:**

Prof. Dr. Raşit Turan

Physics Dept., METU

\_\_\_\_\_

Prof. Dr. Bülent G. Akınoğlu

Physics Dept., METU

\_\_\_\_\_

Prof. Dr. Günnur Koçar

Institute of Solar Energy, Ege Univ.

\_\_\_\_\_

Assoc. Prof. Dr. Zuhale Akyürek

Civil Eng. Dept., METU

\_\_\_\_\_

Prof. Dr. Osman Yılmaz

Physics Dept., METU

\_\_\_\_\_

**Date: 14.02.2013**

I hereby declare that all information in this document has been obtained and presented in accordance with academic rules and ethical conduct. I also declare that, as required by these rules and conduct, I have fully cited and referenced all material and results that are not original to this work.

Name, Last name : Selmin, ENER RUŞEN

Signature :

## ABSTRACT

### LINKING SATELLITE IMAGERY TO BRIGHT SUNSHINE HOURS FOR THE ESTIMATING OF GLOBAL SOLAR IRRADIATION

Ener Ruşen, Selmin

Ph.D., Department of Physics

Supervisor : Prof. Dr. Bülent G. Akinođlu

February 2013, 102 pages

This thesis is on the estimation models for the daily global solar irradiation on a horizontal surface at the surface of the Earth. New approaches are developed and applied to 15 locations of Turkey and Germany. The main idea in developing the new models is to link the surface data to satellite imagery. Totally three new modeling approaches are developed and tested. Surface data of daily bright sunshine hours ( $s$ ) and cloud index ( $n$ ) values derived from satellite images are the main input parameters. In the first approach, monthly coefficients of Angström linear relation between daily solar irradiation and daily bright sunshine hours are used to replace the clear sky irradiance calculations of HELIOSAT model. In the second approach new correlations are obtained between daily bright sunshine hours ( $s$ ) and cloud index ( $n$ ). Last model that is developed uses a new correlation expression between daily solar irradiation and daily data of  $s$  and  $n$  and this expression is derived using a physical consideration. The performances of the proposed models are tested against conventional methods (mainly, satellite-based HELIOSAT and ground-based linear Angström-Prescott type).

The results show that the use of sunshine duration together with the cloud index is quite satisfactory in the estimations of daily global solar irradiation. The accuracy of estimations of the combined models is considerably higher than the conventional approaches. Therefore, we propose to use the new approaches to estimate daily global irradiation whenever the data of bright sunshine hours is available for the location of interest or a

nearby station. In addition, for a point on the earth surface, depending on the data in hand, suitable and most accurate models of estimations are proposed for that point.

**Keywords:** Satellite images, HELIOSAT, Angström model, solar energy, bright sunshine hour.

## ÖZ

### KÜRESEL GÜNEŞ IŞINIMI TAHMİN ETMEK İÇİN UYDU GÖRÜNTÜLERİNİ VE GÜNEŞLENME SÜRESİNİ BİRLEŞTİRME

Ener Ruşen, Selmin

Lisans Sonrası Doktora, Fizik Bölümü

Tez Yöneticisi : Prof. Dr. Bülent G. Akınoğlu

Şubat 2013, 102 sayfa

Bu tez dünya yüzeyine gelen yatay bir düzlemdeki günlük toplam güneş ışınımı için tahmin modelleri üzerinedir. Yeni yaklaşımlar geliştirilerek, Türkiye ve Almanya'da 15 istasyon verileri için uygulanmıştır. Geliştirilen yeni modellerdeki temel yaklaşım uydu görüntülerinden elde edilen bilgiyle, yer verisini birleştirmektir. Toplam üç yeni modelleme yaklaşımı geliştirilmiş ve test edilmiştir. Günlük güneşlenme süresi için yer verileri ( $s$ ) ve uydu görüntülerinden türetilen bulut indeksi değerleri ( $n$ ) ana giriş parametreleridir. Birinci yaklaşımda, günlük güneş ışınımı ve günlük güneşlenme süreleri arasında, Angström doğrusal bağıntısının aylık katsayıları, HELIOSAT modelinin bulutsuz havalar için yaptığı ışınım hesaplamaları yerine kullanılmıştır. İkinci yaklaşımda ise günlük güneşlenme süresi ( $s$ ) ve bulut indeksi ( $n$ ) arasında yeni bağıntılar elde edilmiştir. Geliştirilen son modelde ise günlük güneş ışınımı ( $s$ ) ile bulut indeksinin ( $n$ ), günlük verileri arasında yeni bir bağıntı bulunmuş ve bu bağıntı temel bir fiziksel yaklaşımla türetilmiştir. Önerilen modellerin performansları, geleneksel yöntemlere (özellikle, uydu tabanlı HELIOSAT ve yer tabanlı lineer Angström-Prescott tipi) karşı test edilmiştir.

Sonuçlar, bulut indeksi ile birlikte güneşlenme süresinin kullanılmasının, günlük yatay toplam güneş ışınım tahminlerinde oldukça tatmin edici olduğunu göstermektedir. Birleştirilmiş modellerin tahminlerinin doğruluğu geleneksel yaklaşımlardan oldukça yüksektir. Bu nedenle, güneşlenme süresi verileri ilgilenilen bölge için ulaşılabilir olduğu durumda, günlük toplam ışınımı tahmin etmek için yeni yaklaşımların kullanımı

önerilmiştir. Ayrıca, yeryüzündeki bir nokta için elde edilen verilere bağlı olarak en uygun ve kesin güneş radyasyonu tahmin modelleri belirlenmiştir.

**Anahtar Kelimeler:** Uydu Görüntüsü, HELIOSAT, Angström Model, Güneş Enerjisi, Güneşlenme Süresi.



*to my husband Aydın and my daughter Elif Gökçe ...*

## ACKNOWLEDGEMENTS

I would like to thank to my supervisor Prof. Dr. Bülent G. Akınođlu, for his continuous support, perceptiveness, encouragement. Without his guidance, it would be harder to improve my knowledge.

I would also like to thank to Dr. Annette Hammer for giving me the opportunity to study with her group also for his encouragement and support during my research period in her group. My thanks are also due Bulent Aksoy for his critical comments and advices and also in supplying and reducing the surface data for Turkey.

In addition, I would like to thank to Jan Kühnert for his wonderful friendship, support and encouragement. I would also like to thank Dr. Detlev Heinemann, Dr. Thomas Scheidsteger, Dr. Elke Lorenz, Jethro Betcke, Tanja Behrendt and all other friends in the Energy Meteorology group of Oldenburg University in Germany who were always patient to my questions and for all their sincere friendship.

I also would like to thank to Assoc. Prof. Dr. Zuhale Akyürek and Prof. Dr. Osman Yılmaz for their critical comments and advices during the course of my studies on my thesis.

I want to thank to my friends Arife Gencer İmer, Özge Bayraklı, Merve Demirtaş and Gökhan Alkaç for their friendliness and endless support during this work. I want to thank to Tunay Tansel, for his support both scientifically and mentally during the last period of my study. I would like to thank to Alper Kılıç, Ulaş Canatalı and Murat Ulubay for their technical support. I really learned a lot from them about various concepts.

I would like to give my endless gratitude to my husband Aydın Ruşen for invaluable patience and love, who supported and motivated me with his understanding during the whole period of my study. I want to also thank my family's each member (especially to my parents) for special support on tired days. My special thanks go to my daughter Elif Gökçe Ruşen for making some heavy times enjoyable.

My warmest regards and many thanks go to Başak Atasoy for tutored me in English and Academic Writing Center for supports. Also, I would like to thank to Scientific and

Technical Research Council of Turkey (TUBITAK) for financial support for some parts of this study. I would like to thank State Meteorological Service (TSMS), Mr. Erdem Erdi for providing us some measured data.

This study is supported by ÖYP program of DPT and ODTÜ under the project number: BAP-08-11-DPT2002K120510. I would like to thank also DPT and ODTÜ for their supports.

## TABLE OF CONTENTS

ABSTRACT .....	v
ÖZ.....	vii
ACKNOWLEDGEMENTS.....	x
TABLE OF CONTENTS .....	xii
LIST OF TABLES .....	xv
LIST OF FIGURES .....	xvi
CHAPTERS	
1. INTRODUCTION .....	1
1.1 Objective .....	1
1.2 The Extent of the Thesis .....	2
1.3 The Need for Accurate Solar Irradiation .....	3
1.4 Measured Data and Calculated Quantities .....	3
1.4.1 Available Data .....	3
1.4.2 Calculated Quantities .....	6
1.5 Thesis Outline .....	7
2. SOLAR RADIATION ON THE EARTH .....	9
2.1 Introduction .....	9
2.2 The Sun And Extraterrestrial Solar Radiation .....	9
2.2.1 The Sun and Spectrum .....	9
2.2.2 Solar Constant .....	11
2.2.3 Extraterrestrial Solar Radiation .....	12
2.2.3.1 Instantaneous Extraterrestrial Solar Irradiance .....	12
2.2.3.2 Hourly Extraterrestrial Solar Irradiation on a Horizontal Surface .....	15
2.2.3.3 Daily Extraterrestrial Solar Irradiation on a Horizontal Surface .....	16
2.2.4 Solar Time .....	17
2.2.5 The Length of the Day .....	18
2.3 The Transmission of Energy Through the Atmosphere .....	18
2.3.1 Air Mass .....	22
2.3.2 Clearness Index .....	23
2.3.3 Clear Sky Index .....	24

2.4 Solar Irradiation Measurements .....	24
2.4.1 Direct and Diffuse Solar Irradiation .....	24
2.4.2 Solar Irradiation Detectors .....	26
2.4.3 Sunshine Duration .....	28
2.4.4 Atmospheric Turbidity .....	29
2.5 Satellites .....	31
2.5.1 Meteorological Satellite Orbits .....	32
2.5.2 Meteosat First and Second Generation Satellites .....	33
2.5.2.1 Meteosat First Generation Satellites (MFG) .....	33
2.5.2.2 Meteosat Second Generation Satellites (MSG) .....	34
2.6 Modeling Comparison and Validation Techniques .....	35
2.6.1 Standard Error Analyses .....	35
2.6.2 Cumulative Distribution of the Differences .....	37
3. SOLAR IRRADIATION ESTIMATION MODELS.....	39
3.1 Introduction .....	39
3.2 Statistical Models for the Estimation of Solar Irradiation .....	40
3.2.1 Ground – Based Solar Irradiation Estimation Models with the Statistical Approach .....	40
3.2.2 Remote Sensing Based Solar Irradiation Models with the Statistical Approach .....	42
3.3 Physical Models for the Estimation of Solar Irradiation .....	42
3.3.1 Ground – Based Solar Irradiation Estimation Models with the Physical Base .....	43
3.3.2 Remote Sensing Based Solar Irradiation Models with the Physical Base .....	44
3.4 Combined Models .....	44
3.5 Comparison of Statistical, Physical and coupled Models .....	45
3.6 Conventional Models .....	46
3.6.1 Angström – Prescott Model .....	47
3.6.2 HELIOSAT .....	48
3.7 Simple Satellite Method Applied to Daily Data .....	51
4. MODELLING APPROACHES .....	53
4.1 Introduction .....	53
4.2 Angström – Prescott Equation with Daily Clear Sky Irradiation of HELIOSAT ( $H^*$ ) .....	53
4.3 $H_{model}$ .....	55
4.3.1 Implementation of the $H_{model}$ to the Neighbors .....	58
4.4 Combined Approach Based on the Relation Between $n$ and $s(H_{CA1})$ .....	59

4.4.1 Implementation of the $H_{CA1}$ to the Neighbors .....	60
4.5 Combined Approach by Using Simple Physical Base ( $H_{CA2}$ ) .....	61
4.5.1 Implementation of the $H_{CA2}$ Model to the Neighbors .....	63
5. RESEARCH RESULTS AND DISCUSSIONS .....	65
5.1 Introduction .....	65
5.2 Standard Error Analyses of Models .....	65
5.3 Cumulative Distribution of the Differences for the Models .....	70
6. CONCLUSIONS .....	73
REFERENCES .....	79
APPENDIX A .....	87
APPENDIX B .....	89
APPENDIX C .....	95
CURRICULUM VITAE .....	100

## LIST OF TABLES

TABLES	
Table 1.1 Geographical and climate type information of selected stations .....	5
Table 1.2 A dictionary for the calculated, derived, measured and estimated quantities .....	7
Table 2.1 Major Spectral Regions and the range of wavelengths .....	10
Table 2.2 The concentration of gases constituting dry air at ground level .....	20
Table 2.3 MFG satellites channels with their resolutions .....	33
Table 2.4 MSG satellites channels with their spectral ranges .....	34
Table 3.1 Comparison of statistical, physical and coupled models with an advantages and disadvantages .....	46
Table 4.1 Multiple regression coefficients $A_0, A_1, A_2$ and $A_3$ for all selected stations .....	63
Table A.1 Monthly values of $\alpha_i, \beta_i, c_i$ and $d_i$ coefficients .....	87
Table B.1. $a, b, a^*, b^*, R^2$ values of $K$ vs $s/S$ and $K^*$ vs $s/S$ .....	89
Table C.1. Monthly relative MBE values for proposed models and selected stations .....	96
Table C.2. Monthly relative RMSE values for proposed models and selected stations .....	97
Table C.3. Monthly MBE values for proposed models and selected stations .....	98
Table C.4. Monthly RMSE values for proposed models and selected stations .....	99

## LIST OF FIGURES

### FIGURES

Figure 1.1	Geographical locations for selected stations .....	6
Figure 2.1	Solar spectrum .....	11
Figure 2.2	Sun – Earth Distance .....	12
Figure 2.3	Angle of incidence .....	13
Figure 2.4	Sun position with zenith angle $\theta_z$ , surface azimuth angle $\gamma$ , solar azimuth angle $\gamma_s$ , solar altitude angle $\alpha_s$ , and $\beta$ slope for a receiving tilted surface, and N is surface normal ranges .....	14
Figure 2.5	The equation of time in minutes, as a function of time of year .....	17
Figure 2.6	The schematic representation of solar energy in the atmosphere.....	21
Figure 2.7	Relative air masses with the convenient zenith angles in a plane parallel atmosphere .....	22
Figure 2.8	Solar irradiation measurements for Ankara, Turkey for the year 2004, 2nd March .....	25
Figure 2.9	Hukseflux DR01 Type Pyrheliometers .....	26
Figure 2.10	The parts of the pyranometer.....	27
Figure 2.11	The tracker ball and shadow ring type pyranometers.....	27
Figure 2.12	The classic Campbell-Stokes type sunshine duration recorder and electronic type sunshine duration sensor.....	29
Figure 2.13	Areas of the Earth covered by each of the satellites. ....	31
Figure 2.14	Meteorological satellites orbit and their distances. ....	32
Figure 3.1	Linear regression between the daily values of clearness index $K$ and daily average cloud index $n_{avg}$ for the month of April 2004 in Ankara. ....	51
Figure 4.1	Comparative analysis between daily clearness index $K$ and daily clear sky index $K^*$ versus $s/S$ for the station Ankara for the year of 2004. ....	55
Figure 4.2	Relation between daily clear sky irradiation values of Angström- Prescott relation, $H_{clear,A}$ and daily clear sky irradiation values of HELIOSAT, $H_{clear,H}$ used in the regression analysis. ....	56
Figure 4.3	Relation between monthly values of Linke turbidity $T_L$ and $R^2$ for the correlation of clearness index $K$ (clearsky index $K^*$ ) with sunshine duration $s/S$ . The regression has been performed for all stations. ....	57
Figure 4.4	Regression analysis between the daily average of cloud index $n_{avg}$ and sunshine duration fraction ( $s/S_o$ ) for the month of April 2004 in Ankara. ....	60
Figure 4.5	Schematic representation of the daily global solar irradiation passing through the Earth's atmosphere to the ground.....	62



Figure 5.1 (A) Monthly relative MBE and (B) monthly relative RMSE among calculated models and ground measurement of daily global solar radiation data for the fifteen selected stations for one year. The values were applied to the same location that the models are constructed .....	68
Figure 5.2 Monthly relative MBE (A) and Monthly relative RMSE (B) among calculated models and ground measurement of daily global solar radiation data for the fifteen selected stations for one year. Implementation results of to the neighboring stations. ....	69
Figure 5.3 (A) Cumulative frequency for the daily differences value of the daily differences for a year and for all the models and locations .....	70
Figure 5.3 (B) Cumulative frequency for the absolute value of the daily differences for a year and for all the models and locations. ....	71
Figure 6.1 Schematic representation for the proposed models (Location A have all three data, location B have $s/S_0$ and $n_{avg}$ , location C only have $n_{avg}$ ). ....	76
Figure 6.2 Comparison of the satellite model (HELIOSAT) and ground measured data for snowy days in Erzincan, 01-15.01.2006. ....	77



# CHAPTER 1

## INTRODUCTION

### 1.1 Objective

It has become essentially important to have accurate knowledge of solar irradiation on the surface of the Earth due to the implications it carries for both various technological applications and potential climatic consequences worldwide over the past two decades. The access to high quality solar data is certainly a vital issue to improve the planning and performance of solar systems, and in terms of environmental compliance in any region of the Earth. The most accurate way of obtaining solar irradiation is certainly the use of ground-based measurements of a given site. However, the measurement network is not adequate and the data taken from ground based sensors are not very reliable. In addition, measurements through ground based sensors have extraordinarily high costs, including maintenance and data archiving efforts. For these reasons, in order to derive accurate information on solar irradiation at the ground level, mainly two different estimation approaches have been developed by many researches [1–6]. The first approach is the statistical models that provide high performances for the estimation of global solar irradiation by using measurements obtained on the surface of the Earth. The other approach, which, in recent years, has been profoundly progressing, is satellite derived estimation models that use geostationary weather satellites.

In this thesis, mainly, new coupled approaches are developed to estimate global solar irradiation by making use of statistical and satellite derived models. The results of new proposed approaches, then, are compared with the estimation of a commonly used satellite model and with Angström type models using ground measurements of global solar irradiation.

## 1.2 The Extend of the Thesis

The Sun is the main natural energy source of the Earth, and solar radiation arises from its surface as electromagnetic energy. Instantaneous solar irradiance,  $G$ , is defined as the amount of instant electromagnetic energy incident on a surface per unit time per unit area. In other words, it is the power received per area. The unit is watt per square meter ( $W/m^2$ ) and it refers to the energy emanating from the Sun [7]. To calculate the irradiance at the receiving surface, influence rate of the atmosphere, Sun-Earth geometry, extraterrestrial solar irradiation and position of the Sun with respect to the receiving surface there, should be determined [8], [9]. A more detailed description will be given later in Chapter 2.

The instantaneous values of global solar irradiance,  $G$ , are used to acquire the hourly, daily or monthly average daily irradiation values required for many applications such as the global solar irradiation maps or for the performance calculations of solar energy systems. In this sense, to obtain hourly or daily values of solar irradiation on horizontal surface, the integration of the instantaneous values of global solar irradiance acquired at specific time intervals according to the intended application is required [10], [11]. The hourly solar irradiation ( $I$ ) is the incident of energy accumulated per unit area over the period of time lasting an hour. It is usually given in joule per square meter ( $J/m^2$ -hour), and it can be obtained by Eqn. (1.1) for an hour time period:

$$I = \int_{t_1}^{t_2} G(t)dt \quad (1.1)$$

where  $G(t)$  is the instantaneous value of global solar irradiance, the limits  $t_1$  and  $t_2$  define one hour.

In the same manner, the instantaneous solar irradiance is used to find integrated daily global solar irradiation,  $H$ , on a horizontal surface. This is calculated by integrating  $G$  over the period from sunrise to sunset:

$$H = \int_{Sunrise}^{Sunset} G(t)dt \quad (1.2)$$

Herein,  $G$  is in watt per square meter ( $W/m^2$ ); consequently,  $H$  is in joule per square meter ( $J/m^2$ -day). The monthly-averaged global daily irradiation  $\bar{H}$  is a useful quantity especially for climatic studies, are monthly averages taken over several years (10 to 30), of daily irradiation. The units and symbols are those recommended by Duffie and Beckman [12].

In the present study, the estimation of daily global solar irradiation values are mainly analyzed and reviewed; new coupled estimation schemes has been developed for daily global solar irradiation values ( $H$ ) and they are compared with classical conventional models.

### **1.3 The Need for Accurate Solar Irradiation**

In the recent years, researchers all over the world have been developing methods to generate reliable and accurate solar resource data and maps, based on advanced models, computer software and state of the art geographic information. Nowadays, planners can use these data and maps as an important input parameter to identify the best sites for solar energy systems and to estimate the resources available at any site where solar applications are contemplated. Placement of solar energy systems, performance evaluation for proposed solar systems at any location, investigation of PV capability, power management of solar thermal power plants and solar architecture, building engineering and short-term forecast of solar radiation are a few examples of these applications of solar irradiance data [13], [14], [15].

According to climate change research, it is important to reach higher accuracies for all types of solar energy applications. In recent studies dealing with climate forecasting for agricultural land usage, researchers have been trying to improve the accuracy of solar irradiation estimation [16]. In the present work, we aimed to reach higher accuracies by coupled approach in which we utilized surface measured bright sunshine hours together with the satellite based cloud index values. Such a procedure may also be useful in the research of climate change issues.

### **1.4 Measured Data and Calculated Quantities**

#### **1.4.1 Available Data**

This work presents the analysis of a year's collection of data obtained from daily global solar radiation measurements on a horizontal surface  $H$  and the data to be correlated to  $H$ , which are the surface measured daily bright sunshine hours  $s$  and cloud index  $n$  derived from satellite imagery. The data of ground level global solar irradiation and sunshine duration were obtained from the Turkish State Meteorological Service (TSMS) for four stations in

Turkey and from Deutscher Wetterdienst (DWD) for eleven stations in Germany. Global solar irradiation data measured by pyranometer and sunshine duration observations are either collected by Campbell-Stokes recorder, which is the most common sunshine recorder used in many stations all over the world or by new solid state sensors.

The estimating models presented in this study used Meteosat satellite visible spectral range images from the European Organization for the Exploitation of Meteorological Satellites (EUMETSAT). The calculation of cloud index  $n$ , images from original satellite data was performed in the Institute of Physics Carl von Ossietzky, University of Oldenburg using the HELIOSAT model. The results were attained on an hourly basis. In all calculations, these hourly values were used to calculate the daily totals obtained directly by summing. In addition, the daily averages of the cloud index,  $n_{avg}$  values were calculated for the selected locations to be used for direct daily estimations. A list of the selected stations' names and their geographical locations together with their climate types, namely Cfb, Dfc, Dfb and Bsk are presented in Table 1.1 and locations are given in Fig. 1.1. (Csa: warm Mediterranean climate, Cfb: temperate oceanic climate, Dfc: cool continental climate/subarctic climate, Dfb: temperate continental climate/humid continental climate, Bsk: cold semi-arid climate [17], [18]).

The set of data was obtained over a one-year period in 2004 for the four stations in Turkey and a one-year period in 2006 for the eleven stations in Germany. For the four locations in Turkey, satellite data for January 2004 was missing and thus the satellite images were available starting from February 2004. Therefore, for Ankara, Afyon, Sinop and Bursa, the analyses are carried out for 11 months only. Besides, the data for some of the ground measurements for German stations were missing. Accordingly, a total of ten months were missing out of 180 months (12 months x 15 stations) and we excluded these months in our analysis.

**Table 1.1** Geographical and climate type information of selected stations.

	Selected Stations	Latitude	Longitude	Altitude (m)	Climate types [17]
1	Ankara/Turkey	39.97 N	32.86 E	891	Bsk
2	Afyon/Turkey	38.74 N	30.56 E	1034	Bsk
3	Sinop/Turkey	42.03 N	35.15 E	32	Cfb
4	Bursa/Turkey	43.23 N	29.01 E	100	Csa
5	Braunschweig/Germany	52.30 N	10.45 E	83	Dfb
6	Wittenberg/Germany	51.88 N	12.65 E	105	Dfb
7	Görlitz/Germany	51.17 N	14.95 E	237	Dfb
8	Dresden-Klotzsche/Germany	51.13 N	13.78 E	222	Dfb
9	Ludwigsfelde/Germany	52.22 N	14.12 E	122	Dfb /Cfb
10	Bremen/Germany	53.05 N	8.80 E	24	Cfb
11	Norderney/Germany	53.72 N	7.15 E	29	Cfb
12	Potsdam/Germany	52.37 N	13.08 E	107	Cfb
13	Chemnitz/Germany	50.80 N	12.87 E	418	Dfc
14	Fichtelberg/Germany	50.43 N	12.95 E	1213	Dfc
15	Zinnwald/Germany	50.73 N	13.75 E	877	Dfc

The correlations between  $H$ , and,  $n$  and  $s$  are obtained for all stations in various ways. Thus, to estimate the daily global solar irradiation on a horizontal surface, these correlations are used simply by inserting the given  $n$  and  $s$  values of the selected stations. We should note that these estimations, carried out by inserting  $n$  and  $s$  values of the same station, into the correlations we obtained, only give the goodness of the fits [19].



Figure 1.1 Geographical locations for selected stations [20].

### 1.4.2 Calculated Quantities

Computations about the estimation of global solar irradiance can be separated into two basic parts: measured (or estimated) and calculated quantities. This section presents a short definition for calculated quantities, which are daily global solar extraterrestrial irradiation,  $H_0$ , the day-length  $S$ , and the modified day-length  $S_0$ . Details will be given in Chapter 2.

The daily global solar radiation received at the top of the Earth's atmosphere on a horizontal surface is called the daily extraterrestrial solar radiation  $H_0$ , calculated as a function of the ratio between actual and mean Sun–Earth distance, latitude ( $\phi$ ), solar declination ( $\delta$ ) and solar angle at sunrise ( $\omega_s$ ). The calculation procedures of these parameters can be found in the reference Duffie and Beckman [12] and an extended summary will be presented in Chapter 3.



Another calculated quantity used in our study is the length of the day,  $S$ , which is the maximum possible duration between sunrise and sunset for a day. In order to reduce the effect of low altitude of the Sun, which means that the solar zenith angle is less than  $5^\circ$  or larger than  $85^\circ$ , a modified day-length  $S_0$  proposed by Hay [21] was used in our calculations.

To conclude,  $s/S$  and  $s/S_0$  fractions ( $s$  is measured values obtained from sunshine recorders,  $S$  and  $S_0$  are calculated quantities) are one of the two main input variables in our study. The other one is the cloud index  $n$  derived from satellite images. It is noted that these calculated quantities and the daily extraterrestrial irradiation  $H_0$  (in Angström relation), mentioned above, and the relevant discussion will be given in detail later in Chapter 3. Table 1.2 gives a dictionary for the calculated, derived, measured and estimated quantities.

**Table 1.2** A dictionary for the calculated, derived, measured and estimated quantities.

Symbol	Name	Description
$s$	Bright Sunshine Hour	Measured by Campell-Stokes type recorder or by new sensors
$n$	Cloud index	Derived from Satellite imagery
$H$	Daily Global Solar Irradiation	Measured and/or estimated by the models
$H_0$	Daily Extraterrestrial Solar Irradiation	Calculated (Duffie and Beckman [12])
$S$	Day-length	Calculated (Duffie and Beckman [12])
$S_0$	Modified day-length	Calculated (Hay [21])

## 1.5 Thesis Outline

In this thesis, Chapter 2 provides background information on the concepts related to the work. A brief description of the solar radiation on the surface of the Earth is introduced, and interrelationships among some related definitions are presented. Chapter 3 begins by reviewing methods for the estimation of solar irradiation with the statistical and physical approaches. Then, combined and conventional models are introduced. Three new combined models are proposed for the estimation of daily global solar irradiation in Chapter 4. After

reviewing several functional and multivariate different estimation methods, the estimation accuracy is evaluated and compared using ground measurement data sets and error analyses in Chapter 5. Finally, the conclusions of these investigations are given in Chapter 6.

## CHAPTER 2

### SOLAR IRRADIATION ON THE EARTH

#### 2.1 Introduction

It is certainly known that the most important natural energy source of the Earth is the electromagnetic solar radiation which comes from the surface of the Sun. It affects, not only the climatic processes of the Earth's weather, but also acts as a source of solar energy systems.

This chapter starts with a description of the Sun and extraterrestrial solar radiation; i.e., solar constant, solar geometry and basics of the spectrum of the Sun are introduced in detail. Then, some fundamental definitions and formulations about the most important atmospheric quantities, such as air mass calculation, clearness and clear sky index on a horizontal surface are explained. The global solar irradiation data detectors and bright sunshine recorder (Pyranometers and Campbell-Stokes type recorders respectively) were introduced under the heading "Solar Irradiation Measurements." In addition, atmospheric turbidity and surface albedo that are associated with the calculation of solar radiation in the Earth's atmosphere are given. Finally, information about satellites which are used for estimation of solar irradiation is presented.

#### 2.2 The Sun and Extraterrestrial Solar Radiation

##### 2.2.1 The Sun and Spectrum

The Sun is a sphere composed of hot and dense gaseous formation with a diameter of  $1.39 \times 10^9$  meters. It revolves around its axis, and the distance between the Sun and Earth is approximately  $1.5 \times 10^{11}$  meters [12], [22]. The majority of the mass of the Sun is composed of hydrogen, and the remainder of it is helium and other heavier elements, such as, oxygen,

carbon, neon and iron. The Sun which has a gaseous surface appears as a blackbody with the temperature of around 5800 K [12]. The energy produced inside of the Sun reaches the Earth's surface as electromagnetic waves. The electromagnetic waves from the Sun transport radiation energy of various wavelengths [23], [16].

If any substance has a temperature, it emits electromagnetic radiation at a range of wavelengths depending on its atomic structure. The human eye can perceive the wavelength range of energy, which is called the "wavelength of the visible region." Nevertheless, the radiation emitted in the region of the infrared wavelength cannot be seen by humans [16].

Table 2.1 summarizes the range of major spectral wavelengths for the solar radiation reaching to the Earth's surface, and Figure 2.1 compares solar radiation at sea level, directly with the extraterrestrial (sunlight at the top of the atmosphere) solar irradiation and blackbody spectrum.

**Table 2.1** Major Spectral Regions and the range of wavelengths

<b>Spectral regions</b>	<b>The range of wavelengths</b>	<b>Percentage</b>
ULTRAVIOLET-A and B	around 380 nm and 315 nm	~7 %
VISIBLE	380 to 700 nm	47 %
INFRARED	>700 nm	46 %

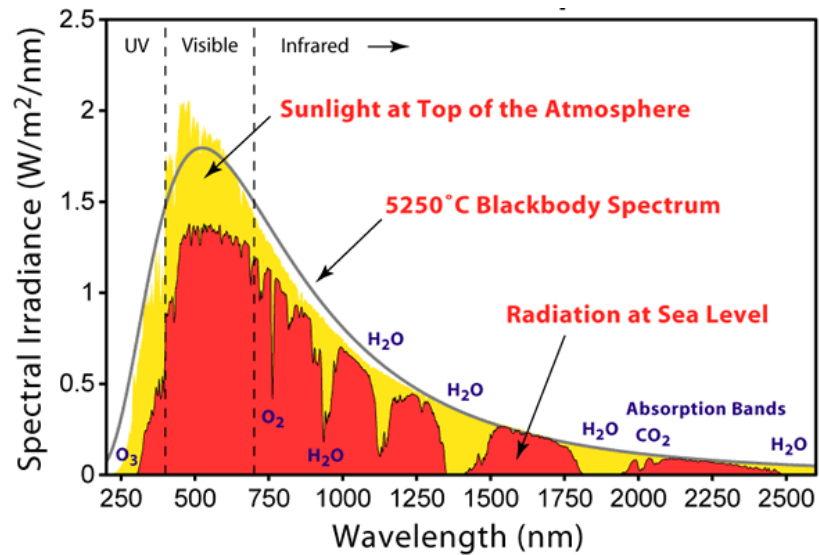


Figure 2.1 Solar spectrum [24]

As seen in Figure 2.1, the total energy of the Sun is in three main spectral ranges which are 7% ultraviolet (UV) radiation, 47% visible radiation and 46% infrared (heat) radiation.

### 2.2.2 Solar Constant

Total solar radiation in all wavelengths striking on a unit area perpendicular to the Sun's rays in unit time, at the top of the Earth's atmosphere, and at the mean Sun-Earth distance is called the solar constant ( $G_{SC}$ ). Its value is averaged at  $1367 \text{ W/m}^2$ . This value is adopted by WMO (World Meteorological Organization [25]) using the results of various measurements. Details are given in the reference Duffie and Beckman [12]. The solar radiation for unit area is determined by the angle between the Sun's rays and the normal to the Earth's surface at any selected point. However, this angle varies depending on time of the day and latitude of location, as well as seasons due to the elliptical orbit of the Earth. That is, all of these variables depend on the distance variation between Sun-and-Earth and rotation of Earth around its axis and around Sun. Sun-Earth distance variation is expressed by the eccentricity correction factor  $\varepsilon$  [26]:

$$\varepsilon = \left[ 1 + 0.033 \cos\left(\frac{360N}{365}\right) \right] \quad (2.1)$$

Here,  $N$  is the number of the day within year. Further investigation was carried out by Iqbal [27] to promote higher accuracy of eccentricity correction as:

$$\varepsilon = \left( \frac{R_{ES}}{\bar{R}_{ES}} \right)^2 \cong 1.00011 + 0.034221 \cos B + 0.00128 \sin B + 0.000719 \cos 2B + 0.000077 \sin 2B \quad (2.2)$$

where  $R_{ES}$  is the actual Sun-Earth distance as shown in Fig. 2.2,  $\bar{R}_{ES}$  is the mean Sun-Earth distance (within one astronomical unit: 1 AU = 1.496 x 10<sup>8</sup> km [27]) and  $B (=2\pi (N-1)/365)$  is the day angle in radians including the number of the day in the year ( $N = 1$  to 365) [23].

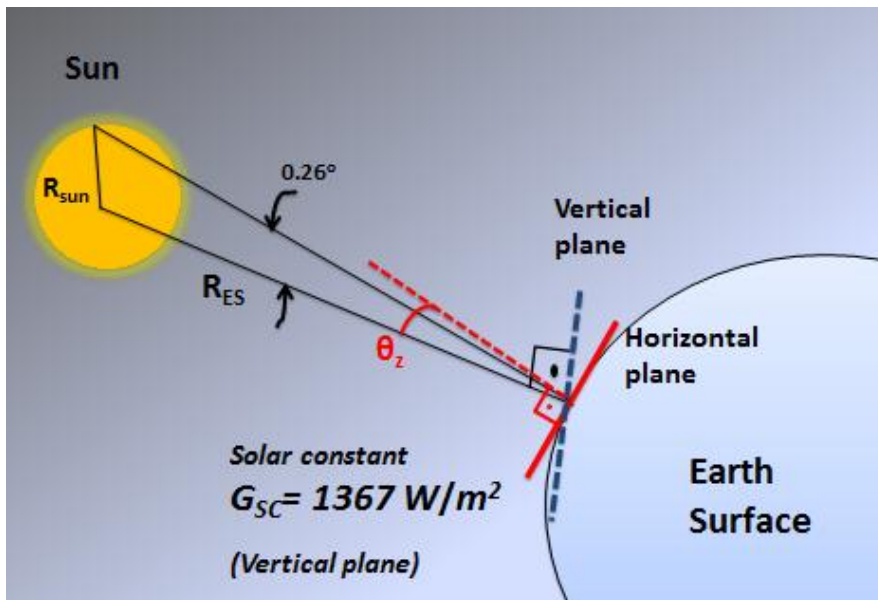


Figure 2.2 Sun –Earth Distance

## 2.2.3 Extraterrestrial Solar Radiation

### 2.2.3.1 Instantaneous Extraterrestrial Solar Irradiance

The instantaneous solar irradiance at the top of the atmosphere on a perpendicular surface at any day is  $G_{0n} = \varepsilon G_{SC}$ . On a horizontal surface, the instantaneous irradiance is:

$$G_0 = \varepsilon G_{SC} \cos \theta_z = G_{SC} \left[ 1 + 0.033 \cos \left( \frac{360N}{365} \right) \right] \cos \theta_z \quad (2.3)$$

where  $N$  is the number of day in the year and  $\theta_z$  is the zenith angle as shown in Fig. 2.4, and the zenith angle will be given later.

In the unit time period, actual solar irradiance on a unit receiving surface depends on the angle between the Sun rays and the normal to the Earth's surfaces. If the receiving surface is inclined, the irradiance should be multiplied by  $\cos \theta$ , which is cosine of the angle of incidence, instead of  $\cos \theta_z$  as is given in Fig. 2.3.

$$G_T = G_n \cos \theta, \quad (2.4)$$

where  $G_n$  is the irradiance on a receiving surface normal to the direct sunlight,  $G_T$  is the irradiance actually received by the sloped surface. These variables are presented in detail in the references Duffie and Beckman [12], Robinson [28], and Fisk and Anderson [29].

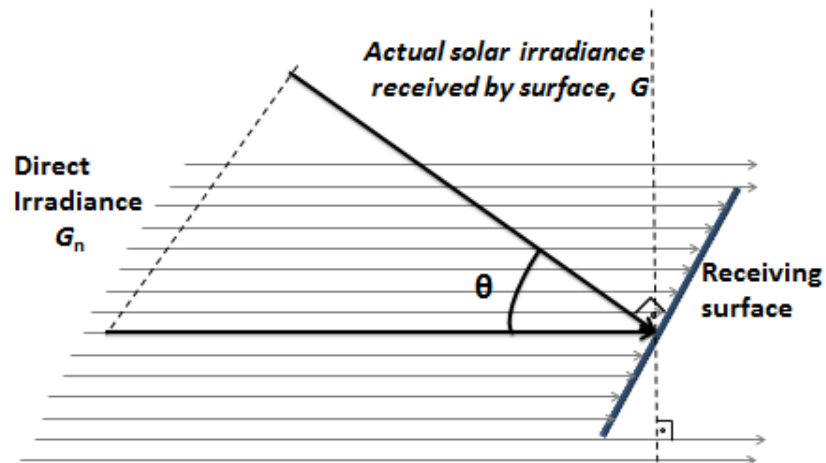


**Figure 2.3** Angle of incidence.

The angle of incidence has to be determined for the calculation of the irradiance received at the tilted surface, taking into account the geometry of the Sun-Earth system and surface orientation [23]. The equation of the angle of incidence on a surface,  $\theta$ , is [12], [30]:

$$\begin{aligned} \cos \theta = & \sin \delta \sin \phi \cos \beta - \sin \delta \cos \phi \sin \beta \cos \gamma \\ & + \cos \delta \cos \phi \cos \beta \cos \omega + \cos \delta \sin \phi \sin \beta \cos \gamma \cos \omega \\ & + \cos \delta \sin \beta \sin \gamma \sin \omega \end{aligned} \quad (2.5)$$

where  $\phi$  is the latitude of the location ( $-90^\circ \leq \phi \leq 90^\circ$ ),  $\delta$  is the declination angle ( $-23.45^\circ \leq \delta \leq 23.45^\circ$ ; its computation equation will be given later),  $\gamma$  is the surface azimuth angle ( $-180^\circ \leq \gamma \leq 180^\circ$ ),  $\omega$  is the hour angle ( $15^\circ$  per hour; morning negative, afternoon positive) and  $\beta$  is the slope angle ( $0^\circ \leq \beta \leq 180^\circ$ ) between the receiving surface (tilted) and the horizontal surface.  $\beta$  equals to  $0^\circ$  for a horizontal plane but equals to  $90^\circ$  for a vertical plane [12].

Therefore, the slope angle  $\beta$  is taken to be zero for a horizontal surface, then  $\cos \theta_z$  can be obtained from  $\cos \theta$  in Eqn. (2.5) by letting  $\beta=0$ . That is,

$$\cos \theta_z = \cos \phi \cos \delta \cos \omega + \sin \phi \sin \delta \quad (2.6)$$

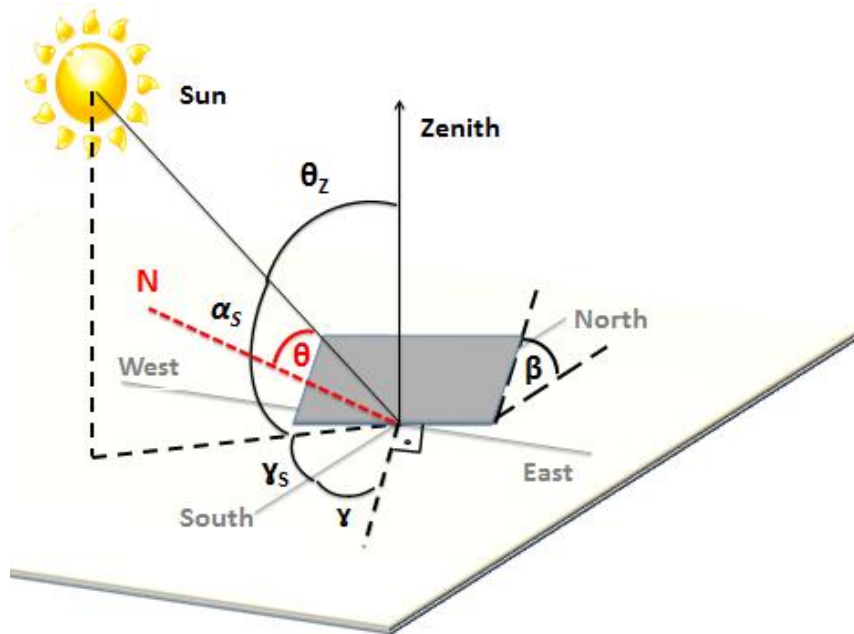


**Figure 2.4** Sun position with zenith angle  $\theta_z$ , surface azimuth angle  $\gamma$ , solar azimuth angle  $\gamma_s$ , solar altitude angle  $\alpha_s$ , and  $\beta$  slope for a receiving tilted surface, and N is surface normal.



Following are the definitions of all related angles which are directly taken from Duffie and Beckman [12]. Fig. 2.4 can be used for the angles.

- *Latitude,  $\phi$* , the angular location north or south of the equator, north positive and south negative.
- *Zenith angle,  $\theta_z$* , the angle between the vertical plane and the direction of sunlight, in other words, the angle of incidence of direct irradiance on a horizontal receiving surface.
- *Surface azimuth angle,  $\gamma$* , the deviation of the projection on a horizontal plane of the normal to the surface from the local meridian.
- *Solar azimuth angle,  $\gamma_s$* , the angular displacement from south of the projection of direct irradiation on the horizontal plane.
- *Solar altitude angle,  $\alpha_s$* , the angle between the horizontal and the direction of sunlight, that is, the complement of the zenith angle.
- *Slope for a receiving tilted surface,  $\beta$* , the angle between the plane of the surface in question and a horizontal surface.
- *Hour angle,  $\omega$* , the angular displacements of the Sun east or west of the local meridian due to rotation of the Earth on its axis at  $15^\circ$  per hour.
- *Declination,  $\delta$* , the angular position of the Sun at solar noon (i.e., when the Sun is on the local meridian) with respect to the plane of the equator, north positive, south negative. The definition of the declination will be given later in Eqn. (2.9)."

### 2.2.3.2 Hourly Extraterrestrial Solar Irradiation on a Horizontal Surface

The equation for extraterrestrial radiation on horizontal surfaces can be calculated for different time periods, i.e., an hour, a day, a month, and so forth. In this section, the integrated value of the instantaneous extraterrestrial solar irradiance over all wavelengths is used as the starting value ( $G_{SC}$ ).

In order to find the hourly extraterrestrial solar irradiation ( $I_0$ ) on a horizontal surface for a period lasting an hour, Eqn. (2.3) must be integrated over a period between angles  $\omega_1$  and  $\omega_2$  (where  $\omega_2 > \omega_1$ ). Thus, using in Eqn. (2.3), we can find that this integral gives:

$$I_0 = \frac{12 \times 3600}{\pi} G_{SC} \left[ 1 + 0.033 \cos \left( \frac{360N}{365} \right) \right] x \left[ \cos \phi \cos \delta (\sin \omega_2 - \sin \omega_1) + \frac{\pi(\omega_2 - \omega_1)}{180} \sin \phi \sin \delta \right] . \quad (2.7)$$

The limits of  $\omega_1$  and  $\omega_2$  are hour angles at the beginning and end of the hourly intervals. The unit is usually given in joule per square meter per hour (J/m<sup>2</sup>-hour) [12].

### 2.2.3.3 Daily Extraterrestrial Solar Irradiation on a Horizontal Surface

The daily extraterrestrial solar irradiation on a horizontal surface ( $H_0$ ) is obtained by integrating Eqn. (2.3) over the period from sunrise to sunset. The unit of it is joule per square meter per day (J/m<sup>2</sup>-day; due to its large daily value MJ/m<sup>2</sup>-day is preferred). Thus, the daily extraterrestrial solar irradiation  $H_0$  can be defined by taking into consideration these basic parameters and after integration the equation takes the form [12], [22]:

$$H_0 = \frac{24 \times 3600}{\pi} G_{SC} \left[ 1 + 0.033 \cos \left( \frac{360N}{365} \right) \right] x \left[ \cos \phi \cos \delta \sin \omega_s + \frac{2\pi\omega_s}{360} \sin \phi \sin \delta \right] . \quad (2.8)$$

where  $\omega_s$  is the sunset hour angle. The declination angle and the sunset hour angle are defined as follows:

$$\delta = 23.45 \sin \left[ 360 \frac{284 + N}{365} \right] , \quad (2.9)$$

and

$$\omega_s = \arccos(-\tan \phi \tan \delta) . \quad (2.10)$$

The daily extraterrestrial solar irradiation on a horizontal surface,  $H_0$ , as a calculated quantity was used in our study to normalize global solar irradiation on a horizontal surface (in Angström relation, which will be described later in Chapter 3).

## 2.2.4 Solar Time

Daily variations of solar radiation are based on the solar time and the length of the day which changes due to the effects of the angular motion of the Sun [12], [23]. In contrast to standard time, solar time is related to the Sun-angle relationships. It is not based on longitudes or the standard meridian. Solar time is defined as a solar day which is the time period between two sequential transitions of the Sun with the local meridian. This time period takes the mean daylength as 24 hours, but it changes from day to day due to the effect of the changing orbital speed of the Earth around the Sun as  $\pm 15$  minute as seen in Fig. 2.5. It is called the equation of time, and the calculation procedures of this can be found in the reference Duffie and Beckman [12].

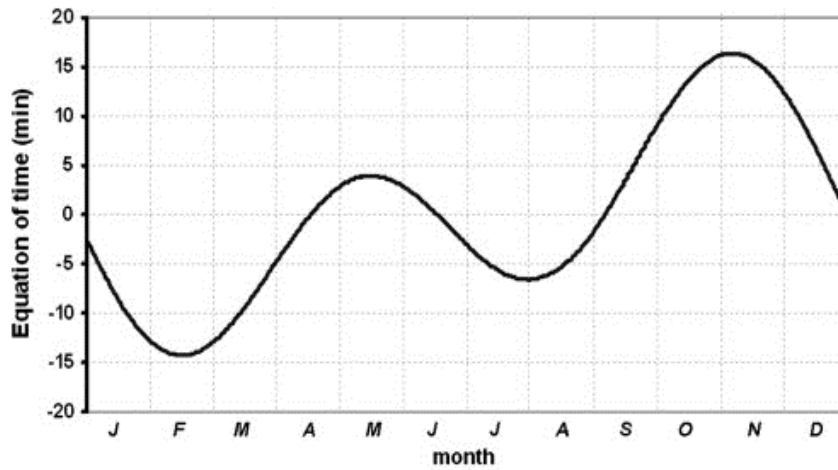


**Figure 2.5** The equation of time in minutes, as a function of time of year [12], [31].

The equation of time is calculated with the Eqn. (2.11) in minutes [26], [27].

$$E = 229.2(0.000075 + 0.001868 \cos B - 0.032077 \sin B - 0.014615 \cos 2B - 0.04089 \sin 2B) \quad (2.11)$$

where  $B (=2\pi (N-1)/365)$  is the day angle in radians including the number of the day in the year ( $N = 1$  to 365). For the determination of solar time the following expression is used:

$$\text{Solar Time} - \text{Standard Time} = 4 (L_{\text{standard}} - L_{\text{local}}) + E \quad (2.12)$$

where  $E$  described above,  $L_{standard}$  is the standard meridian for the local time of the location and  $L_{local}$  is the longitude of the selected location in degrees.

### 2.2.5 The Length of the Day

The most popular method (the Angström method) for estimating global solar irradiation on a horizontal surface uses daily global to daily extraterrestrial irradiation ratio and the fraction of bright sunshine duration (i.e, fraction of clear sky period in a day)  $s/S$ . The length of the day is the maximum possible duration between sunrise and sunset for a day, and it can be calculated in hours using sunset hour angle as [12]:

$$S = \frac{2}{15} \arccos(-\tan \phi \tan \delta) \quad (2.13)$$

During the low altitude of the Sun, which means that the solar zenith angle is less than  $5^\circ$  or larger than  $85^\circ$ , commonly used sunshine recorders to measure bright sunshine hour  $s$  usually do not operate properly. In order to reduce the effect of the low altitude of the Sun, Hay [21] proposed a correction with respect to the zenith angle by means of a modified daylength  $S_0$  (daylength for zenith angle  $\leq 85^\circ$ ):

$$S_0 = \frac{\arccos\left[\frac{\cos 85^\circ - \sin \phi \sin \delta}{\cos \phi \cos \delta}\right]}{7.5} \quad (2.14)$$

To estimate global solar irradiation on a horizontal surface,  $s/S$  and  $s/S_0$  fractions ( $s$  values obtained from sunshine recorders,  $S$  and  $S_0$  calculated by Eqns. (2.13) and (2.14), respectively) are used in classical models and our proposed estimation models. All these mentioned quantities and the relevant discussions will be given next chapter.

## 2.3 The Transmission of Energy Through the Atmosphere

It is known that the electromagnetic waves from the Sun carry solar radiant energy (radiation) at a tremendous rate. These enormous amounts of solar energy are influenced by a number of atmospheric and exoatmospheric factors [30].

As mentioned earlier in this chapter, global solar irradiation on the surface varies depending on such factors as astronomical factors (the solar spectrum, the solar constant, Sun-Earth

distance variation, declination of the Sun, the hour angle), geographical factors (latitude, altitude), and geometrical factors (azimuth, tilt and surface azimuth angles.) In addition to these, solar radiation falling on the Earth's surface is influenced by physical (absorption and scattering in the atmosphere) and meteorological (cloudiness and albedo) factors [28].

Due to the physical and meteorological factors, it is possible to split solar irradiation into parts, which are given as:

- Absorption by water vapor, ozone and carbon di-oxide; and
- Scattering by air molecules, water vapor and dust [27].

The atmosphere of the Earth includes various amounts of different gaseous formations and concentrations. These gases are highly variable and non-homogeneous. The normal composition of dry air at ground level can be seen in Table 2.2.

Actually, the atmosphere air has fluctuating density and it varies with the geographical location, season and elevation [32]. The most frequently encountered gas is nitrogen (78.1%) which absorbs high radiant energy in a number of overlapping bands less than 100nm. Then, solar energy with a wavelength range of 100nm and 210nm is absorbed by atomic oxygen (20.9%) in the upper atmosphere. UV radiation is significantly filtered out by the ozone layer in the stratosphere. There is insufficient absorption of radiant energy by the atmosphere at wavelengths longer than 350nm (see Fig. 2.1) [12], [33].

Water vapor in the atmosphere is variable, and it is impressionable with temperature and winds. The main source of water vapor is from the oceans and inner seas. The effect of the water vapor in atmosphere has led to both scattering and absorption. At wavelengths in the infrared bands of 700-2500nm, it is a major absorber; however, there is very little water vapor absorption at the wavelengths higher than 2500nm. The scattering of water vapor is based on perceptible water and is inversely proportional to the 4<sup>th</sup> power of the wavelength [12], [34].

All plants, industrial waste, gas emission, and also de-composite forms of life in the sea water are the main sources of carbon dioxide in the atmosphere. Carbon dioxide is another strong absorber gas in the atmosphere, absorption is ranging between 1400nm and 1800nm, and above 2600nm [12], [16], [28].

Incoming solar energy passes through the atmosphere, which is an interaction process by air molecules, water vapor, and dust in all directions. This interaction process is called the scattering of the incident radiation, and it increases with the size of the particles. Without the

transformation of energy, there are only changes in the spatial distribution of the incident radiation, so the scattering is an important factor of the attenuation of radiation by the atmosphere [12], [28], [32–34].

**Table 2.2** The concentration of gases constituting dry air at ground level [33],[32].

Gas	Chemical Symbol	Concentrations (%)
Nitrogen	N <sub>2</sub>	78.1%
Oxygen	O <sub>2</sub>	20.9%
Argon	Ar	0.93%
Carbon dioxide	CO <sub>2</sub>	0.035%
Neon	Ne	0.0018%
Helium	He	0.00050%
Methane	CH <sub>4</sub>	0.00017%
Krypton	Kr	0.00011%
Hydrogen	H <sub>2</sub>	0.00005%
Ozone	O <sub>3</sub>	0.000001-0.000004%

Most of the incoming wavelength of the solar radiation is scattered by atmospheric aerosols, which are solid particles or liquid substances. Moreover, air molecules also scatter the solar radiation according to the theory of Rayleigh and Mie scattering with the size of the particles present in the atmosphere. As results of the scattering by air molecules in all directions, the sky seems blue with shorter wavelengths [12], [28], [32], [35], [36]. Dust and water particle, which are of larger sizes and which depends on the seasons, scatter the incoming radiation. Besides, most common models to estimate the global solar irradiation uses these scattering effects for the turbidity calculations [12], [24], [27], [28], [30], [32], [33], [37]. After absorption and scattering by the different components of the atmosphere, the range of the main wavelength of radiant energy reaches the Earth's surface between 300 to 2500nm. The effects of all gasses and atomic particles scattering and absorption on the spectral distribution of solar irradiance are illustrated in Fig. 2.1 [37].

It is well-known that nature has a balance between the energy that reaches the Earth from the Sun and the energy that is emitted to space. This energy balance is demonstrated roughly in Fig. 2.6.

Consequently, most of the incoming solar energy from the Sun is absorbed by the surface (land and oceans) and the atmosphere (51% and 19%, respectively.) The rest of the incoming solar radiation is reflected directly back into space by the atmosphere (6%), clouds (20%), and some is reflected by the Earth's surface (4%) [9], [12], [27], [32], [33], [37]. Earth is heated and it re-radiates the energy that it receives from the Sun in longer wavelengths. The long-term knowledge of the exchange of this radiant energy between the Sun, Earth, and space is very important especially for climate change studies [16].

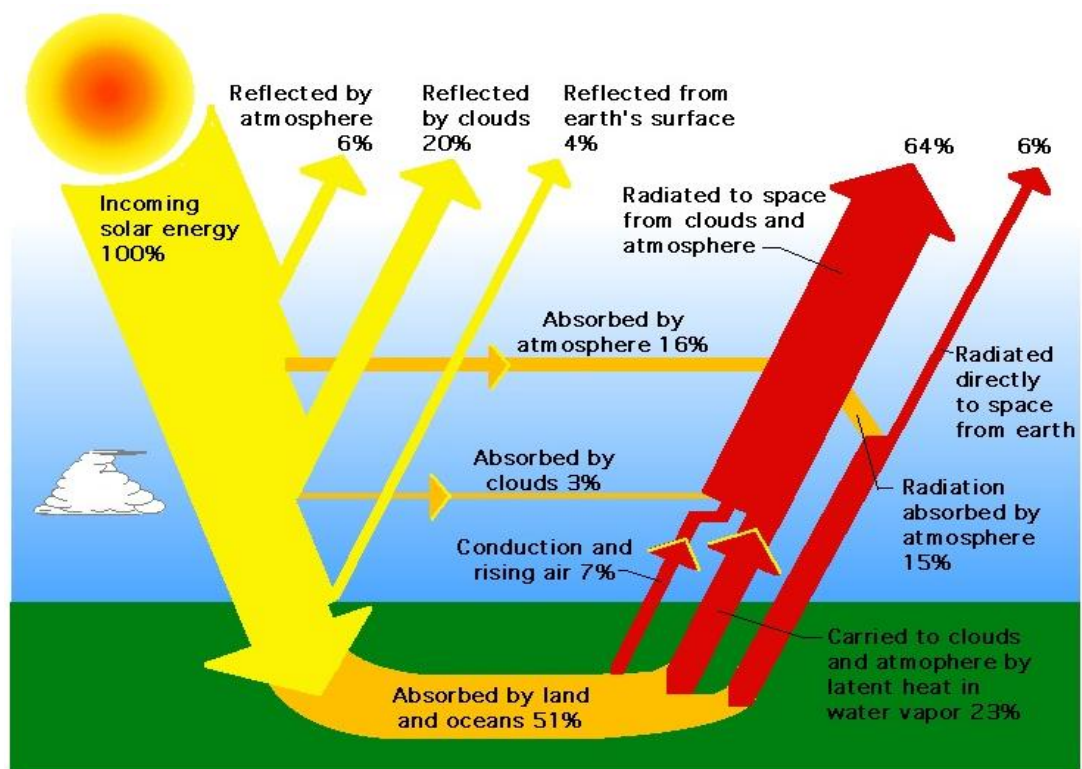


**Figure 2.6** The schematic representation of solar energy in the atmosphere [37].

### 2.3.1 Air Mass

For the analyses of energy transmission process in the atmosphere, it is essential to know total mass of absorption and scattering substances on the path of radiative transfer. This total mass is called air mass, and it is important to know the amount of atmosphere sunlight must pass through before it reaches the Earth. Paltridge and Platt [38] developed the relative air mass ( $m$ ) by taking into account the effect of zenith angle. It can be defined using  $\cos \theta_z$  only for a plane parallel atmosphere:

$$m = \frac{1}{\cos \theta_z} \quad . \quad (2.15)$$

For the calculations of solar energy, commonly used air masses, and their corresponding zenith angles are given in Fig. 2.7. If the Sun is in a perpendicular position (at the zenith angle  $\theta_z = 0^\circ$ ), the path that sunlight reaches the Earth at sea level is called relative air mass 1. At sea level, when the zenith angle is  $\theta_z = 60^\circ$ , it is called relative air mass 2, when the Sun is at the zenith angle  $\theta_z = 70.5^\circ$ , it is called relative air mass 3 in general. The relative air mass 0 is defined as outside of the atmosphere (the extraterrestrial irradiation) because there is no air in space [23], [28], [29].

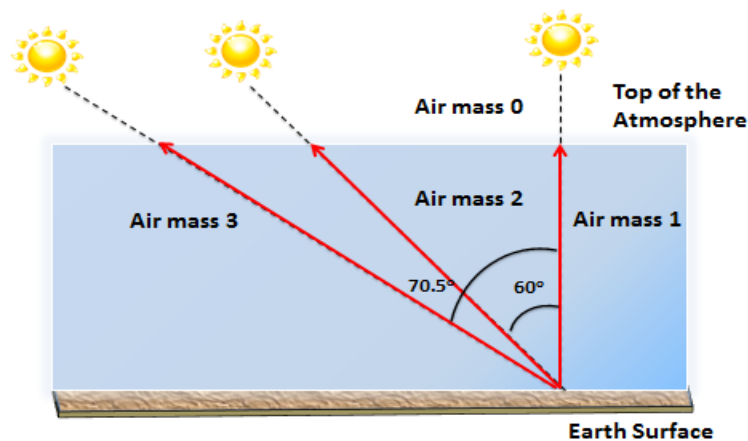


**Figure 2.7** Relative air masses with the convenient zenith angles in a plane parallel atmosphere [23].



In 1989, a detailed study for the relative air mass  $m$  is made by Kasten and Young [39]. It was obtained as:

$$m = \frac{1 - z / 10000}{\cos \theta_z + 0,50572(96,07995 - \theta_z)^{-1,6364}} \quad , \quad (2.16)$$

where  $z$  is the heigth of the site (in meters). To calculate  $G_{clearsky}$  , which will be described in section 3.5.2 this relation is used.

### 2.3.2 Clearness Index

All calculations and definitions to the solar irradiation so far apply in the standard spectrum for clear (cloudless) sky. However, most of the incoming irradiation is reflected directly back into space by clouds (20%), as mentioned in section 2.3. The ratio of the transmitted solar irradiation is defined as the clearness index, classified in three time scales; hourly ( $k$ ), daily ( $K$ ) and monthly average ( $\bar{K}$ ) clearness index.

The hourly clearness index ( $k$ ) is the fraction of the hourly global irradiation on a horizontal surface reaching the Earth ( $I$ ), to the hourly extraterrestrial irradiation on a horizontal surface ( $I_0$ ) (during a period lasting an hour).

$$k = \frac{I}{I_0} \quad , \quad (2.17)$$

and the daily clearness index ( $K$ ) is given by

$$K = \frac{H}{H_0} \quad , \quad (2.18)$$

where  $H$  is the daily global solar irradiation on a horizontal surface and  $H_0$  is the daily solar extraterrestrial irradiation on a horizontal surface. Then, the monthly average daily clearness index  $\bar{K}$  , which usually varies between about 0.3 and 0.8, is given by

$$\bar{K} = \frac{\bar{H}}{\bar{H}_0} \quad . \quad (2.19)$$

Clearness index gives a dimensionless fraction of the solar irradiation that is reaching the Earth surface to that hitting outside the atmosphere [12], [23], [40].

### 2.3.3 Clear sky Index

The hourly clear sky index,  $k^*$ , is similar to the hourly clearness index ( $k$ ) but now, instead of  $I_0$ , calculated values of hourly clear sky irradiation,  $I_{clearsky}$  reaching to the Earth on a clear day is used [41], [42]. It is defined as:

$$k^* = \frac{I}{I_{clearsky}} \quad (2.20)$$

The calculated values of hourly clear sky irradiation  $I_{clearsky}$  will be defined in Chapter 3. The daily ( $K^*$ ) and monthly ( $\overline{K}^*$ ) clear sky indices are also calculated in the same way. Hence, for clear sky index one should know the solar irradiation reaching the Earth in a clear day. It can be either measured or calculated.

## 2.4 Solar Irradiation Measurements

Measurement of solar irradiation for the site of interest is the most accurate way to assess the availability of solar energy reaching the Earth. Many solar irradiation estimation models have been developed by using these measurements. In order to measure solar energy, which comes as global irradiation has two parts: direct and diffuse irradiation and to measure them three types of instruments can be used.

This section will introduce the definitions of various solar irradiations (global, direct, and diffuse solar irradiation) on the Earth's surface and the instruments used to measure the solar irradiation. In addition, the calibrations and errors of these instruments are discussed. Moreover, the measurements of bright sunshine hour with the instruments of Campbell-Stokes type recorders are presented. Atmospheric turbidity ( $T_L$ ) and surface albedo are described briefly.

### 2.4.1 Direct and Diffuse Solar Irradiation

The solar irradiation passes through the atmosphere divided into three main components; beam (direct), diffuse and global solar irradiation. The first component, the beam (direct) solar irradiation, is the energy that is directly reaching the Earth's surface from the Sun

without scattering [22]. Beam solar irradiation is necessary to plan and install solar systems which use concentrating collectors (in water heating, for power and in some PV systems).

Another component gets the name of diffuse solar irradiation which is produced as results of scattering, absorbing, or reflecting due to the air molecules, water vapor, aerosols, and clouds and ground. In a cloudy sky conditions, the values of diffuse solar irradiation may be high, but during clear sky condition it is relatively low [22], [29], [43].

Summation of beam and diffuse components of solar irradiation gives global solar irradiation. Global solar irradiation is the main input for most solar energy applications such as PV-systems, domestic hot water systems, solar power systems etc. [29], [44]. They also carry appreciated information for day lighting design, plant growth, etc. [8]. The total global solar irradiance collected over all the wavelengths on a horizontal surface can be formulated as:

$$G = G_D + G_B \cos \theta_z \quad (2.21)$$

where  $\theta_z$  is the zenith angle  $G_D$  is the instantaneous diffuse irradiation on horizontal surface and  $G_B$  is the instantaneous beam irradiation at normal incidence. As mentioned before, the  $\cos \theta_z$  parameter is used when the receiving surface is not oriented perpendicular to the Sun's rays (see section 2.2.3.1) but instead horizontal. Fig.2.8 shows, as an example, a graphical representation of solar irradiation on a horizontal surface (Global, Beam and Diffuse) for Ankara, Turkey, for the year 2004 in the second day of March.

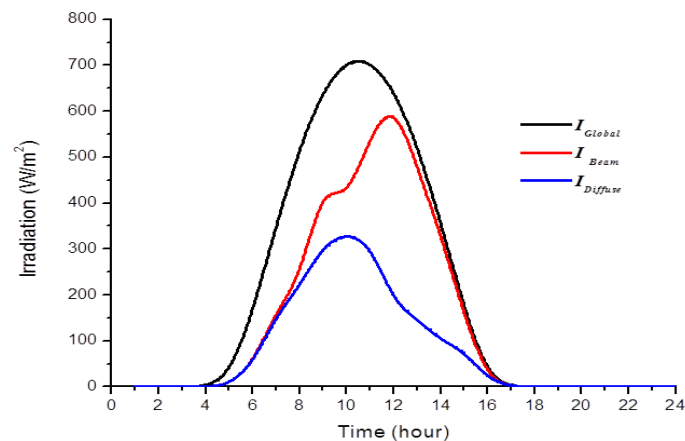


**Figure 2.8** Solar irradiation for Ankara, Turkey for the year 2004, 2<sup>nd</sup> March.

## 2.4.2 Solar Irradiation Detectors

Although solar irradiation data from ground-based detectors have an insufficient spatial density and are often not available for a selected location, the ground measurement data are usually more accurate than the solar irradiation estimations [45]. However, for solar irradiation ground measurements, the accuracies typically are based on calibration and reliability of the detectors. These ground measurements are obtained by basically thermal detectors (pyrheliometer, and pyranometers) [22], [23], [28], [46].

In order to measure direct solar energy, the surface of the beam irradiation detectors should be perpendicular to the incoming irradiation. For this purpose, usually a pyrheliometer mounted on a solar tracker is used. A solar tracker is a collimator tube over the Sun and it follows the Sun continuously [23], [28]. In addition, it has a viewing angle of about  $5^\circ$ , and in this kind of thermal detectors voltage output is directly proportional to the incoming solar irradiation [12], [23], [46]. Such a detector example is given below in Fig. 2.9.

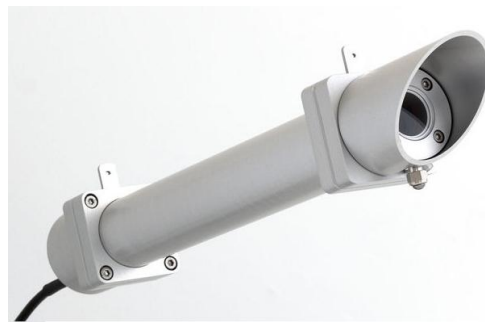


**Figure 2.9** Hukseflux DR01 Type Pyrheliometers [47].

When measuring global solar irradiation, the detectors should be placed to on a horizontal surface in order to measure together, beam and diffuse components of solar energy. Global Solar Irradiation is measured by a pyranometer. It can measure the solar irradiation between approximately 300 to 3000 nm wavelengths spectrum range [12], [22], [23], [28], [46]. The pictural representation corresponding to the parts of the pyranometer is given in Fig. 2.10.

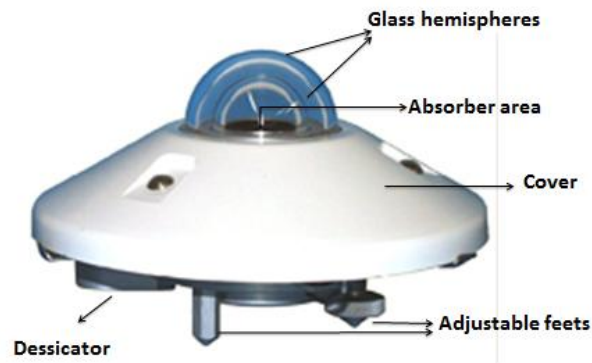


**Figure 2.10** The parts of the pyranometer [48]

In order to measure diffuse solar irradiation for the whole hemisphere, diffuse radiation measurement detectors should have the large view angle ( $180^\circ$ ) and they should be located on a horizontal surface. Diffuse solar irradiation is measured by pyranometers with a shading ring (shadow band) or tracking ball [12], [22], [23], [28], [46]. The combination of a pyranometer and shadow ring or tracker ball offers a wise solution to measure diffuse irradiation. Fig. 2.11 shows these two types of pyranometers.



**Figure 2.11** The tracker ball and shadow ring type pyranometers [47], [49].

Pyranometers should be calibrated regularly, using a pyrliometer or a reference pyranometer. In addition, pyranometers and pyrliometers must correspond to the ISO standard, which is used as a guideline for the selection of detectors [23].

### 2.4.3 Sunshine Duration

Sunshine duration is defined as the number of hours that the Sun is not obstructed by the clouds. In order to measure sunshine duration, two types of detectors are used. Firstly, the classic Campbell-Stokes type sunshine recorder, which is widely used because it is simple and utilizable. Hence, many stations all over the world use this type of sunshine duration recorder. Due to this, long-term and reliable sunshine duration data for at least 100 years are thought to be found all over the world [22], [45], [46], [50], [51]. The main working principle of the classic Campbell-Stokes type sunshine recorder is to focus direct solar irradiation to burn the thin sensitive card bearing a time scale. For this purpose, commonly a solid glass sphere, which is about ten cm in diameter, is used. When the Sun is not obstructed by clouds and intensity of the incoming irradiation is enough to burn, a trail of the Sun is produced on the thin card [28], [46], [50], [51].

The second one is the modern type sunshine duration sensor, which makes use of photo-diodes (special design electronic systems) to measure sunshine duration. According to a report published by WMO (World Meteorological Organization [25]) in 2003, the direct solar radiation per square meter  $120 \text{ W/m}^2$  has been identified as a critical threshold value for this type of sunshine duration recorder. This critical threshold value was obtained from direct solar irradiation measurement comparisons. In addition, it is equal to the value of clear sky solar radiation during times of sunrise and sunset.[46], [50–52]. Fig. 2.12 shows these two types of pyranometers.



**Figure 2.12** The classic Campbell-Stokes type sunshine duration recorder and electronic type sunshine duration sensor [53], [54].

Sunshine duration data are also relevant for the most common estimation model Angström (described in Chapter 3), which includes the global solar irradiation measurements.

#### 2.4.4 Atmospheric Turbidity

Knowledge of the Linke turbidity factor,  $T_L$ , is of utmost importance for the calculation of beam and diffuse solar irradiation in a determined locality, when the HELIOSAT calculation (in Chapter 3) for solar radiation on clear days is adopted. This method used the Linke turbidity for the determination of aerosol and water vapor atmospheric content, in the calculation of the clear sky irradiation. This clear sky irradiation is then used to produce ground level irradiation under any sky condition, at any time of the year.

HELIOSAT clear sky solar irradiation computation model consists of direct and diffuse irradiation parts. The direct irradiation is described by Page [55], and the diffuse irradiation is developed by Dumortier [56] under cloudless skies. Both of them use the Linke Turbidity  $T_L$ , Sun elevation, and the altitude of the site as parameters. Atmospheric extinction, which can be obtained from the relation given by Bourges [57], is described with Linke Turbidity  $T_L$ .

To calculate clear sky irradiation, they first calculated direct and diffuse solar irradiation together with the eccentricity correction  $\varepsilon$ , the Linke turbidity factor for air mass 2 ( $T_L(2)$ ), the Rayleigh optical thickness of a dry and clean atmosphere ( $\delta_R(m)$ ), where  $m$  is the air mass. In an ideal Rayleigh atmosphere,  $T_L = 1$ . The closest to this ideal value ( $T_L(2)$ , at a relative optical air mass equal to 2) is achieved in clear, cold air at high latitudes [58].  $\varepsilon$  is given in Eqn. (2.2). The Linke turbidity factor can be obtained from measurements of direct normal irradiation and it has the problem of being dependent on the air mass,  $m$ . The relative air mass  $m$  is given in detail in section 2.3.1.

The Rayleigh optical thickness  $\delta_R$  is taken from Kasten [59].

$$\delta_R = \begin{cases} \frac{I}{6.6296 + 1.7513m - 1.1202m^2 + 0.0065m^3 - 0.00013m^4}, m < 20 \\ \frac{I}{10.4 + 0.718m}, m > 20 \end{cases} \quad (2.22)$$

For the atmospheric turbidity information, a climatological model is applied. To account for the annual variation of the turbidity, a relation of Bourges [57] is used:

$$T_L(2) = T_o + u \cos\left(\frac{2\pi J}{365}\right) + v \sin\left(\frac{2\pi j}{365}\right) \quad (2.23)$$

$T_o$ ,  $u$  and  $v$  are site specific parameters and a map specifying the parameters for Europe has been prepared in an EU-funded Satel-Light project [60].

Since the experimental determination of the  $T_L$  factor is rather complex, owing to the need for many measurements of beam solar radiation on clear days, setting up a general and reliable calculation method appears to be especially useful.

In light of the aforementioned information, HELIOSAT clear sky model (in section 3.6.2) is computed as the sum of its direct and diffuse components. Direct component of the normal hourly beam solar irradiation ( $W/m^2$ ) is given by Page [55] as mentioned and the quantities  $\delta_R$  and  $m$  are calculated at the center of the hour (at solar noon) [61]. By solving the hourly beam solar irradiation with respect to  $T_L$  and using the solar constant  $G_{SC}$ ,  $T_L$  is obtained as:

$$T_L = \frac{-\ln(I_{dn;clear}) + \ln(G_{SC}\varepsilon)}{0.8662\delta_R m} \quad (2.24)$$



By means of Eqn. (2.24) the hourly values of the Linke turbidity factor can be calculated in every locality in which global daily irradiation  $H$  on the horizontal plane is known. Since reference is usually made to average daily turbidity values, once the hourly values of  $T_L$  are obtained, average daily values are obtained through the following equation:

$$T_L = \frac{\sum_{i=t}^t T_{L_i}}{t} \quad (2.25)$$

where  $T_{L_i}$  is the average hourly values and  $t$  is the number of hours between sunrise and sunset, ignoring those fractions of an hour next to sunrise and sunset [62], [63].

## 2.5 Satellites

In the last two decades, meteorological satellites have been used to obtain reliable, accurate solar resource data and solar irradiation maps. Nowadays, satellite-based solar irradiation estimation provides high spatial and temporal resolution data required for planning and efficient use of solar energy systems. Besides, long term satellite measurements data are available for large regions of the Earth [64]. Fig. 2.13 illustrates the coverage ranges of some of the satellites.

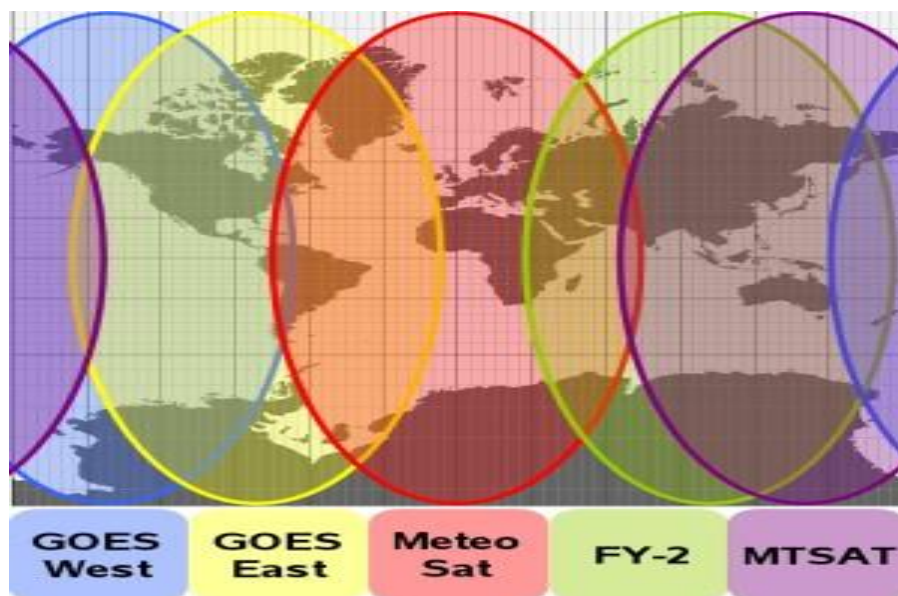
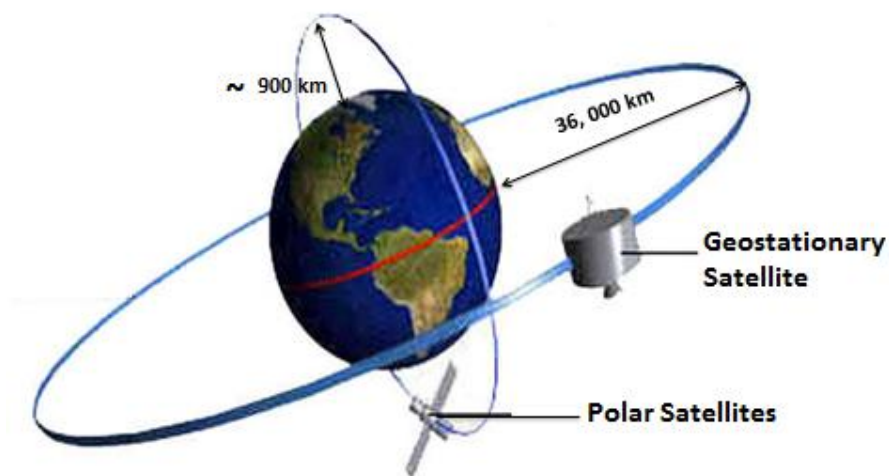


Figure 2.13 Areas of the Earth Covered by each of the Satellites [65].

### 2.5.1 Meteorological Satellite Orbits

Depending on the measurement objectives, there are two types of meteorological satellite; polar and geostationary orbits. Polar- satellites, rotates in a constant circular orbit about 900 km away from the Earth's surface, travel from pole to pole. The polar orbiters fly lower and nearly perpendicular to geostationary orbits [66]. Such a satellite can make one full orbit in approximately a 102-minute period around the Earth. In other words, it makes a total of 14 tours a day. As the polar orbit is lower than the geostationary satellites' orbits, the polar satellite images provide detailed information about the cloud structure [67]. They are useful for the estimation and determination of sea surface temperatures, dust storms, and fire/smoke on the Earth's surface. On the other hand, geostationary satellites which are rotating around the Earth at the same speed as the Earth are used for modeling of solar irradiation. They orbit at about 36000 km, and especially the new generation satellites, can offer a temporal resolution of up to 15 minutes and a spatial resolution of up to 1 km [66]. The geostationary satellite images are not useful for the applications that need great details, because the satellite is too far from the Earth. Fig. 2.14 presents the schematic representation of meteorological satellite orbits with their distances.



**Figure 2.14** Meteorological satellites orbit and their distances [68].

## 2.5.2 Meteosat First and Second Generation Satellites

The Meteosat Satellites (MeteoSat), which are operated by EUMETSAT, are also a geostationary satellite at the same position as its predecessors, 36,000 km above the Earth. It can be seen that they, at position nearly 0°-Longitude, views basically Europe, Africa, Asia, including the Middle East and the North Atlantic [68–70].

### 2.5.2.1 Meteosat First Generation Satellites (MFG)

In 1977, Meteosat-1, which is the first European meteorological satellite, was launched by the European Space Agency (ESA). Since 1983, the EUMETSAT programme has been in operation. From 1977 to 2004, Meteosat-1 to Meteosat-7, there are seven Meteosat first generation satellites in total. They provide continuous meteorological images from space, basically for the researchers involved in climatic studies. MFG satellites include three main channels, and their images were taken every 30 minutes. Table 2.3 shows the main channels of first generation satellites, and the range of the bands with their resolutions.

**Table 2.3** MFG satellites channels with their resolutions [66].

Channels	The range of the channel	Resolution
Visible (VIS)	0,45 - 1,0 $\mu\text{m}$	2,5 km
Thermal Infrared (TIR)	10,5 - 12,5 $\mu\text{m}$	5 km
Water vapour (WV)	5,7 - 7,1 $\mu\text{m}$	5 km

An advantage of the images taken from MFG geostationary satellites was their large area coverage with good spatial resolution and with sufficient temporal resolution [61], [69], [70]. The images obtained from the Meteosat First Generation satellites, weather forecasts and cloud motions and climatic parameters such as solar irradiation can be obtained. Therefore, it is very important to increase the accuracy of such estimations. For this aim, long term, and relatively accurate surface measurements of some climatic studies can be very useful. The last satellite of this family was Meteosat-7, which was launched on 2 September 1997, and it remained operational up to the year 2004 [66].

### 2.5.2.2 Meteosat Second Generation Satellites (MSG)

The second generation geostationary satellites (MSG) are composed of four satellite series Meteosat-8 to Meteosat-11 that will operate consecutively until 2020. Meteosat-8 (MSG-1) was launched in 2002 with the addition of new channels for weather and climate monitoring. It provided an active scanning of Europe, producing images every 5 minutes. Then, Meteosat-9 (MSG-2) was launched in 2005. It provides with imagery for Europe and Africa with the frequency up to 15 minutes. In 2011, Meteosat-7, -8 and -9 are all working. After the seven years, Meteosat-10 (MSG-3) was successfully sent into space at July 2012. The launch of MSG-4 is planned for early 2015. [66].

The main differences between MFG and MSG satellites are channels and capacity. The second generation geostationary satellites have more spectral channels (12 in total) than the first generation satellites. The channel capacities, and ability to transmit information at twice the speed of its predecessor, provide improved applications for users. For the high-resolution visible channel, the image resolution is 1 km, and for the other channels from 2.5 km. The spectral channels of the MSG satellites with their ranges are tabulated in Table 2.4.

**Table 2.4** MSG satellites channels with their spectral ranges [66].

Numbers	Channels	The range of the channel
1	VIS 0,6	0,56 - 0,71 $\mu\text{m}$
2	VIS 0,8	0,74 - 0,88 $\mu\text{m}$
3	IR 1,6	1,50 - 1,78 $\mu\text{m}$
4	IR 3,9	3,48 - 4,36 $\mu\text{m}$
5	IR 8,7	8,30 - 9,10 $\mu\text{m}$
6	IR 10,8	9,80 - 11,80 $\mu\text{m}$
7	IR 12,0	11,00 - 13,00 $\mu\text{m}$
8	WV 6,2	5,35 - 7,15 $\mu\text{m}$
9	WV 7,3	6,85 - 7,85 $\mu\text{m}$
10	IR 9,7	9,38 - 9,94 $\mu\text{m}$
11	IR 13,4	12,40 - 14,40 $\mu\text{m}$
12	High Res VIS, 1km: HRV	0,5 - 0,9 $\mu\text{m}$

These spectral channels will improve the effective observation capacity of second generation satellites more about the atmosphere, and they will be useful for a wider variety of environmental purposes [66–68], [71], [72]. And also, the long-term reliable and comprehensive data from MSG satellites will improve the estimation of serious weather events such as storms, snow, hurricanes, and fogs.

In this thesis, we used the images obtained by Meteosat second generation satellite visible spectral range images from the European Organization for the Exploitation of Meteorological Satellites (EUMETSAT). After 2020, third generation geostationary satellites (MTG) are planned to be launched. The models developed in the present study are adaptable for the cloud index data that will be derived from next generation (MTG) satellite images.

## **2.6 Modeling Comparison and Validation Techniques**

The accuracy of different models is compared using various techniques, but only two techniques will be presented here. The first one is the standard error analyses which widely use the relative root mean square error (rRMSE) and the relative mean bias error (rMBE). The second method is the calculation of the cumulative distribution of the difference between the measured and calculated global solar irradiation  $H$  value and its absolute value. The statistical procedures of calculation and detailed discussions can be found in the literature, some of which are given here.

### **2.6.1 Standard Error Analyses**

To identify the performance of solar radiation estimation models, standard error analyses are carried out. Mean bias error (MBE) and root mean square error (RMSE) are the ones that are applied most commonly in comparing the models. These analyses have been applied for years by many researchers, such as Bevington [73], Davies et al. [74], and Perez et al. [75].

The validation of daily models which calculate irradiation should start by the daily differences ( $\omega_e$ ) and the average of the daily differences which is called the mean bias error (MBE). The differences ( $\omega_e$ ) and mean bias errors (MBE) are defined as:

$$\omega_e = H_{ic} - H_{im} \quad (2.26)$$

and,

$$MBE = \left( \sum_1^d (H_{ic} - H_{im}) \right) / d \quad (2.27)$$

where  $d$  is the number of data pairs,  $H_{ic}$  is the  $i$ th data of estimated irradiation from models, and  $H_{im}$  is the  $i$ th data of measured irradiation from ground. The large positive value of MBE means an overestimation of the estimated values while a negative MBE gives an underestimation of the model. Information on deviations in long term average performance can be directly expressed by MBE [76–79]. In other words, this summation shows us the consideration of the accuracy of the long term predictions of the correlations.

The sum of the squares of the differences is considered as the root mean square error (RMSE) values and it is calculated as:

$$RMSE = \left\{ \left( \sum_1^d (H_{ic} - H_{im})^2 \right) / d \right\}^{1/2} \quad (2.28)$$

The variables of this equation are as previously defined. RMSE provides information on the short term prediction quality of estimation. That is, it may have a high value even when a single measurement has higher differences from that of the calculated irradiation.

The relative mean bias error (rMBE) and the relative root mean square error (rRMSE) are in the form of:

$$rMBE = \left[ \left( \sum_1^d (H_{ic} - H_{im}) \right) / d \right] / H_m \quad (2.29)$$

and,

$$rRMSE = \left[ \left\{ \left( \sum_1^d (H_{ic} - H_{im})^2 \right) / d \right\}^{1/2} \right] / H_m \quad (2.30)$$

where  $H_m$  is the measured values of daily average irradiation on the surface [57].

The goodness of the fit may be also used for the comparison of the models. It shows that the quality of an empirical correlation can be expressed by the regression coefficient  $R^2$  of the regression analysis. The  $R^2$  value, which is an important indicator of the goodness of the fit, should be close to 1.00 for better performance of the models. We used the regression coefficient,  $R^2$ , to test the goodness of the linear relationships obtained by regression analysis between estimated and measured solar irradiation values.

### 2.6.2 Cumulative Distribution of the Differences

The other method to research the accuracy of estimates of global solar irradiation is the cumulative distribution of the differences. In order to analyze the performance of any models, the cumulative distribution of the difference between the measured and calculated values and also absolute value of this difference can be used [80].

To construct the cumulative frequency distribution of the solar irradiation estimation models, the daily differences (Eqn. (2.26), difference between measured and estimated  $H$  values) having certain ranges are calculated in a cumulative manner and these values are used to produce cumulative frequency curves in percentages. In our study, the cumulative distribution curves for the normal distributions in the daily differences and the absolute differences are shown in graphs (in Chapter 5). If the y-axis is the cumulative frequency and the x-axis is the daily difference, then a closer the curve to the  $x=0$  line means a lower difference and hence a better estimation. In the same manner, cumulative distribution curves of the daily absolute values of differences represent the best performances when the curves are closer to the y axis.





## CHAPTER 3

### SOLAR IRRADIATION ESTIMATION MODELS

#### 3.1 Introduction

Solar energy, meteorology, and many climatic applications are directly related to the correct knowledge of solar irradiation at the Earth's surface. In this context, obtaining accurate solar data for solar irradiation is vital. On the surface of the Earth, solar irradiation measurements and estimations are carried out by means of two main approaches. These are models based on ground level measurements with pyranometers and pyrheliometers, and satellite-derived remote estimations.

It is known that ground level solar irradiation data is the most accurate way to characterize the solar resource of a given site [81]. On the other hand, ground measured solar irradiation is hardly obtained for a given site. In addition to this, the measurement network's density is usually far too low and the data taken are not quite reliable [82]. Another approach is satellite image based estimation models, which are quite promising. However, they are indirect methods and not as good as the other models that use nearby surface measurements [69]. However, these models are still developing and the relevant satellite technology has been profoundly improving in recent years. For these reasons, in order to derive accurate information on solar irradiation at the ground level, different estimation models have been developed by many researches [1–6]. These estimation models at ground level can essentially be divided into two categories: statistical and physical approaches [41], [83], [84].

This chapter starts with a presentation of the statistical approach for the estimation of solar irradiation. Then, the physical approach is detailed, before discussing combined models in section 3.4. In section 3.5, examined models for global solar irradiation of estimation are compared. Finally, conventional models are presented in section 3.6, and “Simple satellite data applied to daily data” is given in section 3.7.

## **3.2 Statistical Approach for the Estimation of Solar Irradiation**

Statistical approaches, which are based on relations between the observed data and global solar irradiation, exhibit high performances. Another important issue is that these approaches are simpler than physical approaches since they do not need extensive and precise information on the composition of the atmosphere.

Statistical approaches have many application areas such as the characterization of numerical data, the description of system behavior and the estimation of the uncertainties of subsequent calculations based on observational data. In addition, they can be used to understand the model behavior, assess the model ability, enhance the performance of the model, analyze future behavior of a system based on historical information and estimate input parameters for more complex physical models [72].

As mentioned before, the models using the statistical approach are simpler than those using the physical approach because they use less input information and uncomplicated computing techniques with shorter computation time for the estimation of solar irradiation. In here, mainly two important points should be taken into account. The first one is the availability of data to be used as input by the statistical approaches, and the other is the accuracy of the estimating model [85]. The statistical approach can be classified as the ground-based and remote sensing (satellite) depending on the information obtained on the composition of the atmosphere and/or measured parameters.

### **3.2.1 Ground - Based Solar Irradiation Estimation Models with the Statistical Approach**

Several models have been developed to estimate the global solar irradiation on the Earth's surface from ground level measurements. In these models, the ground measurements such as the global solar irradiation, the bright sunshine duration, cloudiness, temperature and humidity are used as input parameters [45], [46].

One of them is bright sunshine duration which is long-term, reliable and available data [45]. Because of these properties, it is used widely as an input parameter to estimate solar irradiation. The other measured parameter is the global solar irradiation, which is important in terms of the construction and verification of estimation models. Basically, most of the ground-based statistical models depend on the empirical relationship between these two parameters mentioned. As described previously in Chapter 2, the measurements of global

solar irradiation are obtained by pyranometers, and bright sunshine duration observations are taken by Campbell-Stokes type recorders [52], as explained in section 2.4.3.

In the context of estimation of solar irradiation in the statistical way, the first graphical study was proposed by Kimball [86] between the global solar irradiation and bright sunshine duration, which was developed by Angström [87]. In 1940, Prescott [88] modified this regression equation, and proposed the following Angström-Prescott relation, with linear form as follows:

$$K = \frac{H}{H_0} = a + b \frac{s}{S} \quad . \quad (3.1)$$

The empirical values  $a$  and  $b$  are called Angström coefficients and are site dependent.  $H$  is the daily global solar irradiation and  $H_0$  is the daily extraterrestrial solar irradiation on a horizontal surface. The quantities  $s$  and  $S$  are daily bright sunshine hours and day length, respectively.  $H_0$  and  $S$  can be calculated using the known general formulas [12] that are presented in Chapter 2. In order to estimate the solar irradiation, regression analyses are carried out between the normalized daily solar irradiations, namely the daily clearness index ( $K=H/H_0$ ), and the daily sunshine duration fraction ( $s/S_0$ ) by many researchers. Hence, correlations exist in many locations all over the world and are utilized extensively. However, the regression correlation obtained for one location should not be used for the sites having different climates and/or far from the location that the correlation is obtained. Angström-Prescott model will be detailed in section 3.6.1.

Although Angström-Prescott correlation original form was linear, higher order and quadratic forms were also studied by many researches [3], [4]. In 1984, Ogelman et al. [3] proposed an empirical quadratic estimation model for the solar irradiation. A quadratic relation between the daily clearness index  $K$  and daily sunshine duration fraction ( $s/S_0$ ) have been obtained by Akinoglu and Ecevit using site dependent Angström coefficients [4]. This correlation was obtained using Angström coefficients  $a$  and  $b$  for 100 different locations on the Earth's surfaces [4]. This relation is given as:

$$K = \frac{H}{H_0} = 0.145 + 0.845 \frac{s}{S} - 0.280 \left( \frac{s}{S} \right)^2 \quad . \quad (3.2)$$

Although the values of the coefficients depend on the selected location, Eqn. (3.2) has a simple form and needs only the bright sunshine duration. In addition, the model is tested using a large number of data set and the validity of this model was verified [45], [89].

### 3.2.2 Remote Sensing Based Solar Irradiation Estimation Models with the Statistical Approach

Over the last two decades, satellite-derived (remote sensing) solar irradiation estimation has become a worthy tool to quantify the solar irradiation at ground level for large areas. Generally, images taken by geostationary satellites, which are rotating around the Earth at the same speed as the Earth, are used [72]. The whole surface of the Earth is almost covered by seven geostationary satellites positioned at regular intervals above the equatorial line. One of them is Meteosat Satellite operated by the European metrological satellite series [69], [72], [81]. Refer to Chapter 2 for a detailed discussion about the geostationary satellites and their properties.

Some of the early researchers who used satellite data for the estimation of global solar irradiation at the Earth's surface are given in the following references: [1], [90], [91]. In 1986, Cano et al [41] carried out one of the most popular works, (later named as HELIOSAT) for solar irradiation estimations using the pixel counts of the satellite images taken by Meteosat. This is a well-known and frequently used solar irradiation estimation model which is the correlation between ground measurement irradiation data and cloud index derived from Meteosat satellite images [6], [42], [81], [92]. HELIOSAT estimates surface hourly solar irradiation based on the linear relation between the hourly clearness index  $k$  and cloud index  $n$  derived from satellite images at the selected point. The details of HELIOSAT will be discussed in section 3.6.2.

### 3.3 Physical Approaches for the Estimation of Solar Irradiation

Physical approaches basically use the radiative transfer models to formulate a relationship between satellite and ground measurements [72]. In order to describe the radiative transfer model and energy exchanges of atmosphere, there are many physical parameters defined to fulfill this aim. Some of them are the clear atmospheric scattering coefficients, absorption coefficients, cloud albedo and ground albedo. The models using physical approaches which estimate the global solar irradiation employ mathematical equations based on these physical considerations and dynamic motion of the atmosphere. Since these models have very complex and non-linear mathematical equations, the strong computing systems are needed to solve them [85]. In addition, the physical approaches need complementary and calibrated meteorological data to estimate global solar irradiation. They can be listed as the disadvantages of this type of approach. On the other hand, the most important advantage of

this type of approach is that it is possible to apply it anywhere on the Earth's surface. Besides, taking into account the interactions in the atmosphere, it offers the advantage of tracing immediate effects occurring in the atmosphere. Description of the physical approach was detailed by various researchers [45], [84]. Similar to the statistical approach, physical approach is also divided into two parts; ground-based and remote sensing (satellite) solar irradiation estimation models.

### 3.3.1 Ground-Based Solar Irradiation Estimation Models with the Physical Base

The structure of the atmosphere is semi-transparent and of limited thickness. The incoming solar energy transmission of such a structure can be described with physical models. In the physical models, the initial intensity of this incoming (extraterrestrial) solar energy  $I_0(\lambda)$  should be considered as a monochromatic and non-coherent electromagnetic wave with the wavelength of  $\lambda$ . According to the law of conservation of energy, with the influence of atmospheric constituents such as water vapor, clouds, aerosols, and molecular gases, this incoming electromagnetic energy passing through the atmosphere is reflected, absorbed and transmitted. For an initial monochromatic electromagnetic energy, the reflected; transmitted and absorbed intensities are given as:

$$I_0(\lambda) = I_\rho(\lambda) + I_\tau(\lambda) + I_\alpha(\lambda) \quad , \quad (3.3)$$

where  $I_0(\lambda)$  is the incident,  $I_\rho(\lambda)$  is the reflected,  $I_\tau(\lambda)$  is the transmitted and  $I_\alpha(\lambda)$  is the absorbed intensities. In order to calculate the energy transmittance of the dynamic atmosphere, taking into account the different interactions of different spectral wavelengths, different values are determined. They are commonly defined as a function of the air mass including atmospheric parameters.

Given all of these interactions of electromagnetic waves in the atmosphere, it can be seen that the description of the spread of the solar irradiation requires the complex physical parameters in physical models. The difficulties of the solution of these complex expressions and some necessary initial assumptions are denoted as the disadvantages of these models. Nevertheless, the dynamic structure of the atmosphere and the interaction of the electromagnetic wave can be defined as the most important advantage of physical models [93].

### 3.3.2 Remote Sensing Based Solar Irradiation Estimation Models with the Physical Base

An advantage of the images taken from geostationary satellites is their large area coverage with high spatial resolution (up to 1 km) and with sufficient temporal resolution (up to 15 minutes) especially for the second-generation satellites [6], [66]. Therefore, it is possible to increase the accuracy of satellite based estimations [94–96].

There are many methodologies and formalisms for the estimation of solar irradiation on the Earth's surface using satellite images in the physical models [64], [97], [98]. Among these methodologies, a widely-known physical model was developed by Gautier et al [98]. The main principle of this model is that incoming global solar irradiation of satellite is defined in terms of the extraterrestrial irradiation using two different approaches for clear and cloudy sky that is derived from atmospheric parameters.

Gautier et al [98] explained that the solar irradiation was received by the satellite and ground separately, for both the clear and overcast sky, with the cloud albedo and the coefficient of clouds. Considering the short-wavelength irradiation flux  $F_0=1367\cos\theta$  ( $Wm^{-2}$ ), the reflection ( $F_0\alpha$ ) and absorption ( $F_0(1-\alpha)a(u_1)$ ) equations, Gautier et al [98] expressed the solar irradiation received by the satellite ( $SW\uparrow$ ) with the following equation:

$$SW\uparrow = F_0\alpha + F_0(1-\alpha)[1-a(u_1)](1-\alpha_1)[1-a(u_2)]A \quad (3.4)$$

The variables introduced in this formula are  $\alpha$  and  $\alpha_1$ , reflection coefficients for beam irradiation;  $a(u_1)$ , absorption coefficient for slant water vapor path  $u_1$  for the zenith angle;  $a(u_2)$ , absorption coefficient for slant water vapor path  $u_2$  for the zenith angle;  $A$ , surface albedo. More information about satellite based physical model can be seen in detail in the references: Noia et al.[84], Özdemir [93] and Gautier et al. [98].

### 3.4 Combined Models

From a variety of physical models to statistical models, several mathematical models have been developed in the last three decades. However, these models are still evolving with improvements in many aspects. Some researchers stated that the different model combinations can amend the estimation of solar irradiation in an efficient way [45], [94], [99]. The use of the coupled technique plays an important role in the development of solar irradiation accuracy, and therefore combined models are believed to become more popular [95], [100].

The basic idea of the combined work is to use the unique features of each model by combining ground measured type linear correlations with the satellite based models. In other words, the main objective is to couple the measured surface data with the available imagery taken at the top of the atmosphere and this is the main objective of this thesis. These two types of data which encourage their combined use to reach more accurate estimation schemes are essentially complementary [94–96], [99].

Studies about linking the satellite image driven data to the ground measurements of bright sunshine hour  $s$  can be an example of this approach, which was first stated by Olseth and Skartveit [101]. There are also attempts to increase the estimation accuracy of daily solar irradiation by using this idea of linking surface measurements of bright sunshine hours to satellite imagery [94], [96]. In section 4, we present combined models of estimation that we developed. These models are the first model that directly couples the satellite imagery to surface measured bright sunshine hours.

### **3.5 Comparison of Statistical, Physical and Combined Models**

We already stated that estimating models for ground level global solar irradiation are divided into two main groups depending on the used approach: The statistical approaches and physical models. The advantages and disadvantages of the models were given for comparison in Table 3.1.

The models using the statistical approach do not require detailed information on the composition of the atmosphere; therefore, they are simpler than the physical approach. Moreover, ground-based models of the statistical approach which are based on relations between daily bright sunshine duration and daily solar irradiation data provide high performance. On the other hand, they need accurate and precise long term data measured on the surface of the Earth.

The models of the second group provide good results by using radiative transfer models for the estimation of solar irradiation with the applicability of a large area. Furthermore, they do not require solar irradiation data measured on the Earth's surface, except verification. However, the physical approaches need supplementary meteorological data to calculate the interactions of solar irradiation with the atmosphere and use complex mathematical equations of radiative transfer models.

**Table 3.1** Comparison of statistical, physical and combined models with an advantages and disadvantages.

<b>Approaches</b>	<b>Advantages</b>	<b>Disadvantages</b>
<b>Statistical</b>	<ul style="list-style-type: none"> <li>• Operational efficiency</li> <li>• No need for meteorological data</li> <li>• No need for complex calculations</li> </ul>	<ul style="list-style-type: none"> <li>• Need for ground measured data</li> <li>• Lack of applicability</li> </ul>
<b>Physical</b>	<ul style="list-style-type: none"> <li>• Applicability for large areas</li> <li>• No need for ground solar irradiation data</li> </ul>	<ul style="list-style-type: none"> <li>• Need for meteorological data</li> <li>• Need for complex calibration</li> </ul>
<b>Combined</b>	<ul style="list-style-type: none"> <li>• Operational efficiency</li> <li>• No need for meteorological data</li> <li>• No need for complex calculation</li> <li>• Applicability for large areas</li> </ul>	<ul style="list-style-type: none"> <li>• Need for ground measured bright sunshine hour data</li> </ul>

Lastly, with this thesis, some of the advantages of statistical and physical approaches are combined in coupled models. In these models, with the use of ground data, the accuracy of solar irradiation estimation increases, and the applicability to larger areas with the use of satellite data is also improved.

### 3.6 Conventional models

In this part, common estimation models, namely Angström-Prescott model and satellite based HELIOSAT, are briefly explained. The former is based on the ground measured sunshine values, and the latter is based on geostationary satellite data.



### 3.6.1 Angström-Prescott Model

As mentioned before, the statistical models that use ground measurements provide high performances for the estimation of global solar irradiation. Among them, the most popular one; Angström type [87], utilizes surface measured daily bright sunshine duration values ( $s$ ) which strongly correlate with solar irradiation. Bright sunshine hour values have been measured for more than 100 years all over the world. Detailed discussions of Angström models are given in various references such as Akinoglu [102], [45] and Martinez-Lozano et al.[2].

Original form of Angström's relation was the correlation between the daily sunshine duration fraction,  $s/S$ , and the daily ratio of global solar irradiation to that of clear sky irradiation,  $H/H_C$ . A correlation of the form:

$$\frac{H}{H_C} = \alpha + (1 - \alpha) \frac{s}{S} \quad (3.5)$$

was proposed by Angström [87]. In 1940, this model was modified by Prescott [88] in order to obtain a model easily applicable to all sites. Prescott replaced  $H_C$  – which is to be measured for the site – with extraterrestrial solar irradiation on a horizontal surface which can be calculated. With this replacement, the well-known and frequently used solar irradiation estimation formula called Angström-Prescott equation was defined with two empirical site dependent coefficients [88] (Eqn. (3.1)). The values of coefficients  $a$  and  $b$  are calculated by using measured monthly averages of daily global solar irradiation together with monthly average of bright sunshine hour values. The calculation procedures of  $H_0$  and  $S$  can be found in the reference Duffie and Beckman [12] and Chapter 2.

These correlations exist for many locations all over the world and are utilized extensively. For the daily values, the regressions can also be carried out on a monthly basis and regression coefficients  $a_i$  and  $b_i$  can be obtained for each month. In this case, the equation is as follows:

$$K_m = \frac{H_m}{H_0} = a_i + b_i \frac{s}{S} \quad (3.6)$$

where the values of Angström coefficients  $a_i$  and  $b_i$  are calculated by using linear correlations for each month, that is,  $i$  runs from 1 to 12. Monthly Angström coefficients  $a_i$  and  $b_i$  are believed to contain local information which might be used in the satellite models.

Detailed information on different types appearing in the literature and reviews are presented in references [2], [45], [102].

As mentioned before in section 2.2.5, Campbell-Stokes types of sunshine recorders do not work efficiently during the low altitude of the Sun. Because of this, the modified day length  $S_0$  (day length for zenith angle  $\leq 85^\circ$ ) can be used instead of the daylength  $S$ , Eqn. (2.14). To see the performances of Angström-Prescott model and all other models, the model results and the ground measured solar irradiation data was compared. The obtained results will be discussed in Chapter 4 and Chapter 5 in details.

### 3.6.2 HELIOSAT

There are various models to estimate surface solar irradiation, based on geostationary satellite data. One of the important and most common model is HELIOSAT, which is developed and used by Beyer et al.[5] and others [6], [97]. It is essentially based on the early work of Cano et al. [41] as are most of the satellite imagery based solar irradiation estimation schemes.

HELIOSAT is an hourly-based estimation technique to infer the shortwave surface irradiation from satellite images. The general idea of this model is to deal with atmospheric and cloud extinction separately. A calculation of cloud index  $n$  is determined by Meteosat visible channel pixel count and it is used directly in the estimations. Cloud index  $n$  is defined using the relative cloud albedo  $\rho$ . Relative cloud albedo  $\rho$  is calculated from the pixel counts using the pixels of the satellite images on the location of interest [41]. The relative cloud albedo ( $\rho$ ) is calculated as:

$$\rho = \frac{C - C_0}{I_{ext}} \quad , \quad (3.7)$$

where  $I_{ext}$  is the hourly extraterrestrial irradiation outside of the atmosphere. Here,  $C_0$  represents an offset and it is subtracted from the satellite pixel count measurements [5].

Most important step is the definition of the cloud index  $n$ , which is calculated for each pixel as:

$$n = \frac{\rho - \rho_{clear}}{\rho_{cloud} - \rho_{clear}} \quad . \quad (3.8)$$

Here  $\rho_{clear}$  and  $\rho_{cloud}$  are the maximum and minimum values of the relative reflectivity assuming that they correspond to clear and overcast conditions, respectively [5].

In order to estimate the solar irradiation, an empirical form is needed between the normalized hourly solar irradiances, namely the clearness index ( $k$ ) and cloud index ( $n$ ) defined above. Therefore, assuming a linear relation, hourly clearness index  $k$  can be written as:

$$k = \frac{I}{I_0} = \alpha n + \beta \quad (3.9)$$

where  $I_0$  is the hourly extraterrestrial irradiation,  $I$  is the hourly global irradiation values for the site of interest,  $\alpha$  and  $\beta$  are empirical parameters to be determined using regression analysis with the ground data. These parameters would be site dependent and might be affected by the temporal variations of the atmospheric conditions [6], [81]. Cano et al [41] used such linear correlations of the form as in Eqn. (3.9).

In the modified version of HELIOSAT, instead of hourly clearness index  $k$ , a hourly clear sky index  $k^*$  was used [5]. It was defined as:

$$k^* = \frac{I}{I_{clearsky}} \quad (3.10)$$

where  $I_{clearsky}$  is a calculated hourly clear sky irradiation value of the site using a hourly clear sky model. In their model, Hammer et al [6] calculated  $I_{clearsky}$  as follows:

$$I_{clearsky} = I_{dn;clear} \cos \theta_z + I_{dif;clear} \quad (3.11)$$

where  $\theta_z$  is the zenith angle,  $I_{dn;clear}$  is the hourly clear sky direct and  $I_{dif;clear}$  is the hourly clear sky diffuse irradiation. The daily totals of clear sky irradiation can be obtained from the hourly values,  $I_{clearsky}$  by simply summing over the day. To find the values of hourly  $I_{clearsky}$ , firstly, hourly direct normal irradiation  $I_{dn;clear}$  is calculated, which is proposed by Page [55]:

$$I_{dn;clear} = I_{sc} \varepsilon \exp(-0,8662 T_L(2)) \delta_R(m) m \quad (3.12)$$

According to Dumortier [56], the hourly diffuse irradiation can be calculated using an empirical relationship:

$$I_{dif:clear} = I_{ext} \varepsilon \left( \begin{array}{l} 0.0065 + (-0.045 + 0.0646 T_L(2)) \cos \theta_z \\ + (0.014 - 0.0327 T_L(2)) \cos^2 \theta_z \end{array} \right) \quad (3.13)$$

where  $\varepsilon$  is the eccentricity correction,  $\delta_R(m)$  is the Rayleigh optical thickness of a dry and clean atmosphere,  $m$  is the air mass and  $T_L(2)$  is the Linke turbidity factor for air mass (2) [58], [103]. A worldwide database (climatology) given by Remund [104] is based on the monthly values of Linke Turbidity,  $T_L$ .

As described above, cloud transmission can be defined by the hourly clear sky index  $k^*$  which is the ratio of the actual surface hourly irradiation  $I$  and the hourly clear sky irradiation  $I_{clearsky}$  from Eqn. (3.11), and it is correlated with the hourly cloud index  $n$ . Some detailed explanations on the subject can be found in the following references: Beyer et al.[5] Hammer et al. [6], and Girodo et al.[97]. Eqns. (3.10) and (3.11) are then used to obtain the hourly surface irradiation  $I_g$ :

$$I_g = k^* \cdot I_{clearsky} \quad (3.14)$$

Afterwards, measured hourly values of clear sky index  $k^*$  were correlated to the cloud index  $n$  defined above, to obtain the empirical relations. This relation was described in a simple form by Beyer et al. [5], and then it was improved by Hammer et al. [42], as follows:

$$k^* = \begin{cases} 1.2 & \text{for } n < -0.2 \\ 1 - n & \text{for } -0.2 < n \leq 0.8 \\ 2.0667 - 3.6667n + 1.6667n^2 & \text{for } 0.8 < n \leq 1.1 \\ 0.05 & \text{for } n > 1.1 \end{cases} \quad (3.15)$$

In obtaining eqn. (3.15), Hammer [42] used the data of about 23 locations in Germany. The simple relationship within the large range of  $n$  values, -0.2 and 0.8, can be written as:

$$k^* = 1 - n \quad (3.16)$$

The calculation procedure and other relevant information were explained in detail in the references Hammer et al. [6] and Beyer et al. [5]. The same relation for the daily values was considered and presented in thesis study [96], [99].

### 3.7 Simple Satellite Method Applied to Daily Data

As mentioned before, in section 3 Eqn. (3.10), the first version of satellite based models  $H_{Cano}$ , proposed by Cano et al. [41], [105], was a linear correlation between the hourly clearness index ( $k$ ) and hourly cloud index ( $n$ ). To obtain the monthly relations, we carried out regression analyses for the selected locations presented in Table 1.1. It has been assumed that a linear relationship between the daily values of clearness index ( $K$ ) and daily average values of cloud index ( $n_{avg}$ ) exists. That is, the daily clearness index  $K$  can be written as:

$$K = \frac{H_{Cano}}{H_o} = \alpha_i \cdot n_{avg} + \beta_i \quad (3.17)$$

The result of the linear regression of Ankara for a sample month of April 2004 is given in Fig. 3.1 with the data points for 30 daily values. It is expected that the negative sign in front of the constant  $\alpha_i$  is obviously, indicating the complementary behavior of cloud index  $n$  and bright sunshine hour  $s$ . The correlation coefficients  $R^2$  were found to be 0.93 in April. In fact, the values of  $R^2$  are larger than 0.80 for all months of the year and all locations.

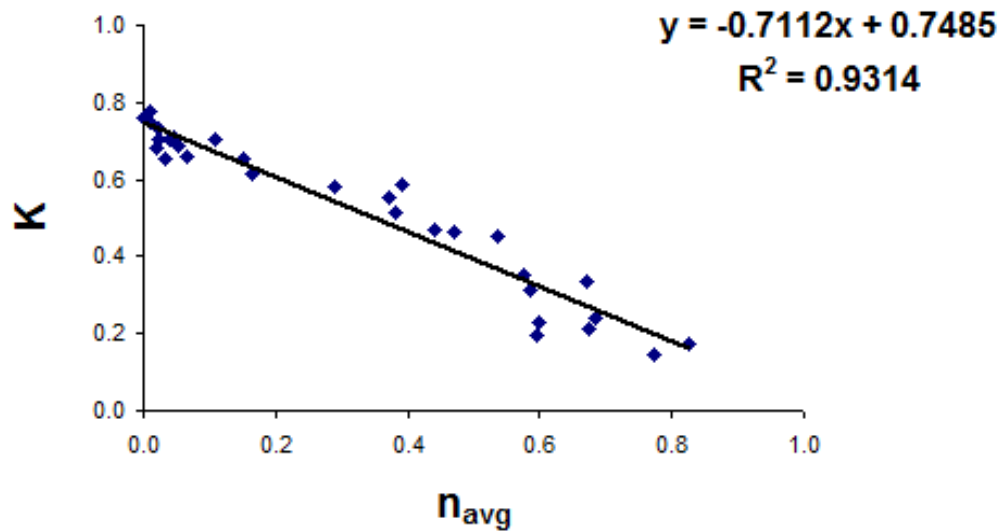


**Figure 3.1** Linear regression between the daily values of clearness index  $K$  and daily average cloud index  $n_{avg}$  for the month of April 2004 in Ankara.

The regression coefficients  $\alpha_i$  and  $\beta_i$  values are found to be -0.71 and 0.75, respectively for the month of April 2004 in Ankara (in Fig. 3.1). The coefficients of the first version of HELIOSAT applied to daily data can be calculated for each month of the year by using 12 pairs of  $\alpha_i$  and  $\beta_i$ . It should be noted that these are the monthly coefficients derived from the surface bright sunshine measurements of the stations under consideration. Considering high values of the correlation coefficients, this simple linear relation can be used to estimate daily global solar irradiation. Therefore, we also compared the results of this earliest version of satellite based estimations applied to daily values, with all the other models explained before and in the following sections (Appendix A).

## CHAPTER 4

### MODELING APPROACHES

#### 4.1 Introduction

Satellite images are heavily used for the estimation of solar irradiation at the Earth's surface. The accuracy of estimations yet should be improved to attain more reliable input values for the use of all types of solar energy systems. For this reason, different approaches and procedures were adopted to link the surface bright sunshine measurements to satellite based procedures [94–96], [99]. In this study, three new models has been proposed, namely  $H_{model}$ ,  $H_{CA1}$  and  $H_{CA2}$ , to increase the estimation accuracy of daily global solar irradiation by coupling the satellite images with surface bright sunshine hour measurements using data from Turkey and Germany. In addition, we tested weather to replace  $H_0$  of the Angström-Prescott (Eqn. (3.1) with  $H_{clear,H}$  ( $=\Sigma I_{clearsky}$ ) of the HELIOSAT would give better performance or not. This procedure is called as  $H_m^*$ .

Nearest neighbor implementation is the simplest method of estimating irradiation at a given point from an existing measuring site. This method has been tested using some classical models ( $H_m$  and  $H_{sat}$ ) and the new models, to use for the neighboring stations where ground data are lacking. The performances of three new models over neighboring sites ( $H_{model\_n}$ ,  $H_{CA1\_n}$ , and  $H_{CA2\_n}$ ) and  $H_m^*$  ( $H_m^*_{-n}$ ) will be compared in detail in Chapter 5 with respect to the statistical errors and cumulative frequency of daily difference and daily absolute difference values.

#### 4.2 Angström-Prescott Equation with Daily Clear Sky Irradiation of HELIOSAT ( $H^*$ )

In the Angström-Prescott linear relation, Eqn. (3.1), vast majority of the works use the extraterrestrial daily solar irradiation  $H_0$  and find the Angström coefficients  $a$  and  $b$  by

regression analysis. We carried out linear regression analysis and determined  $a$ ,  $b$ ,  $a_i$ ,  $b_i$  values of equation (3.1) and (3.6) for all locations intending to couple these coefficients to the satellite model (Appendix B). However, in the original proposal of Angström model, it was the measured clear sky value,  $H_C$  instead of  $H_0$  [87]. Gueymard [106], [107] suggested that the use of a suitable clear sky value could increase the estimation accuracy. Therefore, as mentioned above, we wanted to use also daily summation of hourly clear sky irradiation  $I_{clearsky}$  (Eqn. (3.12)) in the Angström type linear regression analysis on a yearly base. This is the use of  $H_{clear;H}$  ( $=\sum I_{clearsky}$ ) of HELIOSAT instead of  $H_0$  in the Angström relations Eqns (3.1) and (3.6), as explained below:

$$K^* = \frac{H^*}{H_{clear,H}} = a^* + b^* \frac{s}{S} \quad (4.1)$$

where  $a^*$  and  $b^*$  are the new Angström coefficients obtained from the daily data set of the whole year. This regression can also be carried out monthly, and the relation can be written as:

$$K_m^* = \frac{H_m^*}{H_{clear,H}} = a_i^* + b_i^* \frac{s}{S} \quad (4.2)$$

where  $a_i^*$  and  $b_i^*$  are calculated for each month of the year. These values are tabulated in Table B.1 in Appendix B for all selected stations and comparisons are discussed in results and discussion chapter.

We carried out yearly Angström type regressions using all daily data set for all the stations, between  $K$ ,  $K^*$  and  $(s/S)$ , one of which is depicted in Fig. (4.1) for a sample station Ankara for the year 2004.



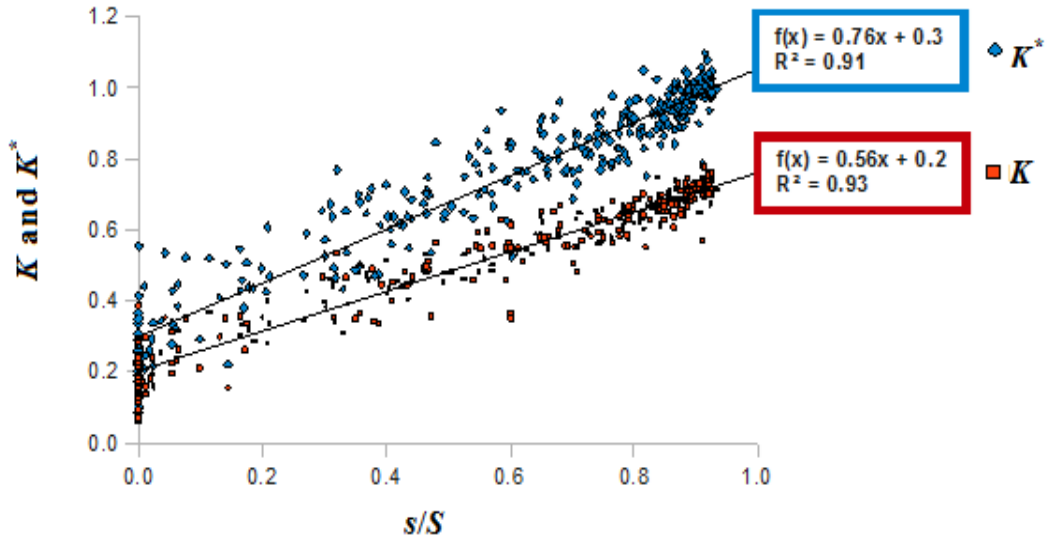


**Figure 4.1** Comparative analysis between daily clearness index  $K$  and daily clear sky index  $K^*$  versus  $s/S$  for the station Ankara for the year of 2004.

When  $H_{clear,H}$  is used in daily clear sky index  $K^*$  for the normalization, yearly values for the linear relation coefficients are 0.30 for  $a^*$  and 0.76 for  $b^*$ , and  $R^2$  is 0.91 as shown in Fig. 4.1. Using  $H_0$  for the normalization in daily clearness index  $K$ , the linear relation yearly coefficients were found to be  $a = 0.20$  and  $b = 0.56$  values with  $R^2 = 0.93$ . Similar results are obtained for other locations (Appendix B).

### 4.3 $H_{model}$

The basic idea of the HELIOSAT is to predict hourly surface global solar irradiation  $I_g$  with hourly cloud index  $n$  calculated from the satellite and  $I_{clearsky}$  (Eqn. (3.12)). To do this, hourly cloud index  $n$  is correlated to the hourly clear sky index  $k^*$ . As mentioned before, Hammer et al. [6] obtained this relationship as  $k^* = (1-n)$  for the largest range of  $n$  values (Eqn. (3.15)). The hourly surface global solar irradiation  $I_g$  was given in Eqn. (3.14).

In this first approach of the thesis, to handle the daily clear sky radiation on horizontal surface  $H_{clear,A}$ , the ground measurements Angström-PreScott relation was used. In equation (3.1), if we take  $(s/S_0) = 1$ , this means that the bright sunshine hour ( $s$ ) for a clear

day must be equal to the modified daylength  $S_0$ , therefore the result is the daily clear sky irradiation on horizontal surface; that is:

$$H_{clear,A} = H_0(a_i + b_i) \quad (4.3)$$

We proposed the use of  $H_{clear,A}$  for the specific month, instead of  $H_{clear,H}$  ( $=\sum I_{clearsky}$ ) in HELIOSAT for the daily global solar irradiation estimations. These values of  $H_{clear,A}$  can either be calculated using yearly values for pair of  $a$  and  $b$  or by using 12 pairs of  $a_i$  and  $b_i$  for 12 months. The regression analysis of the calculated values of  $H_{clear,A}$ , can be obtained from Eqn. (4.3) and also from the daily summation of clear sky irradiation,  $H_{clear,H}$  ( $=\sum I_{clearsky}$ ) of HELIOSAT using Eqn. (3.11). For the period of one year for two sample locations (Ankara and Bremen)  $H_{clear,H}$  versus  $H_{clear,A}$  is given in Fig. 4.2, for comparison.

This regression analysis illustrated that there is indeed a very high correlation ( $R^2 \sim 0.98$ ) between the daily clear sky irradiation of HELIOSAT ( $H_{clear,H}$ ) and values obtained from Angström-PreScott relation ( $H_{clear,A}$ ) for all selected stations. Fig. 4.2 shows the result of the linear regression of sample stations for Ankara and Bremen. But we should note that for a few data for Bremen the deviation reaches about 20%.

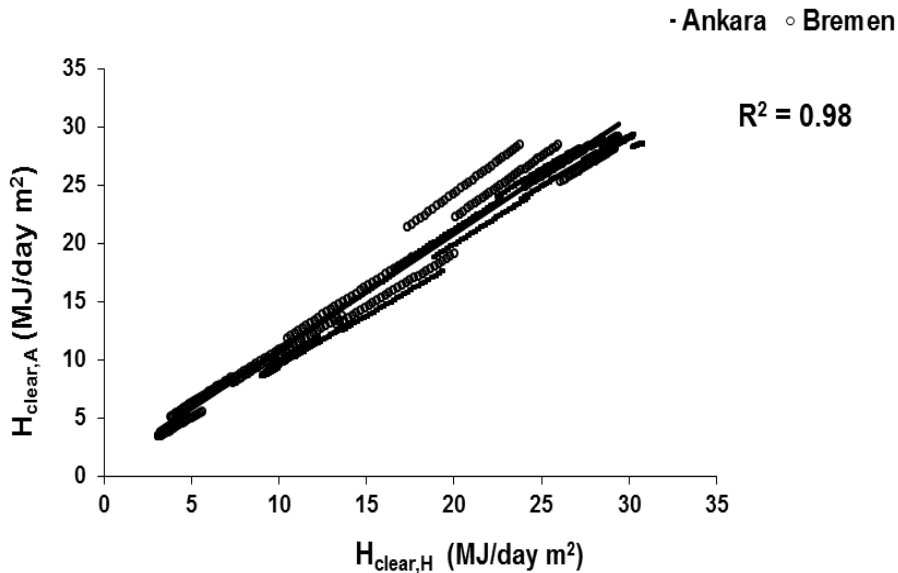


**Figure 4.2** Relation between daily clear sky irradiation values of Angström-PreScott relation,  $H_{clear,A}$  and daily clear sky irradiation values of HELIOSAT,  $H_{clear,H}$  used in the regression analysis [96].

The validity of using  $H_{clear,A} = (a_i + b_i)H_0$  (which is easier to obtain) instead of  $H_{clear,H}$  ( $=\Sigma I_{clearsky}$ ) of HELIOSAT (which uses monthly Linke turbidity  $T_L$ ) is tested using correlation coefficients of regressions between daily clearness index  $K(=H/H_0)$  and fraction of daily bright sunshine duration  $s/S$ , and daily clear sky index  $K^*(=H/H_{clear,H})$  and  $s/S$ . These correlation coefficients derived from monthly regressions are plotted with respect to monthly Linke turbidity  $T_L$  calculated within HELIOSAT formalism. As can be observed from Fig. (4.3) the correlation coefficients are not function of  $T_L$  indicating that Eqn. (4.3) can be used as clear sky irradiation for a location. This certainly encourages the use of surface measured bright sunshine hour data.

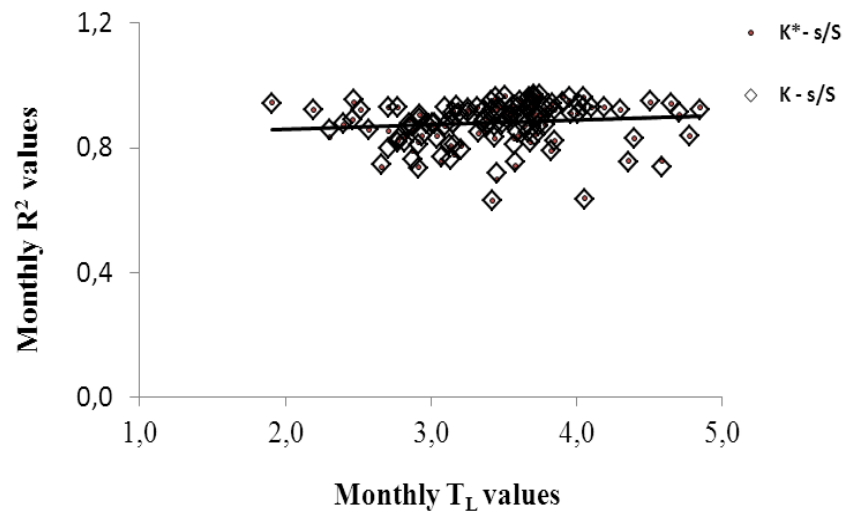


**Figure 4.3** Relation between monthly values of Linke turbidity  $T_L$  and monthly values  $R^2$  for the correlation of clearness index  $K$  (clearsky index  $K^*$ ) with sunshine duration  $s/S$ . The regression has been performed for all stations [96].

Furthermore, it is possible to take the daily average values of the hourly cloud index in Eqn. (3.8) ( $n_{avg}$ ) to find the daily global solar irradiation. In writing this expression, one may use hourly correlation Eqn. (3.16), by assuming that the correlations for the daily averages follow a similar trend, which is essentially  $(1 - n_{avg})$ . Thus, for the daily values of clear sky index  $K^*_{model} (H/ H_{clear,A})$  and daily average of cloud index  $n_{avg}$ , we assumed that a similar correlation can be written as:

$$K_{model}^* = \frac{H_{model}}{H_{clear,A}} = \frac{H_{model}}{(a_i + b_i)H_o} = (1 - n_{avg}) \quad (4.4)$$

Note that  $a_i$ 's and  $b_i$ 's are monthly-based Angström coefficients of the stations under consideration, derived from surface measurements.

In order to clarify this assumption, new linear correlations between daily clear sky index  $K^*$  and daily cloud index  $n_{avg}$  were investigated. Slightly different results were obtained when we compared the results of hourly and daily data sets.

We obtained new correlations for each station using the daily-based data sets. The results showed that there were slightly different relations between clear sky index  $K^*$  and daily cloud index  $n_{avg}$ , as presented next.

#### 4.3.1 Implementation of the $H_{model}$ to the Neighbors

As mentioned above, we assumed that there should be a new linear relation as:

$$K_{model}^* = \frac{H_{model}}{H_{clear,A}} = (c - dn_{avg}) \quad (4.5)$$

where  $c$  and  $d$  are the site-specific regression coefficients.

We verified this model in the regression analysis between  $K_{model}^*$  and  $n_{avg}$  for all locations and the site-specific regression coefficients  $c$  and  $d$  are obtained (Appendix A). For an example, we present the following equations to show the results for only two of them, Ankara and Bremen. As pre-assumed above, these relations are slightly different than  $1-n$ :

$$K_{modelAnkara}^* = \frac{H_{modelAnkara}}{H_{clear,A}} = (0.99 - 0.93n_{avg}) \quad (4.6)$$

$$K_{modelBremen}^* = \frac{H_{modelBremen}}{H_{clear,A}} = (1.00 - 1.02n_{avg}) \quad (4.7)$$

The values of site specific coefficients  $c$  and  $d$  are 0.99 and 0.93 and, 1.00 and 1.02 for Ankara, and for Bremen, respectively. It is noteworthy that, if the daily average values of

hourly cloud index  $n_{avg}$  have higher values,  $H_{model}$  might give negative results. However,  $n_{avg}$  values never reached such high values.

These relations were tested for neighboring stations. We used the coefficients of above selected stations Ankara and Bremen to estimate solar irradiation at neighbor stations Afyon for Turkey, and Braunschweig and Wittenberg for Germany. Results were satisfactory but not considerably better than those obtained using the form of Eqn. (4.4) [95]. Our test results will be given in detail in Chapter 5.

#### 4.4 Combined Approach Based on the Relation Between $n$ and $s$ ( $H_{CAI}$ )

It was proposed [101] and formulated earlier that daily sunshine duration fraction ( $s/S$ ) and daily cloud index ( $n_{avg}$ ) correlated as expected [94], [108]. This correlation is shown in Fig. 4.4 for the data of a sample month of Ankara. Here, the daily average values of the hourly cloud index are used to find daily global solar irradiation. The linear correlations for all locations show similar trends and are of the form:

$$n_{avg} = d_i - c_i \frac{s}{S_o} \quad (4.8)$$

where  $c_i$  and  $d_i$  are the monthly correlation constants. They are 0.76 and 0.76 for the sample month of April 2004 for Ankara. We obtained monthly correlations of these quantities for all the available data sets. It is observed that for the period of one year the correlation coefficient  $R^2$  values rarely drop down to values below 0.80. These monthly coefficients  $c_i$  and  $d_i$  values, which are believed to contain satellite and local surface information, are determined by the linear relationship between the daily average of cloud index  $n_{avg}$  and ( $s/S_o$ ) values for the 12 months of a year for all locations. They are given in Appendix A.

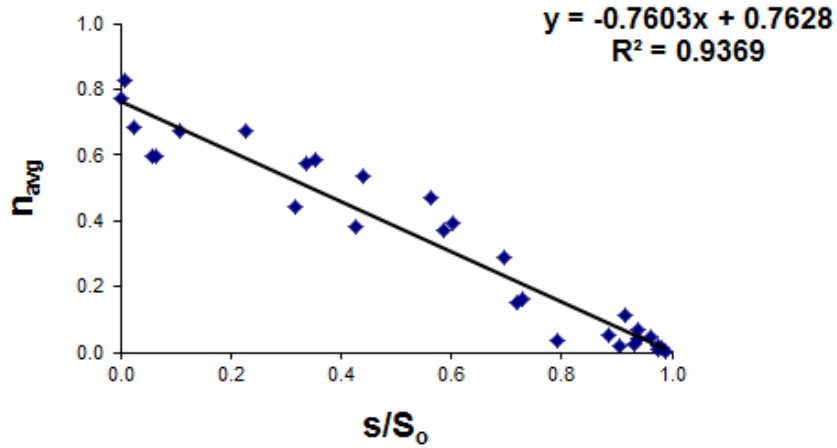


**Figure 4.4** Regression analysis between the daily average of cloud index  $n_{avg}$  and sunshine duration fraction ( $s/S_0$ ) for the month of April 2004 in Ankara.

Using equations (3.17) and (4.8) the daily values of a surface irradiation estimation equation  $H_{CAI}$  can be obtained as follows:

$$K = \frac{H_{CAI}}{H_0} = \alpha_i \left( d_i - c_i \frac{s}{S_0} \right) + \beta_i \quad (4.9)$$

where  $\alpha_i$  and  $\beta_i$  are the regression constants (Appendix A) for a location where the data of ground measured solar irradiation  $H$  is available while  $c_i$  and  $d_i$  are the constants for a location of similar climate where only bright sunshine hour  $s$  data are available (Appendix A).

#### 4.4.1 Implementation of the $H_{CAI}$ Model to the Neighbors

Neighboring stations were selected by taking climate and distance into account, and proposed model  $H_{CAI}$  was applied to this station using the coefficients of its neighbor. In this way, the applicability of the model was tested by using it for neighboring stations. The symbol used for the letter procedure is  $H_{CAI_n}$ . As mentioned before, the subscript  $n$  shows that the coefficients of the neighboring station were used in the estimation model. For comparisons, the analyses were carried out for all the locations and obtained results are discussed in Chapter 5.

#### 4.5 Combined approach by Using Simple Physical Base ( $H_{CA2}$ )

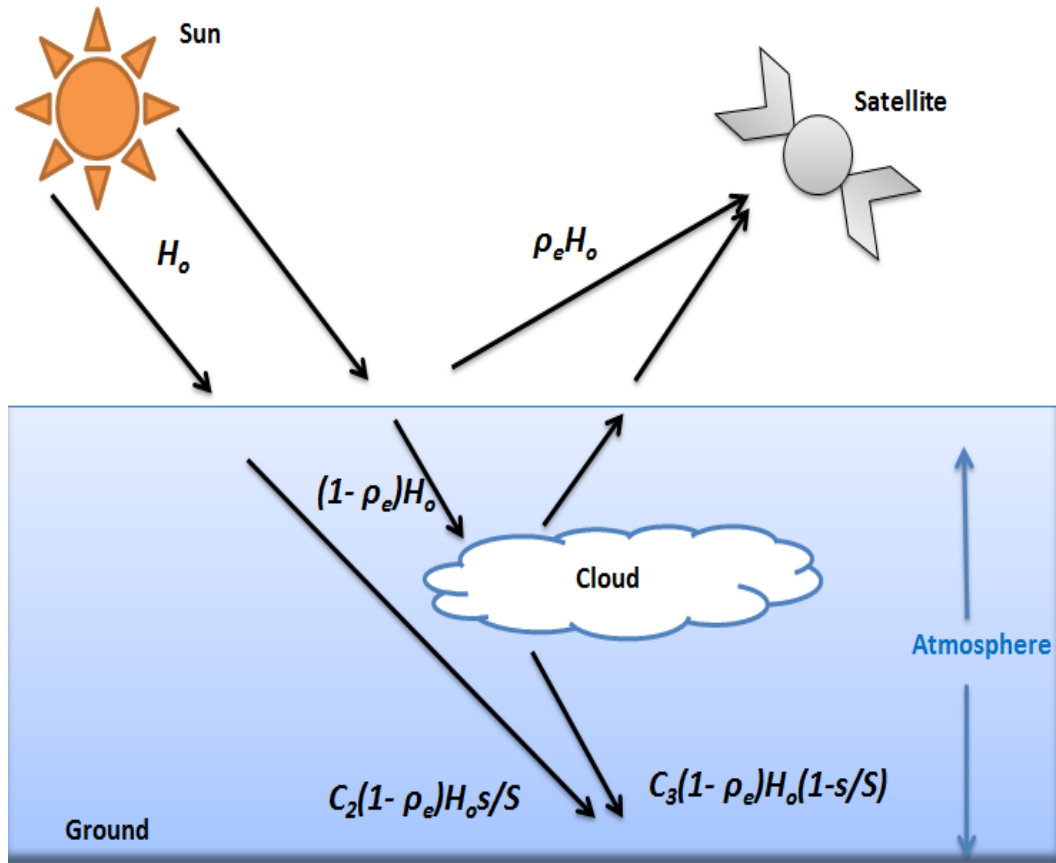
Instantaneous solar irradiance on the Earth surface is mainly determined by the dynamic behavior and the constituents of the atmosphere. That is, Atmospheric parameters are effective in the transmission of the solar irradiation through the atmosphere. If spectral averages of these parameters are used one can reach simple physical equations for the solar irradiance transmitted by the atmosphere. However in solar energy applications integrated and/or averaged values of solar irradiance are used. One can assume that after integration and averaging procedure the form of the obtained physical expressions do not change [45]. In such a consideration one should obviously define new effective atmospheric parameters. We used above assumption for a physical derivation of a functional form between solar irradiation and;  $s/S$  and  $n$  below.

Fig. 4.5 gives a representation of solar irradiation entering to the atmosphere and reaching the Earth, which we will use to explain our physical approach to construct the new correlation. With the above mentioned assumption, we can start with the daily solar irradiation on a horizontal surface  $H_0$ . If the effective reflection of the clouds-atmosphere-ground is  $\rho_e$ , the reflected amount to satellite detector is  $\rho_e H_0$  and the remaining solar irradiation is  $(1-\rho_e)H_0$ . Effective reflection  $\rho_e$  is directly related to the cloud index  $n_{avg}$  derived from satellite imagery. This relation in a simple form can be written as:

$$\rho_e = C_0 + C_1 n_{avg} \quad , \quad (4.10)$$

A fraction  $s/S_0$  of the remaining solar irradiation will pass through the atmosphere in the clear time period while  $(1-s/S_0)$  fraction will pass during cloudy sky. One can consider that the part during clear sky period as  $[C_2(1-\rho_e)(s/S)]H_0$ , and that of the part during cloud sky conditions as  $[C_3(1-\rho_e)(1-s/S)]H_0$ . The constants  $C_2$  and  $C_3$  can be thought as effective atmospheric properties. Adding them up together we obtain solar irradiation reaching the Earth as:

$$K = \frac{H}{H_0} = [C_2(1-\rho_e)(s/S)] + [C_3(1-\rho_e)(1-s/S)] \quad (4.11)$$



**Figure 4.5** Schematic representation of the daily global solar irradiation passing through the Earth's atmosphere to the ground.

This is the main equation for the new combined approach and using Eqn. (4.10), it can be re-arranged in terms of four multiple regression coefficients related to  $C_0$ ,  $C_1$ ,  $C_2$  and  $C_3$ . This equation then reads:

$$K = \frac{H_{CA2}}{H_0} = A_0 + A_1 n_{avg} + A_2 \frac{S}{S} + A_3 \frac{S}{S} n_{avg} \quad . \quad (4.12)$$

This is the form of our new equation. Applying multiple regression analysis, four dimensionless regression coefficients  $A_0$ ,  $A_1$ ,  $A_2$  and  $A_3$  are obtained for each station. The locations considered in this analysis together with the calculated correlation coefficients are given in Table 4.1.



**Table 4.1** Multiple regression coefficients  $A_0$ ,  $A_1$ ,  $A_2$  and  $A_3$  for all selected stations.

Selected Stations	$A_0$	$A_1$	$A_2$	$A_3$
Ankara/Turkey	0.388	-0.268	0.327	0.093
Afyon/Turkey	0.441	-0.282	0.279	0.234
Sinop/Turkey	0.238	-0.039	0.505	0.012
Bursa/Turkey	0.345	-0.212	0.371	0.222
Braunschweig/Germany	0.423	-0.360	0.231	0.393
Bremen/Germany	0.398	-0.350	0.252	0.498
Chemnitz/Germany	0.329	-0.186	0.341	0.354
Norderney/Germany	0.369	-0.294	0.290	0.395
Fichtelberg/Germany	0.352	-0.187	0.360	0.250
Wittenberg/Germany	0.300	-0.165	0.340	0.396
Potsdam/Germany	0.392	-0.307	0.273	0.384
Görlitz/Germany	0.387	-0.257	0.306	0.328
Zinnwald/Germany	0.288	-0.064	0.470	0.218
Dresden-Klotzsche /Germany	0.424	-0.316	0.276	0.399
Ludwigsfelde/Germany	0.405	-0.292	0.268	0.350

As can be seen from Table 4.1, the coefficients for different regions usually have approximately the same values except for two stations ( $A_3$  for Ankara and  $A_1$  for Zinnwald). This may result from the possibility that different surfaces  $K(n,s/S)$  intersect/overlap for the value of ranges for independent variables  $n$  and  $s/S$  (from 0 and 1). Our findings are in agreement with this argument. To illustrate this, when  $A_3$  value was fixed at 0.200 for Ankara, the regression analysis yielded the regression parameters  $A_0=0.410$ ,  $A_1=-0.315$  and  $A_2=0.298$ . These parameters are close to that obtained for the other locations [99] and we tested these coefficients for their performances; accuracy of results was also very high.

#### 4.5.1 Implementation of $H_{CA2}$ Model to the Neighbors

In order to analyze the performance and applicability of the proposed model  $H_{CA2}$ , four calculated multiple regression coefficients for one station were used for its neighbor. The

reason for this investigation is to reveal if the coefficient of the neighbor location can be used for the estimations where there is no ground measured solar irradiation. As described before for previous approaches, the results, when the coefficients of the neighboring station are used for these estimations, is denoted by the subscript  $n$  in  $H_{CA2\_n}$ .

The results are summarized in the discussion section by using relative mean bias error (rMBE) and root mean square error (rRMSE). In addition to these error analyses, cumulative frequency distribution for daily differences and daily absolute differences for the implemented version of all proposed models are presented in Chapter 5. The results of the study suggest that among all the implemented versions of the models,  $H_{CA2\_n}$  gives the most accurate estimation [99].

## CHAPTER 5

### RESEARCH RESULTS AND DISCUSSIONS

#### 5.1 Introduction

To investigate suggested models ( $H_{model}$ ,  $H_{CA1}$  and  $H_{CA2}$ ) and  $H_m^*$ , and compare them with classical models ( $H_{sat}$ ,  $H_m$  and  $H_{Cano}$ ) as previously defined in the fourth and third sections, the data over a period of one-year for the fifteen stations was considered. Neighboring stations were specified according to the characteristics of climate and distance. The symbols used for this procedure are denoted as  $H_{m\_n}$ ,  $H_{Cano\_n}$ ,  $H_m^*_{-n}$ ,  $H_{model\_n}$ ,  $H_{CA1\_n}$  and  $H_{CA2\_n}$  where the subscript  $n$  is to show that the coefficient of the neighboring station are used in these estimations. In this section, some basic discussions about models validation, goodness of the fit and model comparisons are given. The accuracy of different models is compared using two techniques explained in section 2.6.

#### 5.2 Standard Error Analyses of Models

The rMBE and rRMSE values, which are obtained with the daily applications of the models to the same data that the regression coefficients are obtained, are presented in Fig. 5.1 (A) and (B). This only gives the goodness of the models to represent the data that it was obtained. In Fig. 5.2 (A) and (B) we present the error statistics of implantation of the models for neighboring stations for rMBE and rRMSE, respectively.

The Angström type model ( $H_m$ ), which uses ground measured data of the station in its calculation process, is more accurate than the other estimation models as expected. However, implementation of Angström models to neighboring stations, rRMSE values for some of the stations is very high (for example, rRMSE of Wittenberg is 0.29 and rRMSE of Norderney is 0.25, Fig. 5.2 (B)). rMBE values seem low but we note that this value only gives

overestimations or underestimations, and usually negative biasing are canceled by positive to yield a small rMBE. The relative MBE of all cities lies between  $-0.07$  and  $0.04$ , which is within the margin of  $\pm 0.10$ . It is seen that Angström models works only for close neighboring stations ( $H_{m_n}$  and  $H_{m_n}^*$ , in Fig. 5.2 (A)-(B)) The accuracy of the estimated global solar irradiation in this way decreased with increasing distance between the two neighboring stations as expected [69], [75].

Simple use of Cano's model ( $H_{Cano}$ ) for the fifteen selected stations showed relatively good performance with small rMBE and rRMSE. However, it did not add performance better than the hourly satellite model when the  $H_{Cano}$  correlation of a site is used at a neighboring station (see Fig. 5.2 (A)-(B)).

In the satellite derived global solar estimations, better results can be obtained with the use of the surface measurements. One of the proposed models for this purpose was  $H_{model}$  described in Chapter 4.4. In this model,  $H_{clear,A} (= (a_i + b_i) H_0$ , Eqn. 4.3) values was used instead of  $H_{clear,H} (= \sum I_{clearsky})$  of HELIOSAT. The results were good, but not better than HELIOSAT. Although the results when it is applied to the data, it is obtained (Fig. 5.1 (A)-(B)) that  $H_{model}$  have relatively better performance than  $H_{sat}$ , when it is implemented for a neighboring location their performances are quite the same ( $H_{sat}$  and  $H_{model_n}$  in Fig. 5.2 (A)-(B)). The implemented results showed that rMBE and rRMSE of  $H_{sat}$  is in between  $-0.06$  and  $0.04$  while it is  $-0.04$  and  $0.06$  for  $H_{model_n}$ . rRMSE values are in between  $0.07$  and  $0.24$  for  $H_{sat}$  and  $0.08$  and  $0.23$  for  $H_{model_n}$ . With the results obtained for  $H_{model}$ , it is verified that the use of surface information can improve the solar irradiation on the Earth's surface. This is one of important results of this thesis. It encourages for future investigations.

It seems that introducing these surface data to a simple satellite derived model (with  $1-n_{avg}$  in the widest range) is quite similar to the estimation results compared with  $H_{sat}$  in the daily base. However, the use of  $H_{clear,A}$  obtained from surface data instead of  $H_{clear,H}$  with satellite image derived daily cloud index  $n_{avg}$ , is an easier way (because there is no need to use complex calculation for hourly  $I_{clearsky}$  values and knowledge about Linke turbidity) and gives satisfactory results for daily estimations. Therefore, for the daily calculations whenever Angström coefficients can be obtained for a nearby location having similar climate, use of  $H_{model_n}$  may be preferred due to its easy procedure to apply.

Another result is the Sinop rMBE values for the satellite model. The  $H_{sat}$  model results for this location revealed that the values of rMBE unexpectedly higher than the others. This result shows that the recorded ground data might contain high errors due to shadow effect for this location [109]. It might be an important conclusion that the satellite results can be

used to check the accuracy and reliability of surface measured solar irradiation especially when the data of location has metadata problems.

The first combined model ( $H_{CA1}$ ) was basically the use the relation between  $s/S_0$  and  $n$ . It has hoped that a further improvement can be established for daily values. The results showed that the approach produce highly accurate estimations of data that it was developed ( $H_{CA1}$ , Fig. 5.1 (A)-(B)). This verifies the goodness of the procedure of obtaining the model expressions between  $H/H_0$  and,  $n$  and  $s/S_0$ . From Fig. 5.1 (A), rMBE values are in between -0.02 and 0.02. Similarly, from Fig. 5.1 (A) rRMSE values are also very low, in between 0.07 and 0.15. Implementation of this model to a neighboring station also produces good results. The results are between -0.04 and 0.06 for rMBE and between 0.09 and 0.22 for rRMSE. Therefore, we can conclude that this model (or  $H_{CA2}$  as we will discuss next) can be used instead of Angström equations of a nearby location.

It seems that the model  $H_{CA2}$  (which has a physical base) puts a little improvement on  $H_{CA1}$ , in the implementation to neighboring stations. However it must be verified by using data from different locations. The result of implementing the coefficients  $A_0$  to  $A_3$  of a location to a neighboring location has good performance. rMBE value ranges in -0.05 to 0.05 ( $H_{CA2_n}$  in Fig. 5.2 (A)) quite similar to  $H_{CA1}$ , but rRMSE values varies in a smaller range of 0.06 to 0.15, which is a considerable reduction.

For all stations relative MBE, relative RMSE, MBE and RMSE values are given in the in Appendix C.

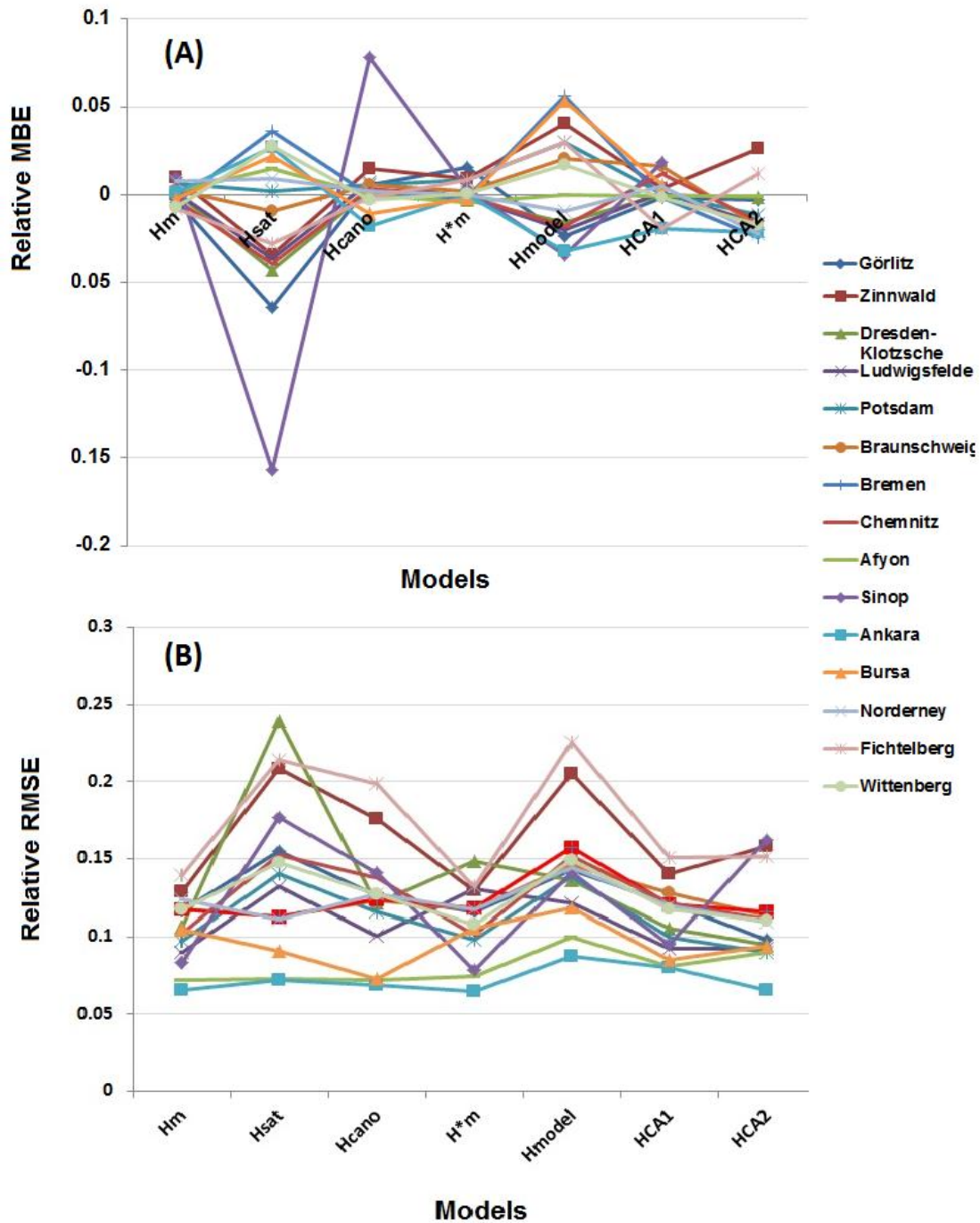
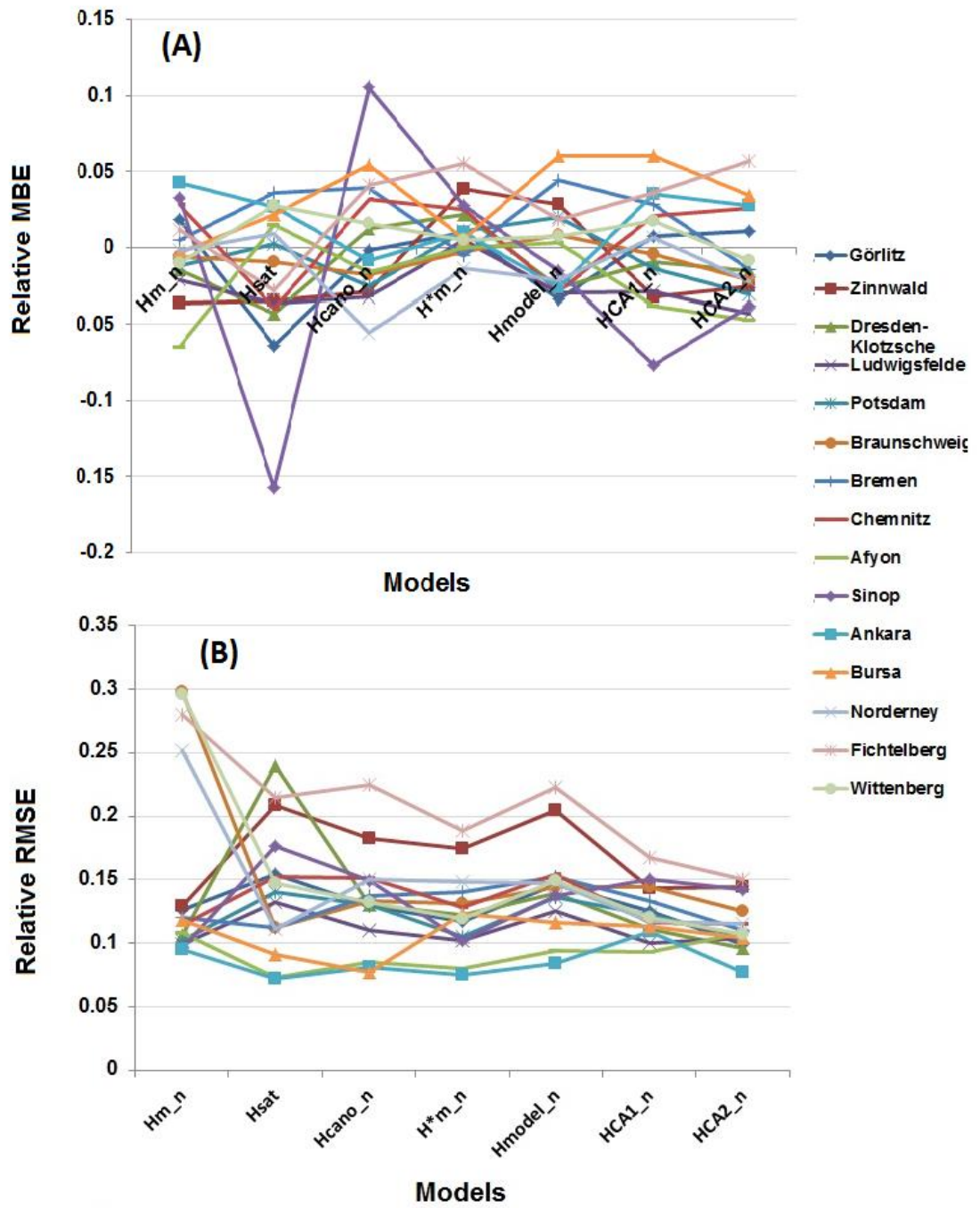


Figure 5.1 (A) Monthly relative MBE and (B) monthly relative RMSE among calculated models and ground measurement of daily global solar irradiation data for the fifteen selected stations for one year. The values were applied to the same location that the models are constructed.



**Figure 5.2** Monthly relative MBE (A) and Monthly relative RMSE (B) among implementation of calculated models and ground measurement of daily global solar radiation data for the fifteen selected stations for one year. Implementation results of to the neighboring stations.

### 5.3 Cumulative Distribution of the Differences for the Models

We exclude the data of Bursa and Sinop due to their metadata problems. This was mentioned before [109] and can be seen in Figs. 5.1 and 5.2. We also exclude  $H_{m\_n}^*$  and  $H_{model\_n}$  as they perform same as  $H_m$  and  $H_{sat}$ .

As it has been mentioned earlier, nearest neighbor implementation constitutes the simplest method of estimating radiation at a given point from an existing measuring site. We used the cumulative distribution of differences as a comparison method to distinguish good models for the estimation of daily solar irradiation. This method has been tested using the implemented version of models in the neighboring stations which ground data are lacking. The performances of five procedures ( $H_{sat}$ ,  $H_{m\_n}$ ,  $H_{Cano\_n}$ ,  $H_{CA1\_n}$ , and  $H_{CA2\_n}$ ) are compared in Figs. 5.3 (A) and 5.3 (B) with the cumulative frequency of daily difference and daily absolute difference values.

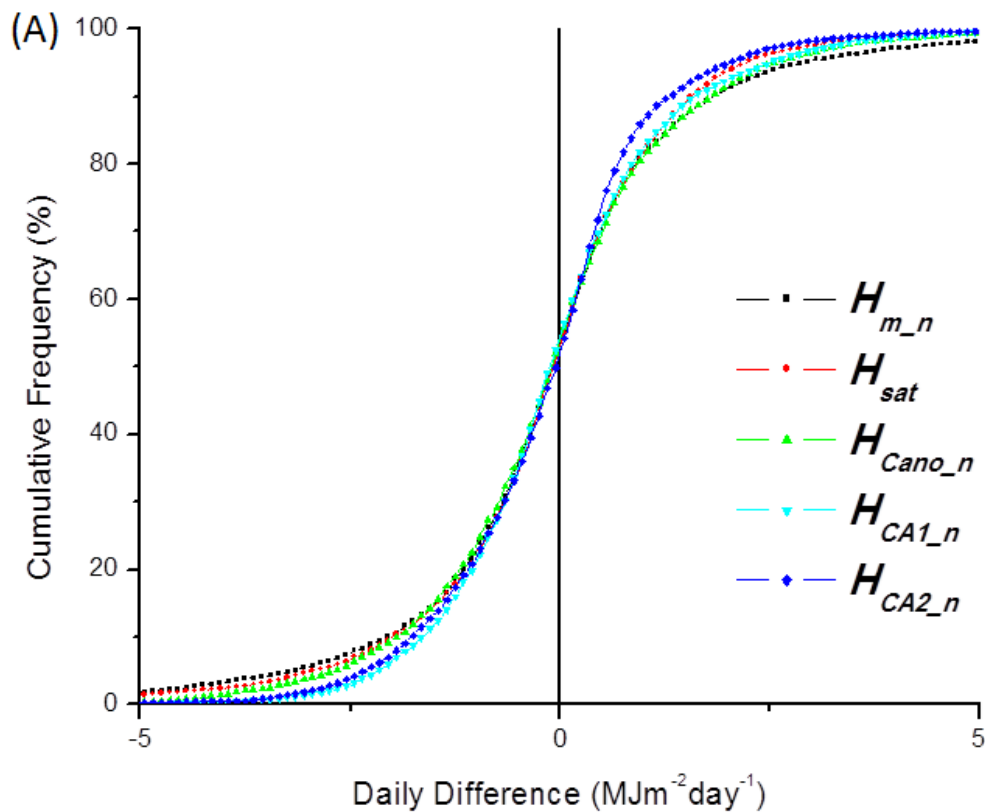


**Figure 5.3 (A)** Cumulative frequency for the daily differences value of the daily differences for a year and for all the models and locations.



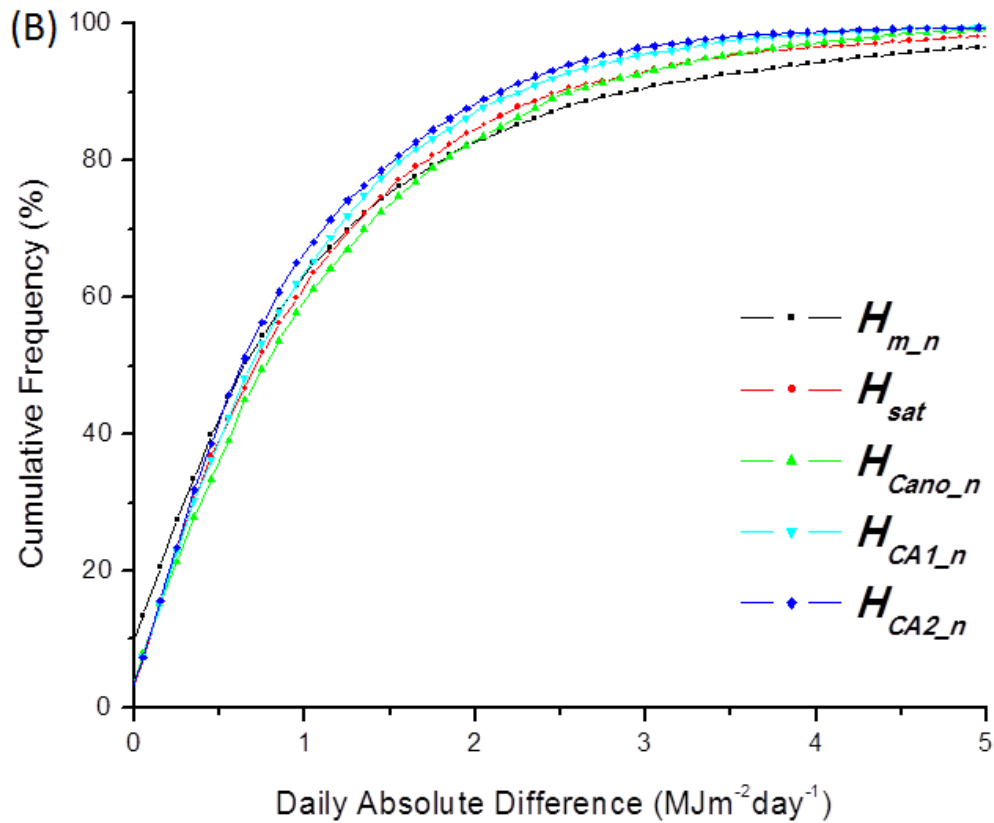


**Figure 5.3 (B)** Cumulative frequency for the absolute value of the daily differences for a year and for all the models and locations.

In the figures the x-axis shows the daily differences in Fig. 5.3 (A), and it is the absolute value of the daily difference in Fig. 5.3 (B). In addition, the y-axis represents the percentage of the cumulative frequency in both Figs. 5.3 (A) and 5.3 (B). The point to be considered when interpreting Fig. 5.3 (A), if the difference between estimated and measured values is very close to the line  $x=0$ , the performance of estimation model is better. On the other hand, in Fig. 5.3 (B), a closer curve to the y-axis shows a good performance for the solar irradiation estimated model.

It can be clearly observed that in Fig. 5.3 (A), the daily cumulative frequency function for daily difference showed slightly better results for  $H_{CA2_n}$  and  $H_{CA1_n}$ . Almost all daily values were estimated with the deviation of less than  $\pm 2.5$  MJ/m<sup>2</sup>day. Cumulative frequency of daily absolute difference is presented in Fig. 5.3 (B). It is seen that  $H_{CA2_n}$  is the best performing model and followed by  $H_{CA1_n}$ . 97% of the daily estimated values with proposed models approximately have an error of less than 2.5 MJ/m<sup>2</sup>day. But  $H_{sat}$  yielded 92% of the

estimates with a deviation of less than 2.5 MJ/m<sup>2</sup>day.  $H_{m_n}^*$  and  $H_{model_n}$  models have relative RMSE cumulative frequency values somewhat lower than the others. For example, for the implemented version of Angström model,  $H_{m_n}$ , only 90% of the daily absolute difference values fall into the range less than 2.5 MJ/m<sup>2</sup>-day. Therefore, the combined models  $H_{CA2_n}$  and  $H_{CA1_n}$  can be utilized to estimate daily global solar irradiation instead of Angström type linear regressions of a nearby location. A last note about the case of  $H_{CA2_n}$  and  $H_{CA1_n}$  is that to use them,  $s$  data of a nearby station is needed.

A final discussion is on the Gueymard's proposal [106] of using a calculated  $H_{clear,H}$  instead of  $H_0$  in Angström-Prescott equation that it would increase the performance. In contrast to this proposal, using  $H_{clear,H}$  ( $=\Sigma I_{clear}$ ) instead of HELIOSAT did not result an improvement on Angström-Prescott equation ( $H_{m_n}$  and  $H_{m_n}^*$ ). However, we should note that further analysis is required to reach a concrete conclusion.

## CHAPTER 6

### CONCLUSIONS

It is known that high-accuracy solar irradiation estimation is very important for all kinds of solar energy applications and also for the climate change studies. For this purpose, satellite images have been commonly used in the last decade to obtain spatially continuous solar irradiation maps. In addition, the ground measured bright sunshine duration, with data source of nearly 100 years, is an extremely important source of information for the estimation of global solar irradiation. In this thesis, we aimed to combine satellite-based values of daily cloud index and the surface measurements of bright sunshine hours to increase the accuracy of the estimations of daily global solar irradiation. The daily values of the proposed models ( $H_{model}$ ,  $H_{CA1}$  and  $H_{CA2}$ ) and the daily values of the familiar equation of Angström ( $H_m$ , and  $H_m^*$ ) the daily global solar irradiation derived from the satellite ( $H_{sat}$ ) and the daily version of simple model that Cano first proposed ( $H_{Cano}$ ) are compared. In addition, implementation of these models for the neighbouring stations ( $H_{m_n}^*$ ,  $H_{model_n}$ ,  $H_{CA1_n}$ ,  $H_{CA2_n}$ ,  $H_{m_n}$  and  $H_{Cano_n}$ ) is also studied in details.

We firstly note that we tried also different forms and chosen the best performing combined forms. Secondly, we tested the models by using a number of different statistical error analysis and chosen to present only the two of these comparison methods.

Validation of all models for predicting daily solar irradiation has been performed by using the statistical errors of relative MBE and RMSE. According to the obtained results, the Angström method ( $H_m$ ) has been found to be the most accurate model for the prediction of daily global solar irradiation on horizontal surfaces for selected stations. However, global solar irradiation ground data that are necessary for the Angström method for most parts of the world are not available, and this method does not seem very applicable for distant places where ground irradiation data are lacking.

Another important result of the presented proposed combined models are quite satisfactory for daily prediction and gives better estimates than all the studied models in terms of the above mentioned standard error analysis (see in Chapter 5). Moreover, global solar irradiation estimation can be carried out easily and more accurately by using the proposed models of the thesis ( $H_{model}$ ,  $H_{CA1}$  and  $H_{CA2}$ ), without complex calculations, such as Linke turbidity, direct and diffuse irradiation. Furthermore, a measurement of the daily duration of bright sunshine hour, which requires values for the calculation of proposed models, is more common than the global solar irradiation ground data all over the world [45].

In order to analyze the implemented version of all models to the neighboring stations, the cumulative frequency function was used for the daily difference and the daily absolute difference values (Figs. 5.3 (A) and (B)). Of the two applied models which use sunshine duration data and cloud index information together,  $H_{CA1_n}$  and  $H_{CA2_n}$  are more accurate than Angström type equations ( $H_{m_n}$ ) and direct application of HELIOSAT ( $H_{sat}$ ). The other models using only satellite information (daily cloud index) had similar trend line values ( $H_{sat}$  and  $H_{Cano_n}$ ) in the cumulative frequency analyses. The results of the study suggest that among all the models' implemented versions,  $H_{CA2_n}$  is the most accurate prediction procedure with the smallest cumulative frequency of daily difference and daily absolute difference values.

In addition, a single equation was obtained using the data of 10 locations, 9 in Germany and one in Turkey for the second combined approach  $H_{CA2}$ . This regression equation was obtained as:

$$K = H / H_0 = 0.352 - 0.225n_{avg} + 0.333\frac{S}{S} + 0.334n_{avg}\frac{S}{S} \quad . \quad (6.1)$$

This expression can be useful for locations where only the data of bright sunshine hour and satellite derived cloud index exist. Eqn. (6.1) was tested using the data of remaining three locations (Bremen, Görlitz and Afyon data were not taken in obtaining this equation) and the results were the best in comparison to the other models [110]. Therefore, Eqn. (6.1) can be used for locations where the data of  $n$  and  $s$  are available, at least for the locations having similar climates to those ten locations.

In order to illustrate the usability of proposed models and Angström type models, three hypothetical stations (points,  $A$ ,  $B$  and  $C$ ) are selected on the ground as schematically shown in Fig. 6.1. Point  $A$  is selected as a reference station, and it has ground measurement of daily global solar irradiation ( $H$ ), bright sunshine duration ( $s$ ) and satellite derived cloud index

( $n$ ) as available data. On the other hand, station  $B$  has  $s$  and  $n$ , and station  $C$  has only cloud index  $n$  as available data. Depending on the available data sets, Fig.6.1 illustrates which models can be applied to the stations  $B$  and  $C$ . Additionally, selected stations, their distances, available data, and models coefficients that can be obtained with this data are summarized in this diagram. The coefficients of the proposed models for the estimation of daily solar irradiation for the stations  $B$  and  $C$  are shown in the rectangular boxes in Fig. 6.1 which are mainly obtained from the data of reference station  $A$ .

As mentioned before, the Angström model is found as the most accurate model for the prediction of daily global solar irradiation on horizontal surfaces. Thereby,  $H_{m_n}$  should be used for the estimation of daily global solar irradiation especially for the locations which are very close (up to ~50 km) and also having similar climate to the reference station ( $A$ ) [69], [75], [99]. We should suggest that, within this distance, combined models can also be used. However, to obtain an accurate estimation of global solar irradiation using Angström type correlation, climate and/or altitude of the stations should be taken into account. For instance, in our study, four stations (Norderney, Fichtelberg, Braunschweig and Wittenberg of Germany) have high altitudes or different climate types. If Angström model is used for these stations with the coefficient of nearby locations, the results are quite unsatisfactory as can be inferred from Fig. 5.2 (A)-(B) ( $H_{m_n}$ ).

From Fig. 6.1, it can be seen that station  $B$  is a distant neighbor to  $A$  (more than 50 km ).  $H_{CA1}$  and  $H_{CA2}$  of this thesis should be used to estimate daily global solar irradiation for the neighbouring station ( $B$ ) which has daily bright sunshine hours and daily cloud index values. This is one of the most important outcome of the present study.

For station  $C$ , where only satellite derived cloud index  $n$  data exist, if the climate types are the same for  $A$  and  $C$  stations, we can propose the use of the model  $H_{model}$  for the daily calculations as it is easier to utilize than satellite model such as HELIOSAT formalism. On the other hand, if satellite images are available, use of HELIOSAT should be suggested for estimation of hourly global solar irradiation and also for daily considerations, for the stations having similar climatic characteristics of Europe all over the world.

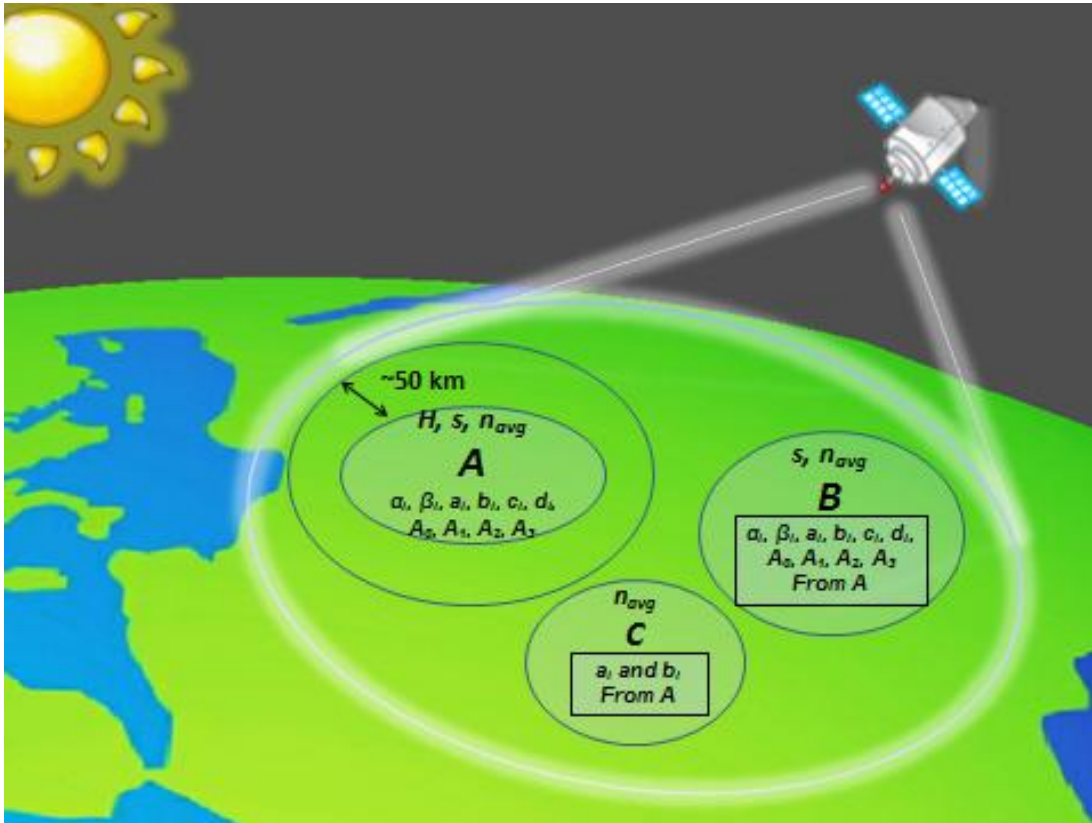


**Figure 6.1** Schematic representation for the proposed models (Location *A* have all three data, location *B* have  $s/S_0$  and  $n_{avg}$ , location *C* only have  $n_{avg}$ ).

It is then acceptable to claim that use of HELIOSAT or other remote sensing estimation models for global solar irradiation is more efficient than using the Angström type correlations with the coefficients obtained by the data of a location which have different climatologic or geographic characteristics of the selected point or which are at long distance from the selected point (longer than about 50 km).

It is known that the first generation satellites (MFG) and the old satellites models, which are not capable of unraveling the snow covered areas with clouds reflections, fail especially in winter seasons [111], [112]. Fig. 6.2 illustrates the comparison of the satellite model (HELIOSAT) and ground measured data for Erzincan in clear days with land area having snow coverage, as example. It is seen that the results of satellite model estimation is lower in clear days which the surface is covered by snow. This situation is verified using snow depth and bright sunshine hours measured at those days.

The second generation satellites (MSG), with 12 channels and high resolutions, currently uses to differentiate the snow coverage from clouds and to increase the estimation accuracy. However, the determination of snow procedure from satellite images needs complex computational procedure with their spectral channels. The models presented in this study can easily be extended in snow detection. In further studies, the accuracy of global solar irradiation estimation can be enhanced by adding a simple procedure about determining the days having clear sky and with snow coverage land surface into the proposed models. Such a procedure can be carried out by using the surface data of bright sunshine hour and snow depth and, satellite derived cloud index. Here in this thesis we only describe a method of applying such a procedure. However, to extend this method and to achieve an accurate algorithm, one needs extended data from different stations and larger number of such specific days.

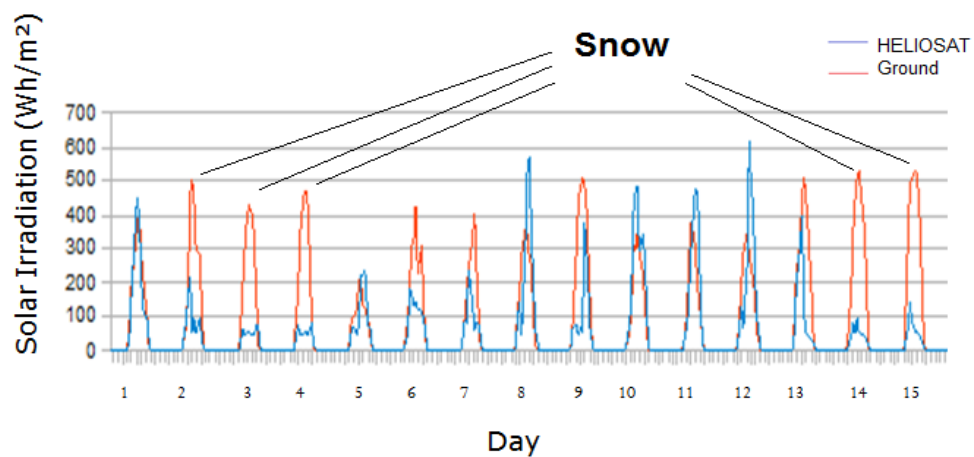


**Figure 6.2.** Comparison of the satellite model (HELIOSAT) and ground measured data for snowy days in Erzincan, 01-15.01.2006.

Consequently, present research results encourage the linking surface measurements to satellite imagery based cloud index  $n$  for the accurate estimation of global solar irradiation. The modeling approaches presented in this thesis can further be applied for hourly and/or monthly average daily global solar irradiation estimation with the use of other ground data. It is noteworthy to state that the use of Angström type regression coefficients of a nearby location may not always give satisfactory results to replace the satellite-based HELIOSAT model. We concluded that selected stations should have similar climatic parameters of the

station from which the regression coefficients are derived and should be close enough. For future studies, long and short-term satellite image data can be used together with the surface measured data to estimate more accurate solar irradiation values. The formalism of present thesis can be applied to hourly data of bright sunshine hours to combine with remote sensing, and this may lead new hourly satellite formalisms like HELIOSAT but without complex calculations such as Linke turbidity of the site of interest. This is an important future topic of investigation.



## REFERENCES

- [1] J. D. Tarpley, "Estimating incident solar radiation at the surface from geostationary satellite data.," *Journal of App. Meteor.*, vol. 18, pp. 1172–1181, 1979.
- [2] J. A. Martinez-Lozano, F. Tena, J. E. Onrubia, and J. de la. Rubia, "The historical evolution of the Angström formula and its modifications: review and bibliography," *Agric. For. Meteorol.*, no. 33, pp. 109–128, 1984.
- [3] H. Ogelman, A. Ecevit, and E. Tasdemiroglu, "A new method for estimating solar radiation from bright sunshine data," *Solar Energy*, vol. 33, pp. 619–625, 1984.
- [4] B. G. Akinoglu and A. Ecevit, "Construction of a quadratic model using modified Angström coefficients to estimate global solar-radiation.," *Solar Energy*, vol. 45, pp. 85–92, 1990.
- [5] H. Beyer, C. Costanzo, and D. Heinemann, "Modifications of the HELIOSAT procedure for irradiance estimates from satellite images," *Solar Energy*, vol. 56, pp. 207–212, 1996.
- [6] A. Hammer, D. Heinemann, C. Hoyer, R. Kuhlemann, E. Lorenz, R. Müller, and H. G. Beyer, "Solar energy assessment using remote sensing technologies," *Remote Sensing of Environment*, vol. 86, no. 3, pp. 423–432, Aug. 2003.
- [7] "Solar Radiation Terminology," 2012. [Online]. Available: <http://www.soda-is.com/eng/education/terminology.html>.
- [8] R. G. Allen, L. S. Pereira, D. Raes, and M. Smith, "Crop evapotranspiration - Guidelines for computing crop water requirements - FAO Irrigation and drainage paper," Rome, 1998.
- [9] "Solar Radiaiton Basics," *University of Oregon*, 2012. [Online]. Available: <http://solardat.uoregon.edu/SolarRadiationBasics.html>.
- [10] J. Tovar, F. . Olmo, F. . Batlles, and L. Alados-Arboledas, "Dependence of one-minute global irradiance probability density distributions on hourly irradiation," *Energy*, vol. 26, no. 7, pp. 659–668, Jul. 2001.
- [11] H. Suehrcke, "On the relationship between duration of sunshine and solar rdiation on the Earth's surface: Angström's equation revisited," *Solar Energy*, vol. 68, pp. 417–425, 2000.
- [12] J. A. Duffie and W. A. Beckman, *Solar engineering of thermal processes*, Third ed. New York: John Wiley and Sons, 2006.

- [13] S. S. Chandel, "Estimation of hourly solar radiation on horizontal and inclined surfaces in Western Himalayas," *Smart Grid and Renewable Energy*, vol. 02, no. 01, pp. 45–55, 2011.
- [14] L. T. Wong and W. K. Chow, "Solar radiation model," *Applied Energy*, vol. 69, no. 3, pp. 191–224, Jul. 2001.
- [15] S. Cros, D. Mayer, and L. Wald, "The availability of irradiation data, IEA-PVPS Task 2," 2004.
- [16] M. D. King, C. L. Parkinson, K. C. Partington, and R. G. Williams, Eds., *Our changing planet*. Cambridge University, 2007.
- [17] M. C. Peel, B. L. Finlayson, and T. A. McMahon, "Updated world map of the Köppen-Geiger climate classification," *Hydrology and Earth System Sciences*, vol. 11, pp. 1633–1644, 2007.
- [18] G. T. Threwartha, *An introduction to climate*. New York: McGraw Hill, 1968.
- [19] L. Dahlgren, *IEA. International energy agency handbook of methods of estimating solar radiation-Task 5*. Stockholm, Sweden: The Swedish Meteorological and Hydrological Institute, 1984.
- [20] "Extracted from google maps," 2012. [Online]. Available: <http://maps.google.com/>.
- [21] J. E. Hay, "Calculation of monthly mean solar radiation for horizontal and inclined surfaces.," *Solar Energy*, vol. 23, pp. 301–307, 1979.
- [22] T. Muneer, *Solar radiation and daylight models*, Second. Amsterdam and New York: Elsevier, 2004.
- [23] D. Heinemann, "Energy meteorology - Lecture notes; Postgraduate programme, Renewable Energy." Oldenburg, 2000.
- [24] "Solar Book On-Line Solar Study Reference," 2012. [Online]. Available: <http://www.solarbook.co.uk/solar-panel-physics.html>.
- [25] "World Meteorological Organization," 2012. [Online]. Available: [http://www.wmo.int/pages/index\\_en.html](http://www.wmo.int/pages/index_en.html).
- [26] J. W. Spencer, "Fourier series representation of the position of the sun," *Search*, vol. 2, pp. 172–172, 1971.
- [27] M. Iqbal, "An introduction to solar radiation; PhD thesis," Academic Press, Toronto, 1983.
- [28] N. Robinson, *Solar Radiation*. Elsevier, 1966.
- [29] M. J. Fisk and H. C. W. Anderson, *Introduction to solar technology*. Addison-Wesley publishing, 1982.
- [30] P. N. Cheremisinoff and T. C. Regino, "Principle and applications of solar energy; SAO/NASA ADS Physics Abstract Service," Ann Arbor Science, 1978.
- [31] L. E. Mavromatidis, M. el Mankibi, P. Michel, and M. Santamouris, "Numerical estimation of time lags and decrement factors for wall complexes including Multilayer

- Thermal Insulation, in two different climatic zones,” *Applied Energy*, vol. 92, pp. 480–491, 2012.
- [32] T. Guide, “Atmosphere,” *Annals of Improbable Research*, vol. 7, no. 2, pp. 7–7, 01-Mar-2001.
- [33] “Atmospheric Composition,” 2012. [Online]. Available: <http://aerial.evsc.virginia.edu/~jlm8h/class/fund1.html>.
- [34] T. W. Schlatter, “Atmospheric Composition and Vertical Structure,” *Environmental Impact and Manufacturing*, vol. 6, pp. 1–54.
- [35] C. McLinden, “Types of scattering,” *Department of Earth System Science*. Irvine, 1999.
- [36] G. Bruno, “Classical theory of rayleigh and raman scattering,” vol. 8, 2002.
- [37] “Earth’s Radiation Budget Facts.,” 2012. [Online]. Available: <http://science-edu.larc.nasa.gov/EDDOCS/images/Erb/components2.gif>.
- [38] G. W. Paltridge and C. M. Platt, *Radiative processes in meteorology and climatology*. Amsterdam and New York: Elsevier Scientific Publishing Company, 1976.
- [39] F. Kasten and A. Young, “Revised optical air mass tables and approximations formula.,” *Applied Optics*, vol. 28, pp. 4735–4738, 1989.
- [40] Ş. Cristina, “Estimating clear sky solar global radiation using clearness index , for Braşov Urban area,” in *3rd International Conference on Maritime and Naval Science and Engineering*, 2009, no. January 2006, pp. 150–153.
- [41] D. Cano, J. Monget, M. Albuison, H. Guillard, N. Regas, and L. Wald, “A method for the determination of the global solar radiation from meteorological satellite data.,” *Solar Energy*, vol. 37, pp. 31–39, 1986.
- [42] A. Hammer, “Anwendungsspezifische solarstrahlungsinformationen aus meteosat-daten.,” Carl von Ossietzky University of Oldenburg, 2000.
- [43] “Direct, Diffuse and Global Solar Radiation,” *The Eppley Laboratory*, 2012. [Online]. Available: <http://www.eppleylab.com/radiation.htm>.
- [44] T. E. Kissell, *Introduction to solar principles*. Pearson Education, 2012.
- [45] B. G. Akinoglu, “Recent Advances in the Relations Between Bright Sunshine Hours and Solar Irradiation,” in *Modeling solar radiation at the earth surface*, V. Badescu, Ed. Verlag Berlin Heidelberg: Springer, 2008, pp. 115–143.
- [46] A. C. Gueymard and D. R. Myers, “Solar radiation measurement: Progress in radiometry for improved modelling,” in *Modeling solar radiation at the earth surface*, V. Badescu, Ed. Heidelberg: Springer, 2008, pp. 1–25.
- [47] “Direct Industry VirtualExpo group,” 2012. [Online]. Available: <http://www.directindustry.com>.
- [48] “Pyranometer; Sutron Corporation,” 2012. [Online]. Available: <http://www.sutron.com>.
- [49] “Geneq Instruments Scientifiques,” 2012. [Online]. Available: <http://www.geneq.com>.

- [50] Y. B. L. Hinssen and W. H. Knap, "Comparison of pyrometric and pyrhelimetric methods for determination of sunshine duration," *Journal of Atmospheric and Oceanic Technology*, vol. 24, pp. 835–846, 2007.
- [51] E. Good, "Estimating daily sunshine duration over the UK from geostationary satellite data," *Weather*, vol. 65, no. 12, pp. 324–328, 2010.
- [52] Japan Meteorological Agency, "Measurement of sunshine duration and solar radiation," in *Lecture notes on WMO Training Workshop, revised version*, 2010.
- [53] "Sunshine duration recorder." [Online]. Available: <http://www.weathershop.co.uk>.
- [54] "Sunshine Duration CSD 3." [Online]. Available: <http://www.kippzonen.com>.
- [55] J. Page, "Algorithms for the Satel-Light program," in *Technical report for the Satel-Light program*, 1996.
- [56] D. Dumortier, "Modelling global and diffuse horizontal irradiances under cloudless skies with different turbidity," in *Technical report for the Daylight II project*, 1995.
- [57] B. Bourges, *Yearly variations of the Linke turbidity factor, climatic data handbook of Europe*. Dordrecht: Kluwer Academic Publishers, 1992, pp. 61–64.
- [58] R. W. Mueller, H. G. Beyer, S. Cros, K. F. Dagestad, D. Dumortier, R. Kuhlemann, J. A. Olseth, G. Piernavieja, C. Reise, M. Schroedter, A. Skartveit, and L. Wald, "The use of MSG data within a new type of solar irradiance calculation scheme," in *2002 EUMETSAT Meteorological Satellite Conference*, 2002.
- [59] F. Kasten, "The Linke turbidity factor based on improved values of the integral Rayleigh optical thickness," *Solar Energy*, vol. 56, pp. 239–244, 1996.
- [60] D. Dumortier, "The satel-light model of turbidity variations in Europe," in *Report for the 6th Satel-Light meeting*, 1998.
- [61] J. Polo, L. F. Zarzalejo, L. Martin, A. A. Navarro, and R. Marchante, "Estimation of daily Linke turbidity factor by using global irradiance measurements at solar noon," *Solar Energy*, vol. 83, pp. 1177–1185, 2009.
- [62] M. Cucumo, A. De Rosa, V. Ferraro, D. Kaliakatsos, and V. Marinelli, "Experimental validation of correlations for the estimation of beam and diffuse components of hourly radiation," in *61st ATI National Congress International Session "Solar Heating and Cooling"*, 1999, vol. 76, no. 3.
- [63] M. Cucumo, D. Kaliakatsos, and V. Marinelli, "A calculation method for the estimation of the Linke turbidity factor," *Renewable Energy*, vol. 19, pp. 249–258, 2000.
- [64] V. Applasamy, "Methods for deriving solar radiation from satellite data in Malaysia," in *IEEE Symposium on Business, Engineering and Industrial Applications (ISBEIA)*, 2011, pp. 208–213.
- [65] "Weather satellite system," 2012. [Online]. Available: <http://www.automatedsciences.com>.
- [66] "EUMETSAT," 2012. [Online]. Available: <http://www.eumetsat.int>.

- [67] "Satellite Technology and Orbits; Satellite Applications for Gescience Education; University of Wisconsin; SAGE Course Unit: Remote Sensing," 2012. [Online]. Available: [http://cimss.ssec.wisc.edu/sage/remote\\_sensing/lesson1/intro.html](http://cimss.ssec.wisc.edu/sage/remote_sensing/lesson1/intro.html).
- [68] "Oracle ThinkQuest Education Foundation; Astronomy Satellites - Library," 2012. [Online]. Available: <http://library.thinkquest.org/C005271F/astronomy.html>.
- [69] A. Zelenka, R. Perez, R. Seals, and D. Renne, "Effective accuracy of satellite-derived hourly irradiances.," *Theoretical and Applied Climatology*, vol. 62, pp. 199–207, 1999.
- [70] K.-F. Dagestad, "Estimating global radiation at ground level from satellite images, PhD Thesis," University of Bergen., 2005.
- [71] "Weather satellites," 2012. [Online]. Available: <http://www.n2yo.com/satellites/?c=3>.
- [72] J. Polo, L. F. Zarzalejo, and Lourdes Ramirez, "Solar radiation derived from satellite images," in *Modeling Solar Radiation at the Earth's Surface*, V. Badescu, Ed. Verlag Berlin Heidelberg: Springer, 2008, p. 449.
- [73] P. R. Bevington and D. K. Robinson, *Data reduction and error analysis for the physical sciences*, 3rd ed. New York: McGraw Hill, 2002.
- [74] J. A. Davies and D. C. McKay, "Evaluation of selected models for estimating solar radiation on horizontal surfaces," *Solar Energy*, vol. 43, no. 3, pp. 153–168, 1989.
- [75] R. Perez, R. Seals, and A. Zelenka, "Comparing satellite remote sensing and ground network measurements for the production of site/time specific irradiance data," *Solar Energy*, vol. 60, no. 2, pp. 89–96, Feb. 1997.
- [76] J. Almorox, M. Benito, and C. Hontoria, "Estimation of monthly Ångström–Prescott equation coefficients from measured daily data in Toledo, Spain," *Renewable Energy*, vol. 30, pp. 931–936, 2005.
- [77] E. Eftimie, "Beam Horizontal Irradiance Simulation for Brasov Urban Area - Clear Sky Model," *Advances in Environmental & Geological Science and Engineering*, pp. 224–229, 2009.
- [78] M. Marcu and V. A. Huber, "Thermal stratification in the depression area forms, Depression effect, Phytogeographical implications," *Anale I.C.A.S.*, vol. 46, pp. 141–150, 1986.
- [79] K. Yang, T. Koike, and B. Ye, "Improving estimation of hourly, daily, and monthly solar radiation by importing global data sets," *Agricultural and Forest Meteorology*, vol. 137, pp. 43–55, 2006.
- [80] M. Trnka, Z. Žalud, J. Eitzinger, and M. Dubrovský, "Global solar radiation in Central European lowlands estimated by various empirical formulae," *Agricultural and Forest Meteorology*, vol. 131, no. 1–2, pp. 54–76, Jul. 2005.
- [81] R. W. Muellera, K. F. Dagestad, P. Ineichenc, M. Schroedter-Homscheidtd, S. Crose, D. Dumortierf, R. Kuhlemanng, J. A. Olsethb, G. Piernaviejah, C. Reisei, L.

- Walde, and D. Heinemann, "Rethinking satellite-based solar irradiance modelling The SOLIS clear-sky module," *Remote Sensing of Environment*, vol. 91, pp. 160–174, 2004.
- [82] B. G. Akinoglu, "On the random measurements of robitzsch pyranographs," in *World Renewable Energy Conferance II*, 1992, pp. 2726–2730.
- [83] M. Noia, C. F. Ratto, and R. Festa, "Solar irradiance estimation from geostationary satellite data: I. Statistical models," *Solar Energy*, vol. 51, pp. 449–456, 1993.
- [84] M. Noia, C. F. Ratto, and R. Festa, "Solar irradiance estimation from geostationary satellite data: II. Physical models," *Solar Energy*, vol. 51, pp. 457–465, 1993.
- [85] F. Wang, Z. Mi, S. Su, and H. Zhao, "Short-term solar irradiance forecasting model based on artificial neural network using statistical feature parameters," *Energies*, vol. 5, no. 5, pp. 1355–1370, May 2012.
- [86] H. H. Kimball, "Variations in the total and luminous solar radiation with geographical position in the United States," *Monthly Weather Review*, vol. 47, pp. 769–793, 1919.
- [87] A. Angström, "Solar and terrestrial radiation.," *Quart. J. Roy. Met. Soc.*, vol. 50, pp. 121–126, 1924.
- [88] J. A. Prescott, "Evaporation from a water surface in relation to solar radiation.," *Trans.Roy.Soc.S.A.*, vol. 64, pp. 114–118, 1940.
- [89] V. Badescu, "Correlations to estimate monthly mean daily solar global irradiation: application to Romania," *Energy*, vol. 24, no. 10, pp. 883–893, Oct. 1999.
- [90] T. H. Vonder Haar and J. S. Ellis, "Solar energy micro-climate as determined from satellite observations," *Optics in Solar Energy*, vol. 68, pp. 18–28, 1975.
- [91] J. S. Ellis and T. H. Vonder Haar, "Solar radiation reaching the ground determined from meteorological satellite data," in *3. Conference on Atmospheric Radiation*, 1978.
- [92] R. Perez, K. Moore, F. Rd, S. Wilcox, D. Renné, C. Blvd, and A. Zelenka, "Forcasting solar radiation-Preliminary evaluation of an approach based upon the national forecast data base," *Solar Energy*, vol. 81, no. 6, pp. 809–812, 2007.
- [93] Y. Özdemir, "Uydu tabanlı kuadratik model ile Türkiye'de güneş radyasyonu dağılımının belirlenmesi," Gazi Üniversitesi, 2012.
- [94] B. Aksoy, S. Ener Rusen, and B. G. Akinoglu, "A simple correlation to estimate global solar irradiation on a horizontal surface using METEOSAT satellite images," *Turkish J. Eng. Env. Sci.*, vol. 35, pp. 125–137, 2011.
- [95] Ener Rusen, S., A. Hammer, and B. G. Akinoglu, "Using sunshine duration and satellite images to estimate daily solar irradiation on horizontal surface.," in *ISES Solar World Congress 2011, Kassel, Germany, 2011*.
- [96] S. Ener Rusen, A. Hammer, and B. G. Akinoglu, "Coupling satellite images with surface measurements of bright sunshine hours to estimate daily solar irradiation on horizontal surface.," *Renewable Energy*, vol. 55, pp. 212–219, 2013.

- [97] M. Girodo, R. W. Mueller, and D. Heinemann, "Influence of three-dimensional cloud effects on satellite derived solar irradiance estimation—First approaches to improve the Heliosat method," *Solar Energy*, vol. 80, no. 9, pp. 1145–1159, Sep. 2006.
- [98] C. Gautier, G. Diak, and S. Masse, "A simple physical model to estimate incident solar radiation at the surface from GOES satellite data," *J. Appl. Meteorol.*, vol. 19, pp. 1005–1012, 1980.
- [99] S. Ener Rusen, A. Hammer, and B. G. Akinoglu, "Estimation of daily global solar irradiation by coupling the ground measurements of bright sunshine hours to the satellite imagery," *Energy (submitted)*, 2013.
- [100] H. M. Diagne, M. David, P. Lauret, and J. Boland, "Solar irradiation forecasting : state-of-the-art and proposition for future developments for small-scale insular grids," in *ASES Resource Application Division Newsletter*, 2012, pp. 1–8.
- [101] J. A. Olseth and A. Skartveit, "Solar irradiance, sunshine duration and daylight illuminance derived from ME- TEOSAT data for some european sites," *Theoretical and Applied Climatology*, vol. 69, pp. 239–252, 2001.
- [102] B. G. Akinoglu, "A review of sunshine-based models used to estimate monthly average global solar radiation.," *Renewable Energy*, vol. 1, pp. 479–497, 1991.
- [103] F. Bason, "Linke ' s turbidity factor applied to worldwide global horizontal irradiance measurements," no. August 2006, pp. 2–7, 2007.
- [104] J. Remund, "Aerosol optical depth and Linke turbidity climatology," in *Description for final report of IEA SHC Meteotest*, 2009, p. Task 36.
- [105] L. Diabaté, G. Moussu, and L. Wald, "Description of an operational tool for determining global solar radiation at ground using geostationary satellite images.," *Solar Energy*, vol. 42, no. 3, pp. 201–207, 1989.
- [106] A. C. Gueymard, "Direct solar transmittance and irradiance predictions with broadband models, Part II: validation with high quality measurements.," *Solar Energy*, vol. 74, pp. 381–395, 2003.
- [107] A. C. Gueymard, "Direct solar transmittance and irradiance with broadband models. Part I: detailed theoretical performance assessment," *Solar Energy*, vol. 74, pp. 355–379, 2003.
- [108] H. M. Kandirmaz, "A model for the estimation of the daily global sunshine duration from meteorological geostationary satellite data," *International Journal of Remote Sensing*, vol. 27, no. 22, pp. 5061–5071, Nov. 2006.
- [109] B. Aksoy, "Personnal communications," 2010.
- [110] B. G. Akinoglu and S. Ener Rusen, "Combining the satellite imagery with bright sunshine hours: A review," *Journal of Renewable and Sustainable Energy (submitted)*, 2013.

- [111] S. Ener Rusen and B. G. Akinoglu, "Türkiye'nin doğusunda güneş enerjisinin uydu verileriyle izlenmesi," in *III. Ulusal Güneş ve Hidrojen Enerjisi Kongresi; tebliğ*, 2012, p. Özet Kitabı s. 12.
- [112] M. D. R. De Wildt, G. Seiz, and A. Grün, "Snow mapping using multi-temporal meteosat-8 data," in *EARSeL proceedings*, 2006, pp. 18–31.



## APPENDIX A

**Table A.1.** Monthly values of  $a_i$ ,  $\beta_i$ ,  $c_i$  and  $d_i$  coefficients

Selected Stations	Months Constants	Months											
		1	2	3	4	5	6	7	8	9	10	11	12
Ankara (Turkey)	$-a_i$	-	0.75	0.69	0.71	0.69	0.68	0.60	0.62	0.57	0.49	0.63	0.61
	$\beta_i$	-	0.71	0.72	0.75	0.75	0.73	0.73	0.72	0.72	0.66	0.67	0.62
	$-c_i$	-	0.71	0.81	0.76	0.75	0.68	0.83	0.76	0.99	0.78	0.78	0.79
	$d_i$	-	0.68	0.77	0.76	0.79	0.73	0.84	0.77	1.00	0.75	0.72	0.67
Afyon (Turkey)	$-a_i$	-	0.36	-	-	0.60	0.69	0.56	0.50	0.73	0.61	0.54	0.60
	$\beta_i$	-	0.51	-	-	0.74	0.74	0.72	0.72	0.72	0.71	0.67	0.62
	$-c_i$	-	0.68	-	-	0.64	0.57	0.71	0.68	0.55	0.71	0.81	0.85
	$d_i$	-	0.65	-	-	0.65	0.58	0.69	0.69	0.52	0.69	0.79	0.58
Braunschweig (Germany)	$-a_i$	0.73	0.60	0.71	0.75	0.64	-	0.64	0.61	0.71	0.73	0.59	0.57
	$\beta_i$	0.65	0.60	0.73	0.75	0.70	-	0.71	0.65	0.68	0.70	0.60	0.58
	$-c_i$	0.49	0.69	0.54	0.72	0.72	-	0.63	0.67	0.57	0.56	0.64	0.52
	$d_i$	0.57	0.59	0.62	0.71	0.73	-	0.66	0.64	0.58	0.62	0.61	0.58
Wittenberg (Germany)	$-a_i$	0.63	0.52	0.70	0.70	0.62	0.65	0.60	0.71	0.66	0.58	0.57	0.52
	$\beta_i$	0.63	0.59	0.71	0.70	0.69	0.69	0.68	0.68	0.66	0.63	0.57	0.53
	$-c_i$	0.50	0.63	0.65	0.53	0.68	0.62	0.63	0.65	0.58	0.64	0.58	0.56
	$d_i$	0.60	0.75	0.68	0.58	0.68	0.63	0.68	0.64	0.58	0.65	0.60	0.60
Görlitz (Germany)	$-a_i$	0.73	0.83	0.75	0.68	0.62	0.68	0.63	0.70	0.74	0.68	0.70	0.65
	$\beta_i$	0.73	0.90	0.86	0.74	0.72	0.75	0.72	0.73	0.72	0.72	0.66	0.65
	$c_i$	0.51	0.57	0.75	0.61	0.66	0.75	0.64	0.73	0.60	0.63	0.70	0.65
	$d_i$	0.62	0.73	0.59	0.65	0.55	0.74	0.63	0.59	0.58	0.64	0.62	0.52

Dresden- Klotzsche	$-a_i$	0.78	0.87	0.77	0.72	0.64	0.65	0.66	0.68	0.72	0.71	0.70	0.73
(Germany)	$\beta_i$	0.74	0.89	0.82	0.76	0.73	0.73	0.73	0.70	0.73	0.74	0.67	0.71
	$-c_i$	0.59	0.65	0.68	0.61	0.64	0.66	0.68	0.65	0.65	0.63	0.62	0.73
	$d_i$	0.64	0.72	0.71	0.64	0.66	0.69	0.70	0.68	0.63	0.67	0.64	0.64
Ludwigsfelde	$-a_i$	0.62	0.67	0.66	0.70	0.71	0.55	0.59	0.74	0.64	0.68	0.63	0.54
(Germany)	$\beta_i$	0.63	0.71	0.73	0.73	0.74	0.71	0.72	0.73	0.70	0.69	0.62	0.57
	$c_i$	0.61	0.67	0.67	0.60	0.63	0.68	0.66	0.66	0.64	0.59	0.61	0.69
	$d_i$	0.65	0.70	0.70	0.64	0.67	0.70	0.69	0.67	0.66	0.64	0.62	0.67
Bremen	$-a_i$	0.66	0.64	0.57	0.74	0.72	0.67	0.68	0.72	0.67	0.71	0.68	0.61
(Germany)	$\beta_i$	0.61	0.63	0.65	0.71	0.71	0.70	0.69	0.69	0.66	0.66	0.62	0.56
	$-c_i$	0.60	0.82	0.78	0.81	0.66	0.65	0.55	0.65	0.56	0.65	0.70	0.68
	$d_i$	0.65	0.72	0.71	0.71	0.66	0.66	0.59	0.62	0.56	0.63	0.64	0.70
Norderney	$-a_i$	0.65	0.67	0.74	0.69	0.68	0.68	0.57	0.65	0.64	0.64	0.60	0.59
(Germany)	$\beta_i$	0.61	0.66	0.73	0.71	0.71	0.73	0.71	0.69	0.67	0.67	0.61	0.58
	$-c_i$	0.66	0.75	0.59	0.76	0.56	0.70	0.72	0.66	0.62	0.62	0.59	0.75
	$d_i$	0.71	0.69	0.64	0.73	0.62	0.74	0.78	0.67	0.63	0.69	0.65	0.73
Potsdam	$-a_i$	0.62	0.74	0.66	0.79	0.70	0.57	0.69	0.66	0.69	0.66	0.67	0.56
(Germany)	$\beta_i$	0.60	0.73	0.69	0.74	0.71	0.70	0.72	0.67	0.70	0.69	0.62	0.57
	$-c_i$	0.62	0.63	0.69	0.63	0.64	0.69	0.57	0.68	0.61	0.61	0.58	0.73
	$d_i$	0.67	0.73	0.70	0.64	0.68	0.70	0.61	0.65	0.60	0.65	0.61	0.67
Chemnitz	$-a_i$	0.86	0.95	0.78	0.71	0.70	0.72	0.73	0.68	0.72	0.66	0.65	0.67
(Germany)	$\beta_i$	0.73	1.00	0.86	0.73	0.72	0.73	0.73	0.68	0.70	0.72	0.62	0.63
	$-c_i$	0.34	0.45	0.49	0.66	0.64	0.62	0.64	0.63	0.62	0.64	0.66	0.54
	$d_i$	0.52	0.75	0.71	0.68	0.64	0.65	0.66	0.64	0.62	0.70	0.64	0.63
Fichtelberg	$-a_i$	0.97	0.74	1.07	-	0.87	0.64	0.75	0.85	0.91	0.66	0.65	0.64
(Germany)	$\beta_i$	0.88	0.79	1.01	-	0.79	0.69	0.72	0.73	0.76	0.69	0.70	0.70
	$-c_i$	0.39	0.48	0.40	-	0.65	0.66	0.63	0.59	0.55	0.66	0.64	0.56
	$d_i$	0.65	0.61	0.64	-	0.67	0.66	0.67	0.61	0.57	0.68	0.69	0.70
Zinnwald	$-a_i$	1.12	0.84	0.82	0.65	0.63	0.61	0.62	0.82	0.83	0.72	0.75	0.85
(Germany)	$\beta_i$	0.86	0.95	0.92	0.73	0.70	0.71	0.71	0.75	0.75	0.75	0.68	0.80
	$-c_i$	0.78	0.77	0.87	0.87	0.84	0.94	0.80	0.87	0.88	0.78	0.89	1.11
	$d_i$	0.70	0.69	0.79	0.80	0.82	0.90	0.76	0.80	0.78	0.75	0.78	0.84

## APPENDIX B

**Table B.1.**  $a, b, a^*, b^*, R^2$  values of  $K$  vs  $s/S$  and  $K^*$  vs  $s/S$

<i>Ankara</i>	<i>month</i>	<i>A</i>	<i>b</i>	<i>a+b</i>	<i>K - s/S</i>	<i>R<sup>2</sup></i>	<i>a*</i>	<i>b*</i>	<i>a*+b*</i>	<i>K*- s/S</i>	<i>R<sup>2</sup></i>
	1	0,19	0,54	0,73	0,73		0,29	0,79	1,08	0,74	
	2	0,19	0,63	0,82	0,89		0,29	0,89	1,18	0,91	
	3	0,18	0,62	0,80	0,97		0,25	0,87	1,12	0,97	
	4	0,19	0,61	0,80	0,96		0,27	0,86	1,12	0,96	
	5	0,19	0,57	0,77	0,96		0,26	0,79	1,05	0,95	
	6	0,21	0,52	0,74	0,91		0,29	0,72	1,01	0,91	
	7	0,23	0,53	0,76	0,92		0,31	0,73	1,04	0,92	
	8	0,18	0,58	0,76	0,95		0,25	0,81	1,06	0,95	
	9	0,19	0,57	0,76	0,63		0,26	0,79	1,04	0,64	
	10	0,27	0,46	0,73	0,87		0,35	0,64	0,99	0,89	
	11	0,21	0,56	0,77	0,88		0,31	0,76	1,06	0,87	
	12	0,21	0,56	0,77	0,88		0,30	0,85	1,15	0,89	
	All	0,20	0,56	0,76	0,93		0,30	0,76	1,06	0,91	
<i>Bursa</i>	<i>month</i>	<i>A</i>	<i>b</i>	<i>a+b</i>	<i>K - s/S</i>	<i>R<sup>2</sup></i>	<i>a*</i>	<i>b*</i>	<i>a*+b*</i>	<i>K*- s/S</i>	<i>R<sup>2</sup></i>
	1	0,17	0,66	0,83	0,75		0,25	0,98	1,23	0,74	
	2	0,20	0,57	0,77	0,79		0,28	0,84	1,12	0,81	
	3	0,30	0,53	0,83	0,83		0,43	0,76	1,19	0,83	
	4	0,20	0,60	0,80	0,91		0,29	0,87	1,15	0,91	
	5	0,19	0,57	0,75	0,94		0,26	0,77	1,03	0,93	
	6	0,20	0,56	0,76	0,93		0,27	0,77	1,05	0,93	
	7	0,23	0,50	0,73	0,87		0,32	0,70	1,02	0,87	
	8	0,15	0,62	0,77	0,95		0,21	0,87	1,08	0,96	
	9	0,16	0,65	0,81	0,75		0,23	0,88	1,12	0,74	
	10	0,25	0,48	0,73	0,76		0,34	0,67	1,01	0,81	
	11	0,18	0,57	0,75	0,89		0,26	0,81	1,07	0,88	
	12	0,28	0,44	0,72	0,49		0,43	0,66	1,09	0,49	
	All	0,22	0,54	0,76	0,85		0,33	0,73	1,06	0,81	
<i>Afyon</i>	<i>month</i>	<i>A</i>	<i>b</i>	<i>a+b</i>	<i>K - s/S</i>	<i>R<sup>2</sup></i>	<i>a*</i>	<i>b*</i>	<i>a*+b*</i>	<i>K*- s/S</i>	<i>R<sup>2</sup></i>
	1	0,25	0,47	0,72	0,63		0,38	0,70	1,08	0,63	
	2	0,26	0,33	0,59	0,74		0,39	0,52	0,91	0,76	
	3	0,00	0,00	0,00	0,00		0,00	0,00	0,00	0,00	
	4	0,00	0,00	0,00	0,00		0,00	0,00	0,00	0,00	

5	0,33	0,42	0,75	0,83	0,46	0,58	1,04	0,83			
6	0,30	0,47	0,77	0,94	0,42	0,65	1,07	0,94			
7	0,35	0,39	0,74	0,84	0,49	0,55	1,04	0,84			
8	0,32	0,41	0,73	0,92	0,44	0,52	0,96	0,93			
9	0,30	0,46	0,76	0,75	0,41	0,64	1,05	0,76			
10	0,27	0,46	0,73	0,92	0,36	0,63	0,99	0,93			
11	0,28	0,43	0,71	0,81	0,39	0,59	0,98	0,78			
12	0,28	0,56	0,84	0,77	0,42	0,82	1,24	0,76			
All	0,27	0,46	0,73	0,87	0,41	0,62	1,03	0,85			
<i>Sinop</i>	<i>month</i>	<i>a</i>	<i>b</i>	<i>a+b</i>	<i>K - s/S</i>	<i>R<sup>2</sup></i>	<i>a*</i>	<i>b*</i>	<i>a*+b*</i>	<i>K*- s/S</i>	<i>R<sup>2</sup></i>
1	0,34	0,65	0,99	0,87	0,52	1,03	1,55	0,86			
2	0,32	0,53	0,85	0,85	0,50	0,80	1,30	0,84			
3	0,26	0,62	0,88	0,90	0,38	0,89	1,27	0,90			
4	0,29	0,57	0,86	0,93	0,42	0,84	1,26	0,93			
5	0,27	0,64	0,91	0,93	0,37	0,89	1,26	0,93			
6	0,32	0,55	0,87	0,93	0,44	0,77	1,21	0,93			
7	0,26	0,59	0,85	0,94	0,36	0,83	1,19	0,94			
8	0,25	0,60	0,85	0,93	0,36	0,86	1,22	0,93			
9	0,29	0,57	0,86	0,93	0,40	0,81	1,21	0,92			
10	0,34	0,52	0,86	0,92	0,47	0,74	1,21	0,92			
11	0,33	0,57	0,90	0,93	0,49	0,81	1,30	0,90			
12	0,32	0,72	1,04	0,93	0,46	1,12	1,58	0,93			
All	0,31	0,55	0,86	0,90	0,47	0,77	1,24	0,85			
<i>Braunschweig</i>	<i>month</i>	<i>a</i>	<i>b</i>	<i>a+b</i>	<i>K - s/S</i>	<i>R<sup>2</sup></i>	<i>a*</i>	<i>b*</i>	<i>a*+b*</i>	<i>K*- s/S</i>	<i>R<sup>2</sup></i>
1	0,16	0,54	0,70	0,92	0,25	0,85	1,10	0,92			
2	0,18	0,68	0,86	0,81	0,29	1,06	1,35	0,80			
3	0,23	0,57	0,80	0,89	0,35	0,86	1,21	0,88			
4	0,20	0,66	0,86	0,87	0,29	0,95	1,24	0,87			
5	0,22	0,52	0,74	0,94	0,31	0,75	1,06	0,94			
6	0,00	0,00	0,00	0,00	0,00	0,00	0,00	0,00			
7	0,27	0,46	0,73	0,90	0,39	0,64	1,03	0,90			
8	0,23	0,54	0,77	0,79	0,33	0,78	1,11	0,79			
9	0,26	0,47	0,73	0,92	0,37	0,67	1,04	0,92			
10	0,21	0,55	0,76	0,91	0,31	0,80	1,11	0,91			
11	0,17	0,62	0,79	0,88	0,27	1,02	1,29	0,91			
12	0,18	0,51	0,69	0,89	0,30	0,84	1,14	0,89			
All	0,20	0,55	0,75	0,89	0,31	0,79	1,10	0,89			
<i>Bremen</i>	<i>month</i>	<i>a</i>	<i>b</i>	<i>a+b</i>	<i>K - s/S</i>	<i>R<sup>2</sup></i>	<i>a*</i>	<i>b*</i>	<i>a*+b*</i>	<i>K*- s/S</i>	<i>R<sup>2</sup></i>
1	0,16	0,53	0,69	0,88	0,28	0,92	1,20	0,89			
2	0,16	0,63	0,79	0,84	0,26	0,97	1,23	0,84			
3	0,22	0,56	0,78	0,87	0,34	0,85	1,19	0,85			
4	0,17	0,72	0,89	0,90	0,25	1,05	1,30	0,90			

5	0,23	0,53	0,76	0,96	0,32	0,77	1,09	0,96			
6	0,25	0,49	0,74	0,95	0,36	0,70	1,06	0,95			
7	0,27	0,45	0,72	0,96	0,38	0,64	1,02	0,96			
8	0,21	0,61	0,82	0,82	0,30	0,88	1,18	0,82			
9	0,26	0,44	0,70	0,90	0,38	0,64	1,02	0,90			
10	0,20	0,59	0,79	0,88	0,30	0,85	1,15	0,88			
11	0,15	0,75	0,90	0,81	0,24	1,21	1,45	0,82			
12	0,14	0,60	0,74	0,83	0,25	1,06	1,31	0,83			
All	0,19	0,56	0,75	0,88	0,30	0,82	1,12	0,87			
<hr/>											
<i>Chemnitz</i>	<i>month</i>	<i>A</i>	<i>b</i>	<i>a+b</i>	<i>K - s/S</i>	<i>R<sup>2</sup></i>	<i>a*</i>	<i>b*</i>	<i>a*+b*</i>	<i>K*- s/S</i>	<i>R<sup>2</sup></i>
	1	0,23	0,41	0,64	0,93		0,40	0,71	1,11	0,93	
	2	0,26	0,50	0,76	0,82		0,38	0,76	1,14	0,83	
	3	0,27	0,54	0,81	0,87		0,41	0,82	1,23	0,87	
	4	0,22	0,55	0,77	0,92		0,32	0,80	1,12	0,92	
	5	0,24	0,48	0,72	0,90		0,33	0,69	1,02	0,90	
	6	0,24	0,48	0,72	0,94		0,34	0,67	1,01	0,94	
	7	0,22	0,49	0,71	0,97		0,32	0,68	1,00	0,97	
	8	0,21	0,53	0,74	0,93		0,31	0,75	1,06	0,93	
	9	0,23	0,49	0,72	0,92		0,31	0,67	0,98	0,92	
	10	0,23	0,47	0,70	0,92		0,34	0,67	1,01	0,91	
	11	0,19	0,45	0,64	0,81		0,31	0,75	1,06	0,83	
	12	0,18	0,43	0,61	0,88		0,31	0,75	1,06	0,88	
	All	0,23	0,47	0,70	0,88		0,35	0,67	1,02	0,88	
<hr/>											
<i>Nordemey</i>	<i>month</i>	<i>B</i>	<i>a</i>	<i>a+b</i>	<i>K - s/S</i>	<i>R<sup>2</sup></i>	<i>b*</i>	<i>a*</i>	<i>a*+b*</i>	<i>K*- s/S</i>	<i>R<sup>2</sup></i>
	1	0,14	0,55	0,69	0,94		0,22	0,85	1,07	0,95	
	2	0,18	0,64	0,82	0,88		0,27	0,93	1,20	0,87	
	3	0,20	0,61	0,80	0,93		0,29	0,91	1,20	0,92	
	4	0,19	0,62	0,80	0,90		0,28	0,91	1,19	0,90	
	5	0,23	0,51	0,74	0,91		0,32	0,71	1,02	0,92	
	6	0,20	0,56	0,77	0,93		0,27	0,75	1,02	0,93	
	7	0,25	0,47	0,73	0,92		0,33	0,62	0,95	0,92	
	8	0,23	0,52	0,75	0,87		0,31	0,72	1,03	0,87	
	9	0,23	0,48	0,71	0,91		0,36	0,74	1,10	0,91	
	10	0,22	0,53	0,75	0,91		0,31	0,76	1,07	0,91	
	11	0,20	0,51	0,71	0,80		0,32	0,87	1,19	0,86	
	12	0,14	0,64	0,78	0,86		0,26	1,12	1,37	0,86	
	All	0,19	0,57	0,76	0,92		0,28	0,77	1,05	0,90	
<hr/>											
<i>Fichtelberg</i>	<i>month</i>	<i>A</i>	<i>b</i>	<i>a+b</i>	<i>K - s/S</i>	<i>R<sup>2</sup></i>	<i>a*</i>	<i>b*</i>	<i>a*+b*</i>	<i>K*- s/S</i>	<i>R<sup>2</sup></i>
	1	0,23	0,51	0,74	0,95		0,35	0,76	1,11	0,95	
	2	0,34	0,42	0,76	0,76		0,48	0,64	1,12	0,79	
	3	0,33	0,51	0,84	0,72		0,47	0,71	1,18	0,70	
	4	0,00	0,00	0,00	0,00		0,00	0,00	0,00	0,00	

5	0,20	0,59	0,79	0,89	0,27	0,80	1,07	0,89
6	0,23	0,56	0,79	0,95	0,30	0,75	1,05	0,95
7	0,20	0,53	0,73	0,93	0,27	0,72	0,99	0,93
8	0,18	0,58	0,76	0,85	0,25	0,79	1,04	0,85
9	0,25	0,50	0,75	0,94	0,33	0,67	1,00	0,94
10	0,20	0,51	0,71	0,96	0,29	0,72	1,01	0,96
11	0,23	0,47	0,70	0,83	0,35	0,72	1,07	0,84
12	0,22	0,43	0,65	0,91	0,37	0,75	1,12	0,91
All	0,25	0,47	0,72	0,86	0,35	0,70	1,05	0,85

<i>Wittenberg</i>	<i>month</i>	<i>a</i>	<i>b</i>	<i>a+b</i>	<i>K - s/S</i>	<i>R<sup>2</sup></i>	<i>a*</i>	<i>b*</i>	<i>a*+b*</i>	<i>K*- s/S</i>	<i>R<sup>2</sup></i>
	1	0,21	0,49	0,70	0,86		0,33	0,77	1,10	0,84	
	2	0,19	0,64	0,83	0,82		0,29	0,97	1,26	0,82	
	3	0,23	0,56	0,79	0,85		0,33	0,84	1,17	0,85	
	4	0,23	0,55	0,78	0,84		0,34	0,80	1,13	0,84	
	5	0,24	0,51	0,75	0,95		0,33	0,73	1,07	0,95	
	6	0,25	0,48	0,73	0,96		0,35	0,66	1,02	0,96	
	7	0,26	0,44	0,70	0,91		0,37	0,62	0,99	0,91	
	8	0,21	0,57	0,78	0,82		0,30	0,82	1,12	0,82	
	9	0,26	0,46	0,71	0,93		0,36	0,66	1,02	0,93	
	10	0,25	0,45	0,70	0,88		0,37	0,67	1,04	0,88	
	11	0,21	0,50	0,71	0,88		0,34	0,85	1,19	0,87	
	12	0,18	0,57	0,75	0,87		0,32	0,98	1,30	0,85	
	All	0,22	0,51	0,73	0,90		0,33	0,72	1,06	0,88	

*Dresden-*

<i>Klotzsche</i>	<i>month</i>	<i>a</i>	<i>b</i>	<i>a+b</i>	<i>K - s/S</i>	<i>R<sup>2</sup></i>	<i>a*</i>	<i>b*</i>	<i>a*+b*</i>	<i>K*- s/S</i>	<i>R<sup>2</sup></i>
	1	0,22	0,48	0,70	0,85		0,34	0,78	1,12	0,84	
	2	0,18	0,65	0,83	0,82		0,31	0,97	1,28	0,81	
	3	0,22	0,54	0,76	0,85		0,31	0,85	1,16	0,86	
	4	0,23	0,56	0,79	0,84		0,35	0,80	1,15	0,84	
	5	0,25	0,52	0,77	0,95		0,33	0,75	1,08	0,96	
	6	0,25	0,49	0,74	0,95		0,34	0,68	1,02	0,95	
	7	0,25	0,45	0,70	0,91		0,37	0,60	0,97	0,90	
	8	0,24	0,56	0,80	0,83		0,29	0,80	1,09	0,83	
	9	0,22	0,45	0,67	0,94		0,35	0,63	0,98	0,92	
	10	0,23	0,45	0,68	0,88		0,38	0,67	1,05	0,88	
	11	0,26	0,51	0,77	0,84		0,34	0,84	1,18	0,86	
	12	0,18	0,58	0,76	0,88		0,32	0,97	1,30	0,86	
	All	0,24	0,50	0,74	0,90		0,31	0,74	1,05	0,86	

*Görlitz*

	<i>month</i>	<i>a</i>	<i>b</i>	<i>a+b</i>	<i>K - s/S</i>	<i>R<sup>2</sup></i>	<i>a*</i>	<i>b*</i>	<i>a*+b*</i>	<i>K*- s/S</i>	<i>R<sup>2</sup></i>
	1	0,23	0,48	0,71	0,85		0,34	0,75	1,09	0,84	
	2	0,20	0,65	0,85	0,83		0,31	0,96	1,27	0,82	
	3	0,24	0,54	0,78	0,85		0,32	0,83	1,15	0,85	

4	0,22	0,55	0,77	0,84	0,34	0,80	1,13	0,84			
5	0,23	0,53	0,76	0,94	0,33	0,74	1,07	0,95			
6	0,24	0,49	0,73	0,96	0,33	0,67	1,00	0,96			
7	0,28	0,43	0,71	0,95	0,36	0,65	1,01	0,91			
8	0,25	0,55	0,80	0,82	0,30	0,82	1,12	0,82			
9	0,26	0,44	0,70	0,94	0,36	0,65	1,01	0,93			
10	0,25	0,46	0,71	0,81	0,38	0,67	1,05	0,88			
11	0,23	0,52	0,75	0,82	0,35	0,81	1,16	0,87			
12	0,18	0,56	0,74	0,84	0,35	0,87	1,12	0,85			
All	0,23	0,51	0,74	0,94	0,30	0,75	1,05	0,88			
<i>Potsdam</i>	<i>month</i>	<i>A</i>	<i>b</i>	<i>a+b</i>	<i>K - s/S</i>	<i>R<sup>2</sup></i>	<i>a*</i>	<i>b*</i>	<i>a*+b*</i>	<i>K*- s/S</i>	<i>R<sup>2</sup></i>
1	0,19	0,50	0,69	0,87	0,87	0,34	0,78	1,12	0,84		
2	0,20	0,64	0,84	0,85	0,85	0,22	0,96	1,18	0,82		
3	0,25	0,55	0,80	0,81	0,81	0,34	0,85	1,19	0,85		
4	0,25	0,57	0,82	0,80	0,80	0,30	0,87	1,17	0,84		
5	0,24	0,53	0,77	0,91	0,91	0,33	0,75	1,08	0,95		
6	0,29	0,47	0,76	0,97	0,97	0,31	0,69	1,00	0,96		
7	0,26	0,44	0,70	0,96	0,96	0,33	0,66	0,99	0,91		
8	0,21	0,53	0,74	0,84	0,84	0,31	0,83	1,14	0,82		
9	0,26	0,48	0,74	0,93	0,93	0,36	0,64	1,00	0,93		
10	0,26	0,47	0,73	0,84	0,84	0,37	0,66	1,03	0,88		
11	0,24	0,50	0,74	0,89	0,89	0,35	0,85	1,20	0,87		
12	0,22	0,53	0,75	0,85	0,85	0,32	0,83	1,15	0,85		
All	0,20	0,51	0,71	0,95	0,95	0,33	0,74	1,07	0,88		
<i>Ludwigsfelde</i>	<i>month</i>	<i>A</i>	<i>b</i>	<i>a+b</i>	<i>K - s/S</i>	<i>R<sup>2</sup></i>	<i>a*</i>	<i>b*</i>	<i>a*+b*</i>	<i>K*- s/S</i>	<i>R<sup>2</sup></i>
1	0,22	0,50	0,72	0,85	0,85	0,30	0,73	1,03	0,86		
2	0,23	0,63	0,86	0,86	0,86	0,29	0,85	1,14	0,82		
3	0,21	0,57	0,78	0,82	0,82	0,33	0,80	1,13	0,80		
4	0,23	0,57	0,80	0,81	0,81	0,34	0,80	1,13	0,81		
5	0,24	0,48	0,72	0,97	0,97	0,33	0,76	1,09	0,97		
6	0,21	0,53	0,74	0,98	0,98	0,34	0,72	1,06	0,96		
7	0,28	0,40	0,68	0,90	0,90	0,42	0,60	1,02	0,91		
8	0,22	0,55	0,77	0,85	0,85	0,35	0,80	1,15	0,86		
9	0,24	0,48	0,72	0,95	0,95	0,36	0,70	1,06	0,93		
10	0,22	0,45	0,67	0,89	0,89	0,35	0,67	1,02	0,87		
11	0,20	0,50	0,70	0,83	0,83	0,32	0,85	1,17	0,84		
12	0,17	0,57	0,74	0,81	0,81	0,31	0,88	1,19	0,83		
All	0,25	0,51	0,76	0,88	0,88	0,29	0,77	1,06	0,88		
<i>Zinnwald</i>	<i>Month</i>	<i>A</i>	<i>b</i>	<i>a+b</i>	<i>K - s/S</i>	<i>R<sup>2</sup></i>	<i>a*</i>	<i>b*</i>	<i>a*+b*</i>	<i>K*- s/S</i>	<i>R<sup>2</sup></i>
1	0,24	0,49	0,73	0,79	0,79	0,30	0,78	1,08	0,80		
2	0,18	0,65	0,83	0,80	0,80	0,35	0,96	1,31	0,78		
3	0,23	0,53	0,76	0,77	0,77	0,33	0,85	1,18	0,80		

4	0,22	0,56	0,78	0,81	0,34	0,79	1,12	0,84
5	0,24	0,55	0,79	0,85	0,33	0,70	1,03	0,86
6	0,22	0,50	0,72	0,94	0,34	0,71	1,05	0,96
7	0,26	0,47	0,73	0,91	0,37	0,63	1,00	0,93
8	0,21	0,52	0,738	0,85	0,31	0,85	1,16	0,87
9	0,27	0,43	0,70	0,90	0,41	0,65	1,06	0,93
10	0,25	0,47	0,72	0,89	0,37	0,63	1,00	0,88
11	0,21	0,53	0,74	0,80	0,36	0,85	1,21	0,85
12	0,17	0,56	0,73	0,83	0,30	0,78	1,08	0,82
All	0,22	0,54	0,76	0,91	0,33	0,75	1,08	0,89

---



## APPENDIX C

Table C.1. Monthly relative MBE values for proposed models and selected stations

rMBE	$H_m$	$H_{sat}$	$H_{cano}$	$H^*$	$H_{model}$	$H_{CA1}$	$H_{CA2}$	$H_{m_n}$	$H_{cano_n}$	$H^*_{m_n}$	$H_{model_n}$	$H_{CA1_n}$	$H_{CA2_n}$
Görlitz	0,00	-0,06	0,01	0,02	-0,02	0,00	0,00	0,02	0,00	0,01	-0,03	0,01	0,01
Zinnwald	0,01	-0,03	0,01	0,01	0,04	0,00	0,03	-0,04	-0,03	0,04	0,03	-0,03	-0,03
Dresden-	0,00	-0,04	0,00	0,00	-0,02	0,00	0,00	-0,01	0,01	0,02	-0,03	-0,01	-0,02
Ludwigsfelde	0,00	-0,04	0,01	0,00	-0,02	0,00	-0,02	-0,02	-0,03	0,01	-0,03	-0,03	-0,04
Potsdam	0,01	0,00	0,01	0,01	0,03	0,00	-0,01	-0,01	-0,03	0,01	0,02	-0,01	-0,03
Braunschweig	0,00	-0,01	0,01	0,00	0,02	0,02	-0,02	-0,01	-0,02	0,00	0,01	0,00	-0,02
Bremen	0,00	0,04	0,00	0,00	0,06	0,00	-0,02	0,00	0,04	-0,01	0,04	0,03	-0,01
Chemnitz	0,00	-0,04	0,00	0,00	-0,02	0,01	-0,02	0,03	0,03	0,02	-0,03	0,02	0,03
Afyon	0,00	0,01	0,00	0,00	0,00	0,00	0,00	-0,07	-0,02	0,00	0,00	-0,04	-0,05
Sinop	0,01	-0,16	0,08	0,00	-0,03	0,02	-0,03	0,03	0,11	0,03	-0,02	-0,08	-0,04
Ankara	0,00	0,03	-0,02	0,00	-0,03	-0,02	-0,02	0,04	-0,01	0,01	-0,03	0,04	0,03
Bursa	0,00	0,02	-0,01	0,00	0,05	0,01	-0,03	0,00	0,05	0,01	0,06	0,06	0,04
Norderney	0,01	0,01	0,00	0,00	-0,01	0,01	-0,02	0,00	-0,06	-0,01	-0,02	0,01	-0,02
Fichtelberg	-0,01	-0,03	0,00	0,01	0,03	-0,02	0,01	0,01	0,04	0,06	0,02	0,04	0,06
Wittenberg	-0,01	0,03	0,00	0,00	0,02	0,00	-0,02	-0,01	0,02	0,01	0,01	0,02	-0,01

**Table C.2.** Monthly relative RMSE values for proposed models and selected stations

rRMSE	$H_m$	$H_{sat}$	$H_{cano}$	$H^*$	$H_{model}$	$H_{CAI}$	$H_{CA2}$	$H_{m_n}$	$H_{cano_n}$	$H^*_{m_n}$	$H_{model_n}$	$H_{CAI_n}$	$H_{CA2_n}$
Görlitz	0,12	0,15	0,13	0,12	0,14	0,12	0,10	0,13	0,13	0,12	0,15	0,13	0,10
Zinnwald	0,13	0,21	0,18	0,13	0,21	0,14	0,16	0,13	0,18	0,17	0,20	0,14	0,14
Dresden-	0,11	0,24	0,12	0,15	0,14	0,11	0,09	0,11	0,13	0,12	0,14	0,11	0,10
Ludwigsfelde	0,09	0,13	0,10	0,13	0,12	0,09	0,09	0,10	0,11	0,10	0,13	0,10	0,10
Potsdam	0,10	0,14	0,12	0,10	0,14	0,10	0,09	0,10	0,13	0,11	0,14	0,12	0,11
Braunschweig	0,12	0,11	0,12	0,12	0,15	0,13	0,11	0,30	0,13	0,13	0,14	0,14	0,13
Bremen	0,12	0,11	0,12	0,12	0,16	0,12	0,12	0,12	0,14	0,14	0,15	0,13	0,11
Chemnitz	0,10	0,15	0,14	0,10	0,15	0,12	0,11	0,11	0,15	0,13	0,15	0,12	0,12
Afyon	0,07	0,07	0,07	0,07	0,10	0,08	0,09	0,11	0,08	0,08	0,09	0,09	0,11
Sinop	0,08	0,18	0,14	0,08	0,14	0,09	0,16	0,10	0,15	0,10	0,14	0,20	0,14
Ankara	0,07	0,07	0,07	0,07	0,09	0,08	0,07	0,10	0,08	0,07	0,08	0,11	0,08
Bursa	0,10	0,09	0,07	0,11	0,12	0,09	0,09	0,12	0,08	0,12	0,12	0,11	0,11
Norderney	0,12	0,11	0,13	0,12	0,14	0,12	0,11	0,25	0,15	0,15	0,15	0,12	0,11
Fichtelberg	0,14	0,21	0,20	0,13	0,23	0,15	0,15	0,28	0,22	0,19	0,22	0,17	0,15
Wittenberg	0,12	0,15	0,13	0,11	0,15	0,12	0,11	0,30	0,13	0,12	0,15	0,12	0,11

Table C.3. Monthly MBE values for proposed models and selected stations

MBE	$H_m$	$H_{sat}$	$H_{cano}$	$H^*$	$H_{model}$	$H_{CA1}$	$H_{CA2}$	$H_{m_n}$	$H_{cano_n}$	$H^*_{m_n}$	$H_{model_n}$	$H_{CA1_n}$	$H_{CA2_n}$
Görlitz	-0,03	0,15	-0,75	0,07	-0,03	0,18	0,11	-0,27	-0,40	-0,02	0,08	-0,03	0,13
Zinnwald	0,11	-0,41	-0,38	0,16	-0,32	0,10	0,43	0,45	0,31	0,04	-0,35	0,29	-0,29
Dresden-	0,01	-0,16	-0,49	0,03	0,14	-0,03	0,25	-0,18	-0,30	-0,01	-0,11	-0,02	-0,17
Ludwigsfelde	0,02	-0,24	-0,42	0,08	-0,36	-0,02	0,06	-0,23	-0,34	0,02	-0,33	-0,19	-0,48
Potsdam	0,07	-0,13	0,03	0,06	-0,28	0,09	0,11	0,33	0,22	0,00	-0,15	-0,12	-0,33
Braunschweig	0,02	-0,06	-0,09	0,05	-0,17	0,02	-0,02	0,19	0,08	0,16	-0,04	-0,17	-0,20
Bremen	-0,04	0,05	0,35	0,00	0,38	-0,01	-0,05	0,55	0,42	-0,02	0,28	-0,24	-0,14
Chemnitz	-0,03	0,32	-0,44	0,04	0,35	-0,01	0,28	-0,20	-0,32	0,13	0,24	-0,17	0,29
Afyon	0,03	-1,16	0,27	0,00	-0,29	-0,08	0,00	0,00	0,06	-0,02	-0,68	-0,01	-0,84
Sinop	0,18	0,56	-2,75	0,75	2,09	0,06	0,48	-0,60	-0,27	0,32	-3,84	-0,28	0,79
Ankara	0,03	0,74	0,46	-0,31	-0,15	-0,01	0,17	-0,56	-0,45	-0,33	0,61	-0,37	0,48
Bursa	-0,04	-0,06	0,35	0,42	-0,43	-0,03	0,09	0,85	0,98	0,09	0,97	0,18	1,14
Norderney	0,08	-0,02	0,09	0,02	-0,56	0,00	-0,14	-0,10	-0,21	0,05	0,07	-0,22	-0,23
Fichtelberg	-0,09	0,12	-0,30	-0,01	0,44	0,09	0,60	0,32	0,19	-0,20	0,39	0,13	0,61
Wittenberg	-0,08	-0,11	0,31	-0,03	0,17	0,01	0,06	0,19	0,08	-0,02	0,19	-0,19	-0,10

Table C.4. Monthly RMSE values for proposed models and selected stations

RMSE	$H_m$	$H_{sat}$	$H_{cano}$	$H^*$	$H_{model}$	$H_{CAI}$	$H_{CA2}$	$H_{m_n}$	$H_{cano_n}$	$H^*_{m_n}$	$H_{model_n}$	$H_{CAI_n}$	$H_{CA2_n}$
Görlitz	1,36	1,47	1,79	1,46	1,50	1,35	1,35	1,65	1,70	1,41	1,45	1,13	1,15
Zinnwald	1,43	1,43	2,31	1,95	2,03	1,43	1,94	2,28	2,27	1,55	1,59	1,75	1,60
Dresden-	1,20	1,20	2,71	1,37	1,48	1,68	1,38	1,54	1,58	1,19	1,26	1,07	1,09
Ludwigsfelde	1,02	1,12	1,50	1,14	1,25	1,47	1,15	1,38	1,42	1,05	1,13	1,04	1,18
Potsdam	1,06	1,12	1,53	1,27	1,42	1,07	1,15	1,51	1,48	1,09	1,33	0,98	1,15
Braunschweig	1,11	2,81	1,06	1,16	1,25	1,11	1,24	1,37	1,36	1,20	1,36	1,07	1,18
Bremen	1,13	1,16	1,08	1,20	1,33	1,14	1,36	1,52	1,47	1,17	1,29	1,12	1,07
Chemnitz	1,14	1,28	1,71	1,54	1,70	1,14	1,44	1,70	1,72	1,36	1,31	1,24	1,29
Afyon	1,28	1,93	1,30	1,29	1,51	1,34	1,44	1,78	1,68	1,45	1,66	1,61	1,94
Sinop	1,46	1,69	3,10	2,74	2,03	1,38	1,79	2,48	1,88	1,66	4,44	1,45	1,56
Ankara	1,14	1,65	1,25	1,20	1,40	1,13	1,30	1,52	1,45	1,39	1,89	1,13	1,34
Bursa	1,69	1,91	1,47	1,35	1,29	1,70	1,99	1,90	1,87	1,37	1,82	1,29	1,34
Norderney	1,26	2,56	1,13	1,29	1,52	1,20	1,51	1,46	1,50	1,22	1,19	1,11	1,16
Fichtelberg	1,50	3,01	2,30	2,14	2,41	1,42	2,03	2,43	2,39	1,62	1,80	1,63	1,61
Wittenberg	1,29	3,25	1,62	1,40	1,45	1,18	1,30	1,64	1,64	1,29	1,32	1,21	1,17

## CURRICULUM VITAE

### PERSONAL INFORMATION

**Surname, Name** : ENER RUŞEN, Selmin  
**Nationality** : Turkish (T.C.)  
**Date and Place of Birth** : 1979, Ankara, Turkey  
**Marital Status** : Married with one daughter  
**Employment** : Research Assistant in Department of Physics, METU  
**Contact Details** : Department of Physics, Room: 121, METU, 06531,  
Ankara/TURKEY  
Phone : +90 312 2104317  
Fax : +90 312 2105099  
E-Mail : eselmin@metu.edu.tr, selmin.enerrusen@gmail.com

### EDUCATION:

- **Bachelor of Science:** Physics Eng. Dept., Ankara University, 1997-2001.
- **Master of Science:** Physics Eng. Dept., Ankara University, 2002-2004.

SUPPORT AREA: Medical Physics

THESIS: The Effect of Clinical Experience to the Radiation Doses Received by the Patient in Interventional Radiological Procedures

- **Doctor of Philosophy** : Department of Physics, METU, 2004-

SUPPORT AREA: Solar Energy

THESIS: Linking Satellite Imagery to Bright Sunshine Hours for the Estimation of Global Solar Irradiation

### RESEARCH INTERESTS:

Renewable Energy, Solar Energy, Climate Effect of Solar Energy, Satellite Images of Solar Radiation, Solar Energy Data Analysis and Estimation Models, Medical Physics-Radiology

## ACADEMIC POSITIONS:

Research Assistant: Sept. 2002- 2013, Middle East Technical University Department of Physics

Visiting Researcher: Nov. 2009 – Dec. 2010, Department of Energy and Semiconductor Research Faculty V - Institute of Physics, Carl von Ossietzky University, Oldenburg, Germany.

Trainee: July 2000 – Sept. 2000 Ankara Nuclear Research and Education Center, Ankara

## LIST OF PUBLICATIONS:

### Article in International Journal; (SCI)

1. B. G. Akinoglu and **S. Ener Rusen**, "Combining the satellite imagery with bright sunshine hours: A review" (Submitted to Journal of Renewable and Sustainable Energy) 2013.
2. **S. Ener Rusen**, A. Hammer, B. G. Akinoglu, "Estimation of daily global solar irradiation by coupling the ground measurements of bright sunshine hours to the satellite imagery" (Submitted to Journal of Energy) 2013.
3. **S. Ener Rusen**, A. Hammer, B. G. Akinoglu, "Coupling satellite images with surface measurements of bright sunshine hours to estimate daily solar irradiation on horizontal surface", Renewable Energy, 55 (2013), 212-219.
4. B. Aksoy, **S. Ener Rusen**, B. G. Akinoglu, "A simple correlation to estimate global solar irradiation on a horizontal surface using METEOSAT satellite images" , Turkish J. Eng. Env. Sci., 33 (2011), 125-137.
5. D. Bor, T. Sancak, T. Toklu, T. Olgar, **S. Ener**, "Effects of Radiologists' Skill and Experience on Patient Doses in Interventional Examinations", Radiation Protection Dosimetry 129 (1-3), (2008), 32-35.

### Conference Papers in International Symposium;

1. **\*S. Ener**, E. Yilmaz, B.G.Akinoglu, "An Investigation of the Effect of Climate on Monthly Mean Global Solar Radiation using the Data on Earth Surface", Proc. ISES Asia-Pacific Conf. of International Solar Energy Society, 17-20 October, GwangJu, South Korea, 2004.
2. **\*S. Ener Rusen**, B. Aksoy, B.G. Akinoglu, "Preliminary results of linking the surface data with the satellite images to estimate the solar radiation for Ankara", World Climate Conference 3, 31 August - 4 September, Geneva, Switzerland, 2009.

3. **\*S. Ener Rusen**, A. Hammer, B.G. Akinoglu, "Using Sunshine Duration and Satellite Images to Estimate Daily Solar Irradiation on Horizontal Surface", ISES Solar World Congress 2011, 28 August- 2 September, Kassel, Germany, 2011.
4. D. Bor, T. Sancak, T. Toklu, T. Olgar, **S. Ener**, Effects of radiologist's skill and experience on patient doses in interventional examinations. Sentinel (Safety and Efficacy for New Techniques and Imaging using New equipment to support European Legislation) Meeting Delft, 18-20 April, Netherlands, 2007

(\*: Presented by Selmin ENER RUŞEN)

#### **Conference Papers in National Symposium;**

1. B. Aksoy, **S. Ener Rusen**, B. G. Akinođlu, Global Güneş Radyasyonunun Tahmin Edilmesine Yönelik Angström Denklemi ve Uydu Yaklaşımının Karşılaştırılması, 1. Meteoroloji Sempozyumu, 2010, 27-28 Mayıs, Ankara, Türkiye, 2010.
2. **\*S. Ener Ruşen** & B. G. Akinođlu, "Türkiye'nin Doğusunda Güneş Enerjisinin Uydu Verileriyle İzlenmesi", III. Ulusal Güneş ve Hidrojen Enerjisi Kongresi (UGHEK 2012), 14-15 Haziran, Eskişehir- Türkiye, 2012.

#### **Assisted Courses and Laboratories:**

- PHYS 105-106 Freshmen Physics Laboratories 1-2,
- PHYS 181-182 Basic Physics Laboratories 1-2,
- PHYS 471 Solar Energy-1.

#### **Languages:**

English, German (A1)

#### **Computer Skills:**

Matlab, C++, Windows, OriginPro 7.5-8.0, MapInfo, TNT MIPS, FORTRAN

#### **Scientific Awards & Scholarships:**

Dean's High Honor List of Students, Ankara University (for six times),  
"Successful Student Scholarships" Turkish Physical Society, 1997-2001,  
"TÜBİTAK Yurt Dışı Araştırma Bursu" (for Ph.D. students), November 2009 - May 2010.